

**SMALL SCALE DECENTRALIZED SYSTEMS FOR  
GREYWATER TREATMENT AND RECYCLING**

Thesis

Submitted in partial fulfillment of the requirements for the award of the degree of

**DOCTOR OF PHILOSOPHY**

in

**CIVIL ENGINEERING**

By

**Pragada Sarath Chandra**

Roll. No. 177CV008



**DEPARTMENT OF CIVIL ENGINEERING**

**NATIONAL INSTITUTE OF TECHNOLOGY KARNATAKA, SURATHKAL**

**March, 2022**

# **SMALL SCALE DECENTRALIZED SYSTEMS FOR GREYWATER TREATMENT AND RECYCLING**

Thesis

Submitted in partial fulfillment of the requirements for the award of the degree of

**DOCTOR OF PHILOSOPHY**

in

**CIVIL ENGINEERING**

By

**Pragada Sarath Chandra**

Roll. No. 177CV008

Research Guide

**Dr. Arun Kumar Thalla**



**DEPARTMENT OF CIVIL ENGINEERING**

**NATIONAL INSTITUTE OF TECHNOLOGY KARNATAKA, SURATHKAL**

**March, 2022**

## DECLARATION

I hereby *declare* that the Thesis entitled "**SMALE SCALE DECENTRALIZED SYSTEM FOR GREYWATER TREATMENT AND RECYCLING**", which is being submitted to the **National Institute of Technology Karnataka, Surathkal**, in partial fulfillment of the requirements for the award of the **Degree of Doctor of Philosophy** in the **Department of Civil Engineering** is *a bonafide report of the research work carried out by me*. The material contained in this Thesis has not been submitted to any University or Institution for the award of any degree.

*Sarath 3/3/22*

Place: NITK-Surathkal

Date: 03-03-2022

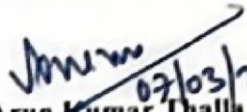
Sarath Chandra Pragada

(177016CV008)

Department of Civil Engineering

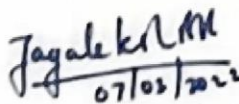
## CERTIFICATE

This is to *certify* that the Research Thesis entitled "SMALL SCALE DECENTRALIZED SYSTEM FOR GREYWATER TREATMENT AND RECYCLING" submitted by **Mr. SARATH CHANDRA PRAGADA (177016CV008)** as the record of the research work carried out by him, is *accepted as the Research Thesis submission* in partial fulfillment of the requirements for the award of the degree of **Doctor of Philosophy**.

  
07/03/2022  
Dr. Arun Kumar Thalla

Research guide  
Department of Civil Engineering  
(Signature with date and seal)



  
07/03/2022  
Prof. B.R. Jayalekshmi  
Chairperson-DRPC

(Signature with date and seal)  
Chairman (DRPC)  
Department of Civil Engineering  
National Institute of Technology Karnataka, Surathkal  
Mangalore - 575 025, Karnataka, INDIA

## ACKNOWLEDGEMENT

It is an immense pleasure to express my heartfelt gratitude to various people who helped and motivated me to carry out the Ph.D. dissertation.

I express my sincere gratitude and thanks to my esteemed Supervisor **Dr. Arun Kumar Thalla**, Associate professor, Department of Civil Engineering, for the valuable guidance, suggestion, constructive criticism, and motivation, which played an inspiring role throughout the research work to fulfil the criteria.

I owe my thanks to Professor **Dr. B. R. Jayalekshmi**, Head of the Department, Civil Engineering and **Dr. K. Swaminathan**, and **Dr. Varghese George**, previous Head of the Department, Civil Engineering, NITK Surathkal, for extending the facilities and wonderful supports in every stage of research work in the Department. I also extend my sincere gratitude towards **Prof. Vidhya Shetty**, Academic Dean, NITK Surathkal, for the support rendered throughout the work.

I would like to thank my RPAC committee members **Dr. Subhaschandra Kattimani and Dr. A. U. Ravi Shankar**, for their continued support and encouragement. I offer my sincere appreciation for the learning opportunities provided by the RPAC members. Also, I would like to express my heartfelt gratitude to all faculty and staff members, Department of Civil Engineering, NITK Surathkal. Their continuous encouragement and support were inspiring towards work.

I would like to express my heartfelt gratitude to all my **friends and colleagues** for their unremitting encouragement, help and support. I am grateful to my **family** members, whose endless encouragement and supports was an endless source of inspiration for this work. I thank the god almighty for his loveliness upon me all through my life. Once again, I thank one and all who have helped me directly or indirectly complete my project in time.

**NITK Surathkal**

**Sarath Chandra Pragada**



## ABSTRACT

As the world's freshwater supply becomes more limited, a greater focus on alternative water resources is required. Wastewater reuse promotes sustainability by lowering global environmental pollution and economic concerns. Greywater reuse and recycling can be essential practices to decrease the demand for clean water. Greywater refers to all domestic wastewater, excluding restroom effluents. Because of the lower levels of contaminants, greywater is easier to treat and recycle than sewage. Thus, greywater reuse is a promising alternative water source that can be used continuously for non-potable purposes. Greywater treatment methods vary depending on site and greywater characteristics. The water quality, quantity to be treated, and reuse applications determine a greywater treatment system design. The present study develops a pilot-scale multi-stage greywater treatment system to treat it to recyclable levels. The study is carried out in two phases. In the first phase, the performance evaluation of a primary treatment unit consisting of an anaerobic-aerobic biological system, followed by a sand filter, was done to remove COD, nutrients, and surfactants. In the second phase, post-treatment of biologically treated greywater by immobilized TiO<sub>2</sub> based solar photocatalytic system is evaluated for removing triclosan effectively.

In Phase I, the performance of the integrated anaerobic-aerobic-sand filter (pilot plant) is assessed based on the results obtained over 12 months of operation of the system. The removal efficiencies of the pilot plant for COD, BOD, anionic surfactants, TN, TSS, and TP are 89%, 95%, 99%, 85%, 88.5, and 87%, respectively

Greywater, predominantly being wash water, where cleansers, mainly composed of surfactants, create huge shock loads and hamper the efficacy of the conventional treatment systems. Therefore, in the present study, experiments were conducted under surfactant shock loads (SSL) to study the reactors' stability in handling the same. Results revealed that anionic surfactants were removed with efficiencies of 96.02%, 96.21%, 94.81%, and 98.42% for hydraulic retention times (HRT) of 32 h, 24 h, 16 h, and 8 h, respectively. The maximum effluent anionic surfactant concentrations obtained are 44.28, 59.12, 73.35, and 88.36 mg/L under the SSL of 85.94, 121.2, 155, and 180.5 mg /L, respectively. The reactor is recovered to steady-state conditions in about 8, 16,

20, and 28 h after removing the SSL of 85.94, 121.2, 155, and 180.5 mg/L, respectively. A linear relationship with  $R^2 = 0.95$  indicates that recovery time is proportional to surfactant loading rate increase. Furthermore, the optimum surfactant-loading rate on the integrated system is 19.38 g/m<sup>3</sup>/h, with a removal efficiency is 91.8%. However, the effluent from the biological treatment unit needs further treatment to eliminate leftover pollutants.

Phase II of the study involves developing a novel solar photoreactor. A ternary film of Fe<sub>2</sub>O<sub>3</sub>-TiO<sub>2</sub>/PVP is coated on the glass tube that stands in a parabolic trough concentrator (PTC) for an effective post-treatment of biologically treated greywater effluents. This ternary film of Fe<sub>2</sub>O<sub>3</sub>-TiO<sub>2</sub>/PVP coated on the glass tube is characterized by Field Emission Scanning Electron Microscope (FESEM), X-ray diffraction (XRD), Fourier-transform infrared spectroscopy (FTIR), UV-visible spectroscopy, and thermogravimetric analysis (TGA). Furthermore, the scratch hardness of photocatalysts at different Fe<sub>2</sub>O<sub>3</sub>/TiO<sub>2</sub> compositions is investigated based on the width measurement of scratch using FESEM analysis. Results show that at an optimum coating of 5% of Fe<sub>2</sub>O<sub>3</sub>/TiO<sub>2</sub> composition catalytic film, the maximum scratch hardness (7.984 GPa) is obtained. The photocatalyst has the highest cohesive bond strength and wearing resistance. The degradation of triclosan (TCS) in treated (anaerobic-aerobic treatment system) greywater has been investigated using a solar photocatalytic reactor. Box Behnken design (BBD) has been employed to screen the significant parameters (such as contact time, pH solution, and initial H<sub>2</sub>O<sub>2</sub> concentration) and identify the most relevant interactions between the operating parameters. After carrying out the different trials of the various operational parameters, the response surface analysis has led to the optimal conditions for the yield of TCS degradation, resulting in an 83.27% removal. Based on LC-MS results, it is evident that the photocatalytic degradation of TCS has resulted in eleven intermediate products.

**Keywords:** *Greywater; Surfactant shock load; Integrated anaerobic-aerobic-sand filter system; Hydrodynamic studies; Immobilized Fe<sub>2</sub>O<sub>3</sub>-TiO<sub>2</sub> /PVP catalyst; Spray coating; Solar photocatalysis.*



# CONTENTS

	<b>Title</b>	<b>Page no.</b>
	<b>LIST OF TABLES</b>	v
	<b>LIST OF FIGURES</b>	vii
	<b>LIST OF ABBREVIATION</b>	ix
	<b>CHAPTER 1 INTRODUCTION</b>	1
1.1	BACKGROUND	1
1.2	GREYWATER	2
1.3	HOW GW CAN BE HANDELED	4
1.4	ORGANIZATION OF THESIS	5
	<b>CHAPTER 2 LITERATURE REVIEW</b>	7
2.1	GENERAL	7
2.2	CHARACTERISTICS	8
	2.2.1 Physical Parameters	9
	2.2.2 Chemical Parameters	10
	2.2.3 Xenobiotic Organic Compounds	10
	2.2.4 Biological Parameter	14
2.3	RECYCLABLE LIMITS	14
2.4	GW FLOW RATE ESTIMATION	16
2.5	TREATMENT OPTIONS	18
	2.5.1 Physical Treatment	19
	2.5.2 Chemical Treatment	21
	2.5.3 Biological Treatment	23
	2.5.3.1 Constructed Wetlands	23
	2.5.3.2 Rotating Biological Contractor	25
	2.5.3.3 Membrane Bioreactor	26
	2.5.3.4 Sequencing Batch Reactor	27

2.5.3.5	Upflow Anaerobic Sludge Blanket Reactor	28
2.5.4	Integrated treatment systems	31
2.6	<b>POLISHING TREATMENT</b>	31
2.6.1	Heterogeneous Photocatalyst	32
2.6.2	Homogeneous Photocatalyst	33
2.6.3	Doping of Semiconductors	33
2.7	<b>SUMMARY</b>	37
2.8	<b>RESEARCH GAP</b>	40
2.9	<b>OBJECTIVES OF PROJECT WORK</b>	41
 <b>CHAPTER 3 MATERIALS AND METHODOLOGY</b>		 43
3.1	<b>GENERAL</b>	43
3.2	<b>MATERIALS &amp; METHODOLOGY</b>	43
3.2.1	Integrated Anaerobic-Aerobic-Sand Filter System	43
3.2.1.1	Compositions of GW	43
3.2.1.2	Culture development in reactors	44
3.2.1.3	Sand filter media	44
3.2.1.4	Experimental Setup	45
3.2.1.5	Reactor Operation	47
3.2.1.6	Start-Up and Operation of the Reactor	50
3.2.1.7	Shock Loading Application	50
3.2.1.8	Analytical Methods	51
3.2.2	Preparation of the immobilized TiO <sub>2</sub> based catalyst	53
3.2.2.1	Preparation of Ternary Composite (Fe <sub>2</sub> O <sub>3</sub> - TiO <sub>2</sub> /PVP) Solution and Catalytic Film Coating	53
3.2.2.2	Characterization of Ternary Composite (Fe <sub>2</sub> O <sub>3</sub> - TiO <sub>2</sub> /PVP) Film	53
3.2.2.3	Experimental Set-Up for Photocatalytic Treatment	55
3.2.2.4	Operational Procedure	55
3.2.2.5	Experimental design and Optimization	56

<b>CHAPTER 4 RESULTS AND DISCUSSION</b>	<b>57</b>
4.1 PERFORMANCE OF INTEGRATED ANAEROBIC-AEROBIC-SAND FILTER SYSTEM	57
4.1.1 organic matter and nutrient removal at steady-state condition	57
4.2 PERFORMANCE EVALUATION OF INTEGRATED GWT UNDER VOLUMETRIC SHOCK LOAD	60
4.2.1 Integrated GWT Systems Performance Prior to Surfactant Shock Loading (SSL)	63
4.2.2 Performance of Integrated GWT System Under Organic Shock Loads	63
4.2.2.1 Overall Performance of the Integrated System During SSL	66
4.2.2.2 Effect of SSL on Integrated Anaerobic-Aerobic-Sand Filter System	66
4.2.2.3 Optimum Loading Rate	66
4.2.3 Characterization of Sludge in an Integrated System	71
4.2.3.1 Fourier Transformation Infrared Spectroscopy Analysis (FTIR)	71
4.2.3.2 Effects of SSL on the Microbial Characteristics of Biomass	72
4.3 IMMOBILIZATION PHOTOCATALYST PREPARATION AND APPLICATION FOR TCS TREATMENT IN GW	75
4.3.1 Structures and Surface Morphologies of Immobilized Ternary Composite (Fe <sub>2</sub> O <sub>3</sub> -TiO <sub>2</sub> /PVP) Coated Film	75
4.3.2 BET analysis	80
4.3.3 Mechanical stability of Fe <sub>2</sub> O <sub>3</sub> -TiO <sub>2</sub> /PVP catalyst	81
4.3.4 Immobilized Photocatalytic Degradation of TCS	82
4.3.4.1 Kinetics of Photodegradation	82
4.3.4.2 Response Surface Methodology (RSM)	85
4.3.4.3 RSM Results	85

4.3.4.4	Model Validation	89
4.3.4.5	Optimization	89
4.3.5	Plausible Degradation Pathway of TCS	91
4.3.6	Toxicity Studies	95
4.3.7	Cost Implications/Energy Consumption	96
<b>CHAPTER 5 CONCLUSIONS</b>		<b>99</b>
<b>APPENDIX</b>		<b>101</b>
<b>REFERENCES</b>		<b>107</b>
<b>PUBLICATIONS</b>		<b>122</b>

## LIST OF TABLES

<b>Table no.</b>	<b>Title</b>	<b>Page No.</b>
2.1	Physicochemical characteristic of greywater	09
2.2	Regulations of GW Reuse	17
2.3	Various operating parameters for filtration	21
2.4	Comparison of organic matter and nutrient removal efficiencies of integrated or combined biological treatment systems for GW	30
3.1	Physical and chemical characteristics of the synthetic GW	44
3.2	Particle size distribution for sand filter media	45
3.3	Design of holding tank, AnSBR, ASBR, and sand filter	45
3.4	Automation and data logging for the pilot-scale operation system	49
3.5	The AnSBR dimensions and operation conditions	51
3.6	Characteristics of influent at various shock loads	52
3.7	Test Methods	52
4.1	Effect of the anaerobic treatment	59
4.2	Aeration effect at dissimilar times on the characteristics of chemical and physical by AnSBR effluent	60
4.3	Effect of up flow sand filter of GW on the chemical and physical characteristics	61
4.4	Effect of overall GWT of physical and chemical characteristics	62
4.5	Comparison of reactor performance at various HRT	64
4.6	Scratch hardness at different ratio Fe <sub>2</sub> O <sub>3</sub> -TiO <sub>2</sub> coated samples	77
4.7	Compounds identified in the different composite samples using XRD	79
4.8	The BET summary of prepared samples	83
4.9	Box Behnken Design matrix in the photocatalyst process	88
4.10	ANOVA of Quadratic model for TCS degradation rate	90
4.11	Comparison of the present study with other photocatalytic treatments of TCS from the aqueous medium	92

4.12	Concentration of metal ions released from the coated catalyst into solar photocatalysis outlet as determined by ICP-OES	95
4.13	Comparison of power consumption of present system with other systems	96

## LIST OF FIGURES

Figure No.	Title	Page No.
1.1	Decentralized wastewater treatment system	02
1.2	Sources of GW	04
2.1	Types of surfactants	12
2.2	Band structure of 'n' and 'p' type semi-conductors	34
3.1	Particle Size Distribution Curve for a) Crushed stone (large size), b) Crushed stone (medium size), and c) Coarse sand	46
3.2	a) Experimental setup and b) Schematic diagram of Integrated anaerobic-aerobic-sand filter system	47
3.3	Operation procedure for Integrated anaerobic-aerobic sequence batch reactors	48
3.4	Scheme of the thermal spray method for immobilization of (Fe <sub>2</sub> O <sub>3</sub> -TiO <sub>2</sub> /PVP) supported on a glass pipe	54
3.5	Synthesis coated sample and solar photocatalysis reactor setup	56
4.1	Overall removal efficiencies of COD, BOD, and TSS in anaerobic, aerobic, and sand filter stages.	58
4.2	Overall removal efficiencies of surfactants and nutrients in anaerobic, aerobic, and sand filter stages.	58
4.3	Effects of SSL before and after the treatment on three-stage (R <sub>1</sub> -R <sub>2</sub> -R <sub>3</sub> ) integrated system: (a) Surfactants and (b) COD	65
4.4	COD variation in influent, R <sub>1</sub> , R <sub>2</sub> and R <sub>3</sub> at shock loads of (a) 640, (b) 800, (c) 960 and (d) 1104 mg/L	68
4.5	Variation of anionic surfactants in influent, based on R <sub>1</sub> , R <sub>2</sub> and R <sub>3</sub> at shock loads of (a) 85.94, (b) 121.2, (c) 155 and (d) 180.5 mg /L.	69
4.6	Evaluation of a) R <sub>1</sub> at SSL of 85.94 mg/l, b) R <sub>2</sub> at SSL of 85.94 mg/l, c) R <sub>3</sub> at SSL of 85.94 mg/l, d) overall system at SSL of 85.94 mg/l, e) R <sub>1</sub> at SSL of 121.2 mg/l, f) R <sub>2</sub> at SSL of 121.2 mg/l, g) R <sub>3</sub> at SSL of 121.2 mg/l and h) whole system at SSL of 121.2 mg/l.	70
4.7	Performance of a) R <sub>1</sub> at SSL of 155 mg/l, b) R <sub>2</sub> at SSL of 155 mg/l, c) R <sub>3</sub> at SSL of 155 mg/l, d) overall system at SSL of 155 mg/l, e) R <sub>1</sub> at SSL of 180.5 mg/l, f) R <sub>2</sub> at SSL of 180.5 mg/l, g) R <sub>3</sub> at SSL of 180.5 mg/l and h) SSL of 180.5 mg/l.	72
4.8	Removal efficiency of the overall system and the effective surfactant loading rate	73
4.9	Fourier transformation infrared spectroscopy (FTIR) analysis for a) Coir fibre, b) attached biofilm in anaerobic sludge	74
4.10	Surface morphology studies for (a) initial seed of anaerobic sludge, (b) initial seed of activated sludge, (c) Biofilm after the application	75

	of shock load-1, (d) Biofilm after the application of shock load-2, (e) Biofilm after the application of shock load-3 and (f) Biofilm after the application of shock load-4	
4.11	(a) TGA thermogram (b) DTA trace for Fe <sub>2</sub> O <sub>3</sub> -TiO <sub>2</sub> /PVP composite solution and (c) FESEM micrographs of scratches on coated samples with scratch width dimensions at different ratios of Fe <sub>2</sub> O <sub>3</sub> /TiO <sub>2</sub> compositions of (i) 1 atomic wt.%, (ii) 3 atomic wt.%, (iii) 5 atomic wt.%, (iv) 7 atomic wt.% and (v) 9 atomic wt.%.	78
4.12	(a) XRD patterns, (b) FTIR spectra, (c) FESEM image, (d) EDAX mapping, and (e) Thickness of coated samples.	81
4.13	Elemental compositions of Ternary composite annealed at 320°C	82
4.14	Surface roughness R-profile of ternary composite annealed at 320°C	82
4.15	BET surface area: a) Fe <sub>2</sub> O <sub>3</sub> -TiO <sub>2</sub> /PVP after annealing @ 3200 C, b) Fe <sub>2</sub> O <sub>3</sub> -TiO <sub>2</sub> /PVP after drying @ 600 - 800C	84
4.16	Surface topography of the worn surfaces after pin on disc wear test (a) coating at 5N load (b) coating at 10N load.	85
4.17	Variation in friction coefficient with respect to sliding time under (a) 5N (b) 10N load	86
4.18	Pseudo second-order kinetics for TCS removal (under natural GW pH)	87
4.19	Pseudo-second-order kinetics for TCS removal	87
4.20	The point zero charges (PZC) of the Fe <sub>2</sub> O <sub>3</sub> -TiO <sub>2</sub> /PVP show the final pH as a function of initial pH <sub>0</sub> .	88
4.21	Response surface analysis (a) experimental and theoretical responses, (b) predictable model's residual analysis, (c) Response surfaces, and (d) contour plots showing the effect of the contact occasion and the value of pH solution of the TCS degradation	91
4.22	Plausible degradation pathway of TCS by immobilized ternary composite (Fe <sub>2</sub> O <sub>3</sub> -TiO <sub>2</sub> /PVP) coating catalyst	94



## ABBREVIATIONS

GW	Greywater
CW	Constructed Wetland
BOD	Biochemical Oxygen Demand
COD	Chemical Oxygen Demand
TKN	Total Kjeldahl Nitrogen
TN	Total Nitrogen
TP	Total Phosphorous
WHO	World Health Organization
NTU	Nephelometric Turbidity Unit
DO	Dissolved Oxygen
TSS	Total Suspended Solids
LPL	Low Pollutants Load
LGW	Load Grey Water
SS	Suspended
XOC	Xenobiotic Organic Compounds
OMP	Organic Micro Pollutants
SAR	Sodium Adsorption Ratio
PAH	Polycyclic Aromatic Hydrocarbons
SRICPS	Short Rotation Intensive Cultural Plantation System
NPDES	National Pollutant Discharge Elimination System
EPA	Environmental Protection Agency
HSFCW	Horizontal Substance Flow Constructed Wetland
HLR	Hydraulic Loading Rate
OLR	Organic Loading Rate
MBR	Membrane Bio Reactor
GWT	Greywater Treatment

AnSBR	Anaerobic Sequential Batch Reactor
PVC	Poly Vinyl Chloride
SBR	Sequencing Batch Reactor
RBC	Rotating Biological Contactor
FSW	Free Surface Wetland
RVFCW	Vertical Flow Constructed Wetland
HFCW	Horizontal Flow Constructed Wetland
EC	Electrical Conductivity
TDS	Total Dissolved Solids
VFF	Vertical Flow Filter
MF	Micro Filtration
UF	Ultra-Filtration
NF	Nano Filtration
RO	Reverse Osmosis
UVC	Ultra Violet c
AOP	Advanced Oxidation Processes
CB	Conduction Band
VB	Valance Band
ASBR	Aerobic Sequential Batch Reactor
PVP	Polyvinyl pyrrolidone
TCS	Triclosan

# CHAPTER 1

## INTRODUCTION

### 1.1 BACKGROUND

Among the whole world population, it is assessed that one-third of people do not have admittance to hygienic potable water (World Health Organization., 2017). Universal water scarcity is due to the integration of a growing population, a developed society with extensive water resources in farming and production, the increasing standard of living, and climate change (Boano HH *et al.* 2020). If the current trend continues, the total number of people living in water-stressed or scarce-water nations will rise by 0.5 billion to 3 billion by 2025 (Hanjra and Qureshi 2010). Water reuse is gaining popularity in discussions about sustainable water management, green economies, and urban planning (Chong *et al.*, 201 5). Water supply is a difficult challenge for all growing cities worldwide, both in quality and quantity. The increasing urbanization and population growth have exacerbated the burden on water bodies. Therefore, every metropolitan and municipal government had been pushed to enact legislation requiring mandatory wastewater recycling and reuse. Economic and energy-based analyses demonstrate the energy of high capital, operating, and maintaining demands in traditional treatment, whereas the potential for energy generation is negligible (Svardal and Kroiss 2011).

The challenge of providing clean water and sanitation needs the development of novel approaches. The decentralized wastewater treatment system is a promising approach for preserving natural water resources because it allows for the reuse of treated wastewater and reduces freshwater consumption. According to source separation principles, unwanted domestic water is separated into two types: blackwater and greywater (GW). Blackwater generation in residential structures is typically modest, less than 30% of the total, and significantly lower in systems of non-resident (Li *et al.* 2009). As a result, greywater treatment (GWT) may recycle most of the wastewater produced (Dixon *et al.* 1999). Separating the GW and blackwater and then treating GW reduces the volumetric burden on the existing centralized conveyance and

treatment system. Hence, the decentralized system approach proves a strong economy for conveyance and treatment by treating the GW and blackwater separately, as shown in Figure 1.1. For the GWT, various technologies such as combined treatment systems with high efficiency are used, resulting in treated water that meets the standards and norms of reuse for non-potable applications.

## 1.2 GREYWATER

Wastewater, which does not include faecal sludge or wastewater from septic tanks, is defined as GW. Organic loading matter is a remarkable difference between GW and black water. In comparison with GW, sewage has a substantially higher organic content. Kitchen wastewater is sometimes referred to as "black water" because it has a higher organic range than other types of wastewaters, such as bathwater (Drechsel *et al.*, 2015). Untreated wastewater from residential areas is dumped into the environment, contributing to the many contaminants that enter the aquatic system. Therefore, the reuse of GW is becoming more popular, and the name "wastewater" has become a misnomer in many ways. Perhaps "Used Water" would be a better moniker for this liquid. When freshwater supply in the world grows increasingly constrained, more emphasis is paid to alternate water sources. The GW characteristics depend on the number of residents, lifestyle and water usage patterns, living standards, social and cultural habits, type and quantity of household chemicals used, and storage time. Bathroom GW contains soaps, shampoos, body care products, shaving waste, skin, hair, body fats, lint, and traces of urine and feces.

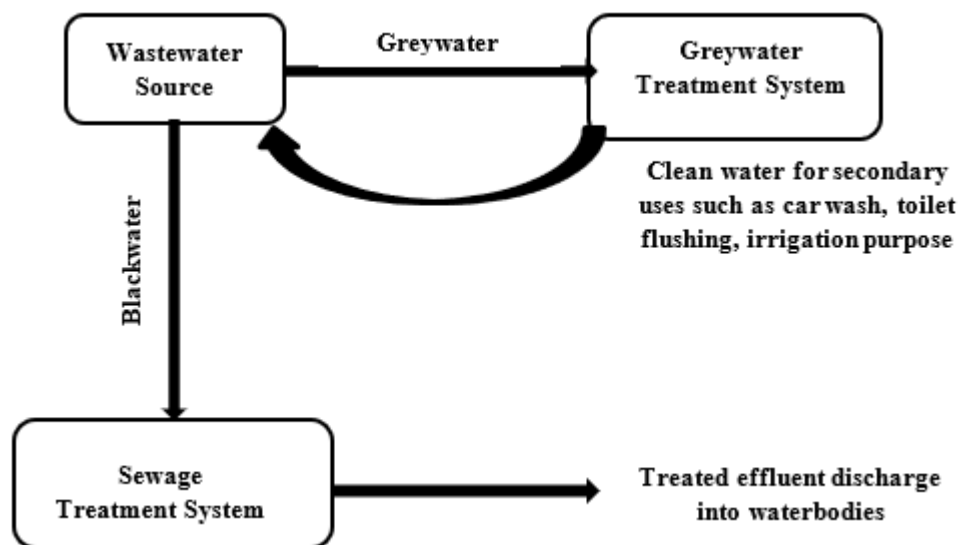


**Figure 1.1** Decentralized Wastewater Treatment System (Siang *et al.* 2018)

Laundry GW contains high concentrations of chemicals from soap powders, bleaches, oils, paints, solvents, and non-biodegradable fibers from clothing. GW originated from washing machines with high pH, temperature, nitrate, surfactants, oil and grease, phosphate, salinity, sodium, suspended solids, and turbidity. GW generated from the kitchen sink contains oil and grease, food scraps, dishwashing detergents such as liquid handwashing. Some of the GW sources and constituents are shown in Figure 1.2.

GW is frequently utilized for irrigation or grass watering in private residences without treatment. It is unlikely harmful to the environment or hygiene of individuals on such a tiny scale. However, adequate treatment is essential when contemplating reuse (apartments, buildings, or communities) on a bigger scale. It will demand a GW characterization, determining the treatment strategy to be used. The treated GW must meet the appropriate criteria (depending on the country's rules). Eventually, treated GW can flush toilets, irrigation, car washing, and fire-fighting.

Compared to other water-capture techniques, such as rainwater harvesting, which depends on hydrology, reuse GW has been regarded as a stable technique for ensuring water security (Janet *et al.* 2010). The quantity of GW depends on the water consumption, GW generation, and GW utility. Typically, GW quantity is generated around 65% of the total wastewater flow. (Jamrah *et al.*, 2011). So, there is a high prospect for recycling and reuse of GW.

GW is a different type of water, and the amount of GW created in emerging nations is higher than in affluent countries. Washing and dip water accounts for around 50-60% of the GW considered the slightest polluted kind of the GW (Sharma *et al.*, 2010). Moreover, it has some faecal contamination due to body washing. Around 25-35% of total GW is generated by water used in fabric washing (Long *et al.* 2019). Chemical pollutants like detergents and cleaning products, i.e., emerging pollutants and various personal care compounds, are also found in the GW (Rajarshi and Oindrila 2012).

Despite its reuse potential, there are specific concerns about the reuse of GW, particularly the risks of direct or indirect exposure to toxic compounds if this stream is not adequately treated. Furthermore, environmental consequences, such as soil and groundwater pollution, are caused by irrigation with water containing with higher

amount of micropollutants such as surfactants. Emerging contaminants found in GW at lower concentration levels may also pose a risk, a problem that has received little attention.

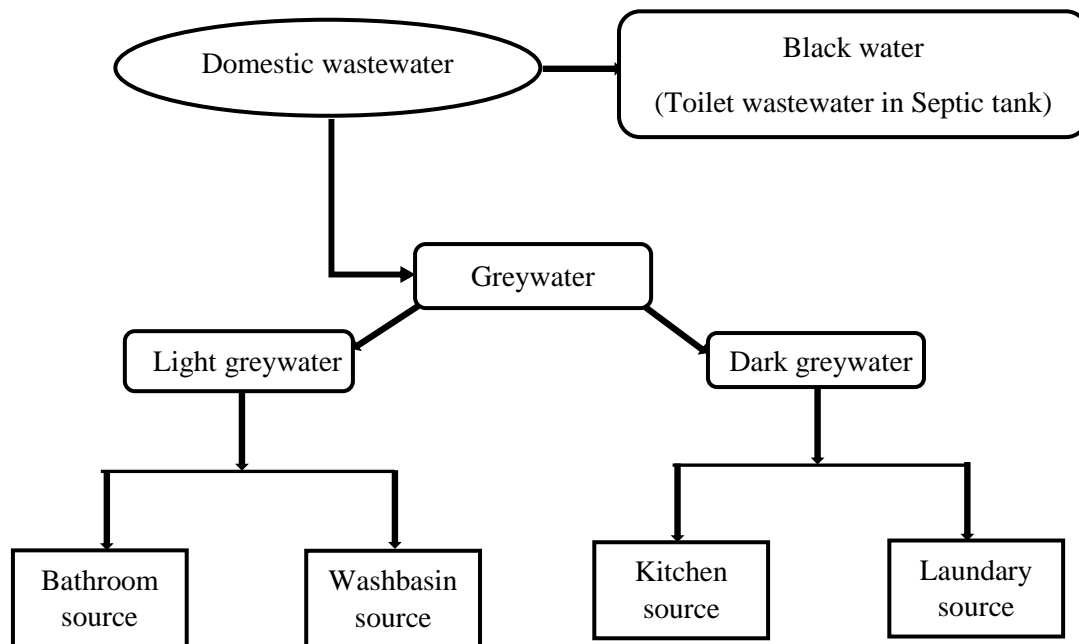


**Figure 1.2** Sources of GW (Ghaitidak and Yadav 2013)

### 1.3 HOW GW CAN BE HANDLED?

In many parts of the world, GW reuse and recycling are essential. Water scarcity is a possible and significant reason, as countries with insufficient rainfall, high evaporation, and excessive population demand for freshwater. On the other side, the importance of recycling wastewater is environmental and economic considerations. GW reuse will lower the total handling cost since there will be a reduced load of water to the treatment plants (Eriksson *et al.*, 2002). So far, India lacks a focused policy framework for managing and utilizing natural resources. Despite some wastewater treatment guidelines, policy and technological interventions must be implemented in India to regulate the recycling and reuse of GW. Furthermore, GW must be adequately treated and not discharged directly into the environment because GW's organic and inorganic constituents can frequently cause irreparable damage, such as depletion of natural oxygen and the development of septic conditions.

GWT methods primarily depend on the volume of GW, physicochemical and biological properties of GW, and energy required. There is no universally accepted technology for GWT. For instance, GWT technologies include physical, chemical,

biological, and combinations of these processes (Manna 2018). Eventually, GWT needs to remove organic matter, nutrients, suspended particles, oil, grease, turbidity, micropollutants, etc., to achieve the quality standard of non-potable water.

#### **1.4 ORGANIZATION OF THESIS**

This thesis contains five chapters, including an introduction, literature survey, materials and methodology, results and discussion, and conclusions.

Chapter 1: Introduction and discussion on water shortage, water availability, current status, methods to handle, the extent of recycling treated GW, and outline of the Thesis.

Chapter 2: Detailed discussion on integrated wastewater treatment technology and various literature surveys on biological treatment (secondary treatment), post-treatment (heterogeneous photocatalysis), and combined physical, chemical, and biological advanced technologies adopted in various modes of treating the GW.

Chapter 3: Materials used for treatment technology and characterization analysis and the methodology section focused on laboratory experiments conducted by different modes of operation.

Chapter 4: The performance results and discussions were evaluated by an integrated anaerobic-aerobic-sand filter system as secondary treatment and immobilized  $\text{Fe}_2\text{O}_3\text{-TiO}_2/\text{PVP}$  composite catalyst for solar photocatalysis continuous reactor as tertiary treatment.

Chapter 5: Outlines the summary and conclusion of the current study and future scope on combined GWT.





## CHAPTER 2

### LITERATURE SURVEY

#### 2.1 GENERAL

Wastewater and GW reuse are evolving as an essential part of water management, helping to conserve high-quality freshwater recycling and reuse of GW, reducing environmental pollution and overall supply costs (Al-hamaiedeh and Bino, 2010). GW was frequently used in some countries like Syria, South Africa, and Australia for gardening and lawn watering (Dalahmeh *et al.*, 2009). GW is difficult to classify as a wastewater type due to its variation in composition from light GW to dark GW. However, GW generally has a similar organic strength to a low to medium strength influent municipal sewage with a characteristic similar to tertiary sewage effluent in terms of biodegradability and physical pollution. The significant issues in treatment are related to the organic strength of the water because of its relationship with characteristics and the need to meet legislative standards. The impact on health concerns directly results from the chlorine demand that residual organics exert on the system, which, if not probably controlled, can result in insufficient disinfection before reuse (Albalawneh and Chang, 2015). Raw GW treatment is a prerequisite for storage and use. Untreated GW reuse would pose health risks to human beings and their environment; hence it should be treated to a higher standard before reusing (Ghunmi *et al.*, 2011).

In addition, the Pathogens contemporary in GW has been broadcasted as volatiles during irrigation and toilet reddening. Irrigation using untreated GW for a long period can cause surfactants, oil, boron, alkalinity, salt, and grease build-up. Moreover, it affects the properties of soil that result in very low yield of crops, at the same time, GW also gets contaminated (Christova-Boal *et al.*, 1996; Travis *et al.*, 2008; Wiel-Shafran *et al.*, 2006; Misra and Sivongxay, 2009; Pinto and Maheshwari, 2010). Filtration is the least expensive treatment required for irrigating the GW. Furthermore, subsurface irrigation was preferred for GW filtering (Gulyas, 2007; Christova-Boal *et al.*, 1996).

GW management is not only necessary for clean and healthy living conditions, but it also has a high potential for reuse. In GWT, technologies have concentrated on 66\*parameters such as BOD and COD, nutrients, and pathogens. Only a few studies have focused on identifying and characterizing other substances, such as organic micropollutants, found in low concentrations in GW.

## **2.2 GW CHARACTERISTICS**

The composition of any wastewater is the sum of materials in the initial water and all the products that are added during usage. In the case of GW, the additional materials consist of soap, shampoo, inorganic dirt or unwanted materials, traces of personal care products, and skin cells during washed off the hands and bathing. Existing literature can contribute to our understanding of hand washing water inputs by two different approaches. The GW treatment often presents real-world handwashing water. The composition of greywater varies, and it is largely a reflection of the lifestyle and the type and choice of chemicals used for laundry, cleaning and bathing. The quality of the water supply and the type of distribution network also affect the characteristics of greywater. There will be significant variations in the composition of greywater in both place and time which may be due to variations in water usage in relation to the discharged quantity. The composition may also be affected by chemical and biological degradations of some compounds within the transportation and storage network. Generally, greywater contains high concentrations of easily biodegradable organic materials and some basic constituents which are largely generated from households. These include nutrients such as nitrates and all its derivatives, phosphorus and its derivatives, but others include xenobiotic organic compounds (XOCs) and biological microbes such as faecal coliforms, salmonella and general hydro chemical constituents (Reynaert et al., 2018). Many researchers have documented that greywater constituents are partly recalcitrant, i.e. slowly or even non-biodegradable. The presence of these contaminants in greywater is an indication of the gradual increase in the level of complexity in the composition of greywater (Abh-ghunmi et.al 2010).

The GW composition can be categorized based on physicochemical properties of water quality parameters, as shown in Table 2.1.

### 2.2.1 Physical parameters

Temperature, Electrical conductivity (EC), turbidity, suspended particles, and other parameters are elements linked with the physical appearance of GW. GW has a range of temperature 18-35 °C, and the comparatively high temperature because of the warm water used in personal hygiene and cooking. Large temperatures may encourage undesired development of microbiology and carbonate's precipitation, like CaCO<sub>3</sub>, salts of inorganic, becomes low soluble at large temperature (Oteng-Peprah *et al.*, 2018; Edwin *et al.*, 2014). According to Prathapar *et al.* (2005), total suspended solids (TSS) concentrations at GW ranged between 190 and 537 mg L<sup>-1</sup>. Higher TSS is because of wastewater from vegetables, fruit, and the kitchen. The EC of GW has been measured in 14 to 3000 S/cm. Due to dissolved minerals, the high EC is commonly linked with groundwater sources and water scarcity places. Due to leaking into GW sources, aged plumbing material also increases EC (Ciabatti *et al.*, 2009). The turbidity of GW is measured in the range of 19–44 NTU, primarily impacted by water usage.

**Table 2.1** Physicochemical characteristic of greywater (Calafat et al. 2008; Gross et al. 2007; James and Ifelebuegu 2018; Reynaert et al. 2018; Rodda et al. 2011; Smith and Bani-Melhem 2012)

Parameter	Laundry	Bathroom	Kitchen Sink	Household greywater
pH	9.3-10	5-8.1	6.3-7.4	6.7-8.34
Turbidity, NTU	-	-	26.5-164	38-158
EC (µS/m)	190-1400	82-20000	-	360-655
BOD <sub>5</sub> , mg/L	48-380	76-200	-	150-530
COD, mg/L	250-375	280-8000	26-1600	210-740
Nitrate, mg/L	0.4-0.6	0-4.9	0.2-3.9	0.12-7.48
Phosphate as PO <sub>4</sub> <sup>3-</sup> , mg/L	4-15	4-35	0.4-4.7	0.23-4.11
TN, mg/L	6-21	0.6-7.3	13-60	20-80
TP, mg/L	0.062-57	0.11-2.2	3.1-10	0.1-69.6
Surfactants, mg/L	-	-	-	2.76-80.5
Triclosan, mg/L	-	-	-	0.0024-3.79

The EC, TSS, turbidity vary from 29–505 mg L<sup>-1</sup> for LGW 190 to 3,000 S cm<sup>-1</sup>, 12–315 mg L<sup>-1</sup> for HGW, 19–444 NTU, and 14–1,241 S cm<sup>-1</sup>, 12.6–375 NTU. HGW has more remarkable physical properties than LGW due to input in kitchen laundry GW.

### 2.2.2 Chemical parameters

Chemicals used for cleaning, cooking, and bathing are significant chemical constituents in greywater. It is critical to understand the contaminants' sources to identify the various chemical components in greywater. Due to a greater detergent content, the range of pH for HGW (6.35–10) is often more extensive than LGW (6.4–8.1). HGW has dissolved BOD and COD in the ranges of 44–1056 and 50–2568 mg L<sup>-1</sup>, whereas LGW has dissolved BOD and COD in the ranges of 23–300 mg L<sup>-1</sup> and 23–633 mg L<sup>-1</sup>. GW of the kitchenette has biologically degradable pieces of food that are dissolved that contribute to BOD. The significant dissolution of COD for HGW is the most likely cause of laundry detergent powders and washing dish solutions. Due to GW of kitchen and phosphates from laundry detergents, TN, TP is more significant inside HGW (2.75–57.7, 0.062–42 mg L<sup>-1</sup>) than in LGW (4.1–16.4, 0.11–1.8 mg L<sup>-1</sup>). Due to the saving of water fittings employed, BOD<sub>7</sub> has been examined rather than BOD<sub>5</sub> the high BOD, COD values of dissolved in 300, 633 mg L<sup>-1</sup>, LGW at Germany resulted (Nolde, 2000). The extremely large dissolving of COD value at the UK, LGW collected from a university campus (maximum of 575 mg L<sup>-1</sup>) was also linked to the cleaning agent used time of residence of LGW in the system of collection (Pidou *et al.*, 2008).

The primary chemical constituents found in GW generated due to cleaning or washing activities are surfactant and triclosan, which have been categorized as emerging pollutants (Oteng-Peprah *et al.*, 2018). These emerging pollutants can act as recalcitrant in the environment due to their long-term persistence behaviour. So, the Xenobiotic organic compounds (XOCs) must be studied and effectively treated.

### 2.2.3 Xenobiotic organic compounds

The main components of GW are organic micropollutants (OMP) and cations like magnesium, nitrate, potassium, and calcium resulting from the cleaning agent (Chan and Tanksale, 2014). According to Eriksson *et al.* (2002), GW in Denmark had almost 200 different forms of OMP, including antioxidants, dyes, perfumes, plasticizers, and surfactants. Surfactants are used to remove the highest amount of organic chemical compounds from home GW (Kobayashi *et al.*, 2015). They are the ingredients active

in most detergents used in personal care products (Aroera *et al.*, 2012; Ying, 2006). Linear alkylbenzene sulphonates (LAS) are the most commonly used anionic surfactants (Temminck and Klapwijk, 2004). Because the detergent qualities differ from ordinary wastewater, traditional effluent treatment techniques for wastewater are ineffective in treating GW (Shafran *et al.*, 2005). Surfactant biological impacts in the environment must be studied to assess surfactants' dangers, division, behaviour, and destiny (Ghunmi *et al.*, 2011).

Surfactants are the most prevalent OMPs in GW because they help make detergents and hygiene products widely used in showering and laundry. Compounds produced by cationic, amphoteric, non-ionic, and anionic detergents are surfactants. These classes may also include cationic compounds, the surfactants of Ionics like olefin sulphonate, methyl ester sulphonate, isotridecanol ethoxylates, alkyl ether sulphates, alkyl benzene sulphonates, ammonium chloride, benzalkonium chloride, and n-hexadecyl trimethyl. Surfactants are the most common ingredients. Surfactants are divided into four categories: non-ionic, cationic, amphoteric, and anionic (Schouten, 2009). Ionic hydrophilic surfactants have a negative charge, whereas cationic surfactants have a positive charge. As seen in Figure 1.1, surfactants of non-ionic had no charge, but surfactants of amphoteric had both positive and unresponsive charges at their end. The pH of the solution determines the surfactant charges. It has anionic characteristics at low pH value and cationic characteristics at sharp pH value, and it can have together charges of unenthusiastic, optimistic at times (Schouten *et al.*, 2009; Salager *et al.*, 2002).

XOCs are one of the most frequent organic pollutants reflecting the actual problems of environmental pollution remediation. Due to their complex organic compound composition, they have had a high degree of ecological persistence for several years. Additionally, while it carries a moderate hazard risk, it poses a threat to aquatic life in a short period due to the presence of a toxin active in tiers.

XOCs are found in daily medication and chemicals. Chemicals that had been partly changed by chemical or biological treatment can also produce XOCs (Fatta-Kassinos *et al.*, 2010). XOCs are dangerous because resistance to treatment can build up in the animal-planet, causing consequences of biology (Fatta-Kassinos *et al.*, 2010). On another side, little medications, like antibiotics, may cause the formation or

expansion of resistant bacteria strains when free into the environment (Le-Minh *et al.*, 2010). It is hard to assess every hazardous compound's potentially chemical contribution in dangers connected to wastewater due to many of them (Palmquist and Hanus, 2005). Benzene, 4-nitrophenol's presence in GW was detected by Revitt *et al.* (2011). Out of 81 tested chemicals, 46 harmful organic chemicals were found in GW (Palmquist and Hanus, 2005). Based on simple contents, several varieties of typical detergent, which Denmark used, Eriksson *et al.* (2002) found 900 probable XOCs in GW. While GW used to clean the floor and flush the toilet, XOCs are usually not a concern, but they could consider if water reused irrigating replenishment (Gulyas *et al.*, 2007b).

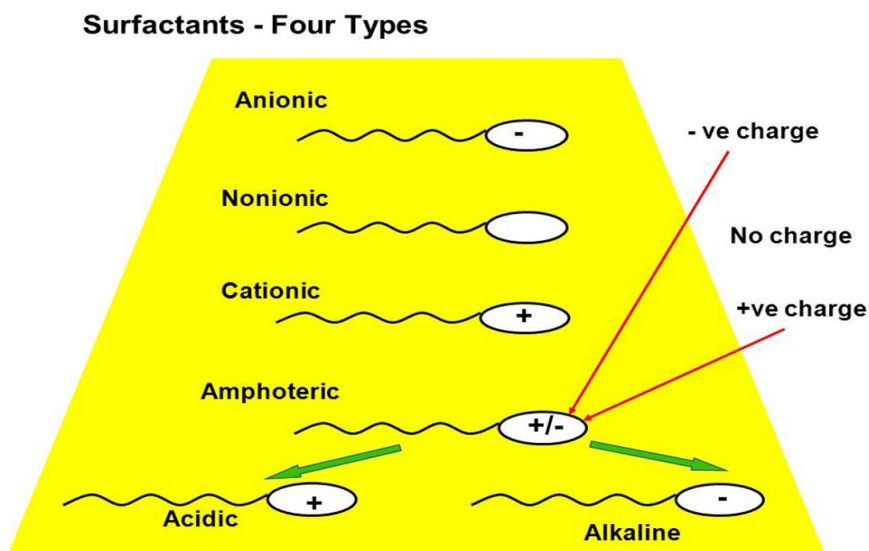


**Figure 2.1** Types of surfactants (<https://slidetodoc.com/surface-chemistry>)

XOCs are significant threats; also, these compounds are artificial to living organisms. Moreover, these substances are not predicted using naturally collected degradative enzymes. Hence, it has a wide range of possibilities to continue in water and sand (Eyer *et al.*, 2004). XOCs originate in the GW based on personal care elements and chemicals such as toothpaste, detergent, softeners, shampoos, and liquids like dishwashing (Etchepare and Hoek, 2015). Detergents and personal care items are used to create XOCs in GW. These chemicals can stay in the environment and negatively affect many species over time, such as toxicants and bioaccumulation in cells (Aonghusa and Gray, 2002; Jenkins, 1998; Donner *et al.*, 2008).

GW generally contains high concentrations of nutrients, xenobiotic organic compounds (XOCs), and biological microbes (Shaikh and Ahammed 2020). GW disposal with a high amount of XOCs can reduce the surface tension of water and create undesired environmental conditions for aquatic organisms. The most common mutual XOCs are polycyclic aromatic hydrocarbons (PAH), nonylphenol, organotin compounds, and monocyclic aromatics. However, recent studies have found many pharmaceuticals and personal care products (PPCPs), pesticides, pigments, and toxic heavy metals in significant concentrations in greywater (Czech et al. 2020). Hence, it is essential to treat greywater with low-cost physicochemical or biological techniques (Ansari and Shrikhande 2019). The term PPCPs refers to a broad range of uncontrolled products, including anti-depressants, anti-inflammatory drugs, antibiotics, and antimicrobial agents, which are utilized by human health care, cosmetic reasons, and livestock productivity (Sharma et al. 2020). For instance, triclosan (TCS) is one such common PPCP.

TCS ( $C_{12}H_7Cl_3O_2$ ) is a broad-spectrum synthetic antimicrobial agent, under the category of emerging contaminants, widely used in PPCPs, soaps, toothpaste, shower gels, body lotions, deodorants, cleansers, and hand sanitizers (Jagini et al., 2019). Liquid hand soaps generally contain TCS in concentrations of 0.1% to 0.45% (% w/v) (Harrow et al., 2011). Due to its extensive use as a prophylactic, the high concentrations it is employed, and its inherent stability, TCS accumulates to high levels in the environment (Orhon et al., 2017). Moreover, TCS reacts with free chlorine and can form chloroform, categorized as a carcinogen (Lépesová et al., 2019). Besides, several studies have confirmed that conventional wastewater treatment systems cannot eliminate TCS complexes due to their least decomposability (Pycke et al., 2010). Consequently, it is necessary to obtain an effective process that allows its degradation to non-toxic substances.

In addition, TCS was usually occurring at the level of ng/L to  $\mu$ g/L concentrations in the atmosphere atmospheres. Hence, the proficient score of the conventional treatment function is adequate to remove the pollution content (Luo et al., 2014). Owed to the shape of the chemical, TCS can persevere in the atmosphere for several years. For example, a high conflict of phenol has been exhibited in natural degradation. Even though the old treatment technologies of GW have been diminished pathogens, nutrients, BOD and COD are not related to XOCs but these compounds are

active in the biological condition (Grčić et al., 2015). Because of the potential impact, XOCs have triggered specific properties on the environment and collapsed the wildlife environmentally, known as bioaccumulation (Yu et al., 2011).

#### **2.2.4 Biological Parameter**

Microorganisms like protozoa, bacteria, helminths are injected into GW because of the interaction of humans. Pathogenic such as *Campylobacter*, *Salmonella* has been found GW due to improper handling of food in the kitchen and treatment food adulteration (Maimon *et al.*, 2014; Ottoson and Stenstrom, 2003). It contaminates fecal frequently inside GW, linked to poor personal hygiene and the dumping of laundered diapers in GW. In a microbiological monitoring study conducted in Melbourne, *Escherichia coli* and the enteric virus was discovered within GW, with most water coming from the source of laundry (O'Toole *et al.*, 2012). During the investigation, viruses in enteric were found 18 %, enterovirus in 7 %, and *E. coli* in 11 % (Jeong *et al.*, 2018; Eriksson *et al.*, 2002), Ottoson and Stenstrom (2003) found a substantial number of excreta infections connected with GW in their studies.

### **2.3 REUSE AND RECYCLABLE LIMITS**

For reuse, GW reclaimed must meet four criteria: safety of sanitary, aesthetics, tolerance of environmental, economic viability (Nolde, 2000). Varied reuse needs a variety of water quality criteria, which necessitates various treatments ranging from simple to complex. Monitoring of GW standards differs per country. Recycling of GW is only mentioned in a few reuse standards (Li *et al.*, 2009). In reality, most nations hold recovered wastewater of municipal to the same standards as GW. Some countries, like the UK, Jordan, Germany, Australia, had set specialized reuse of GW requirements (Table 2.2). WHO rules for GW reuse were developed using the framework of Stockholm, which combines assessment management of risk to compact water-borne illnesses (Bartram *et al.*, 2001).

Furthermore, the recommendations no longer focus on the quality of water criteria, but rather on the actual health defense events to meet health depend on goals. Then describing treating water as the only way of reusing GW, the WHO recommendations refer to it as one of several alternatives for reducing the risk associated with GW. According to WHO standards, health protection methods such as crop limitation, in-between application of water, waiting periods and without resorting



to advanced treatment, sanitary handling of food, the technique to preparing food can reduce dangers connected to GW. However, implementing these principles has been problematic (Sinclair, 2010) since it requires complete understanding and collaboration from all stakeholders to assess and manage risks. As a result, WHO created procedures for the planning of sanitary safety in 2015 and published them in the booklet, addressing safe use, disposal of wastewater (WHO, 2015).

For reuse, the GW recovered must meet four criteria: security, appearances, tolerance for the environment, and feasibility of economic (Nolde, 1999). The absence of good quality of directive of water or norms, on the extra hand, has impeded the reuse of GW (Lazarova *et al.*, 2003). Many reuse applications need varied quality water criteria, which necessitates various treatments ranging from simple to complex. There has never been a globally enforceable worldwide reuse of water guidelines to manage recovered wastewater quality. National reuse of water rules differs from state to state in several circumstances (Rana *et al.*, 2014). There is a lot of diversity in these rules, recognizable and limited parameters (Braun *et al.*, 2019). Discrepancies in need, applications and societal variables are reflected in the differences discovered between stated criteria of reuse (Pidou, 2006). There are very few criteria of reuse designed explicitly for the recycling of GW. Reuse of regulating GW and their standards are frequently created by local governments, emphasizing the implication of health and the environment. WHO published reuse of guideline of GW for limited and non-restricted irrigation of agriculture in 2006. Microbiology standards are exclusively mentioned in the approach, and no additional physical or chemical factors are considered (Sami, 2019). The Amount of Helminth eggs and *E. coli* must be lesser than 1/1 l, 105/100 ml, for limited irrigation (WHO, 2006). The number of Helminth and *E. coli* eggs is less than 1/1 l, 103/100 ml, for unrestricted irrigation (WHO, 2006). The reuse of GW guidelines has been produced by the Housing and building office in Berliner Senate of Germany, including metrics like BOD<sub>7</sub>, oxygen content, coliform of the total, coliform of faecal, and *pseudomonas aeruginosa* (Nolde, 1999). Every country has developed its reuse of water criteria based on its demands (Pidou *et al.*, 2007).

Some reuse of GW requirements had been modified from recovered wastewater of domestic regulations. GW reuse rules are available for nations such as Australia and the US, where the Recycling of GW is a well-established industry (Jefferson *et al.*, 2000). European bathing system irrigates utilized as recommendations in some

countries, such as the United Kingdom and Germany. Each nation had its level of strictness; for example, the Environmental agency for protection in the US, water quality required for irrigation is far greater than Jordan's / European bathing system quality of water criteria (Bart, 2018).

## 2.4 GW FLOW RATE ESTIMATION

There is overall stress on the economy when it comes to freshwater scarcity. As a result of human obstruction, inadequate freshwater supply, and corrupt administration, toxins accumulate in the water.

GW contributes nearly 70% of all household wastewater, which is far cleaner than black water (with significant contaminants) and free of heavy metals and microorganisms (Pandey et al. 2014). So therefore, it permits optimal pollutant concentration to make nutrients while recycling and reusing pollutants. Through green management technologies such as the Short Rotation Intensive Cultural Plantation System (SRICPS), the long-term usage of wastewater as a resource may be further mitigated, and the available nutrients can be harnessed.

To assess wastewater generation and pollutant load, measurement of created wastewater and load is an essential precondition. Many nonpoint sources of pollution produce wastewater, and thus make GW characteristics and discharge flow rate dependent on each other (Piao 2010; Wagener 2010; Koutsouris et al. 2010; Bring and Destouni 2011). The constant variation in wastewater generation time series from minute to minute, day to day, and monthly is a significant challenge to implementing any wastewater treatment plan (Henze et al. 2000). Therefore, the current situation calls for high-quality information on wastewater created daily, hourly, and seasonal. More frequent monitoring of wastewater flow and pollutant load is required for this. Meanwhile, a mathematical formula also computes the quantification of the water flow rate. Compared with other methods, this cone formula is very effective for all water resource applications. Moreover, possible fitness is obtained from the following Eqn. (2.1).

$$Q = aH^b \quad (2.1)$$

**Table 2.2** Regulations of GW Reuse (Albalawneh and Chang 2015; Boano et al. 2020; Muhlemann 2005; Manna 2018; Abu-Ghunmi et al. 2011)

Parameter	CPCB, India	US EPA	India NGT	WHO
TSS	100	30	20	-
pH	5.5-9	6-9	5.5-9	6.5-8.5
BOD	30	10	10	-
COD	-	-	50	-
Turbidity, NTU	2	2	-	5
TN	10	-	10	50
TP	1	-	1	-

*\*Except pH and Turbidity, all other parameters are expressed in mg/l*

Where GW flow rate is represented as Q, H is denoted as head completed wire. Moreover, the cone formula has two coefficients, a and b, where a is denoted as coefficients of regression and b is the water flow variable in Eqn. (2.2). The ranges are calculated as per the NPDES.

$$Q = 1.34H^{2.48} \quad (2.2)$$

Here, let us assume the values a and b where a=1.34 and b=2.48 respectively also defined the overhead height due to the observations. The range for H is 0.07 to 0.13m, which is explored by specific authoring (Robert 1986).

GW is discharged due to organic pollutant loading; GW is primarily determined by pollutant strength and flow rate. Consequently, the organic pollutant load of the GW is measured frequently, that is, daily measured, hourly measured, annually measured, and finally seasonal measured. Moreover, these measurements are mainly based on the organic pollutant load. The design mitigation is used to analyze the proper investigation of the GW organic pollutant load. Furthermore, the EPA formula in Eqn. (2.3) is used to measure the organic pollutant load.

$$OL (kg/day) = \frac{Q \left( \frac{m^3}{day} \times BOD_5 (mg/l) \right)}{1000} \quad (2.3)$$

Where OL is represented as organic load (kg/day) of the given GW, Q is denoted as regular flow (m<sup>3</sup>/day), BOD<sub>5</sub> is defined as BOD reserved at the 5 days (mg/l), and also kilogram per day is converted into gram per day that is 1000 times.

## **2.5 TREATMENT OPTIONS**

In the GWT, various methods have been used, mainly based on the loading of pollution, formation, the procedure of treatment, and its characteristics. The appropriate forms are chosen by various factors such as organic contents, amount of GW, accepted level of standard, and the last applications. The treatment process is enclosed with the different levels: primary, preliminary, and secondary. Nevertheless, this is not a detailed model for the GWT approach worldwide, but certain nations have utilized this model, like America and Australian countries. The design of this model depends upon the relationship of various factors like the quantity and quality of GW resources, the condition of the field, and the replaced recycled item (Edwin *et al.*, 2014).

GWT is considered into various levels, preliminary, primary, secondary, tertiary, and advanced treatments. Preliminary treatment involves removing sticks, grit, oil, grease, tar, cloth pieces, etc., that may damage equipment to create operational problems during treatment. Primary treatment does focus on settleable, suspended solids removal, secondary treatment includes biodegradable organic matter and nutrients removal, and tertiary treatment includes nutrients and disinfection removal. Advanced treatment can handle the removal of dissolved and suspended materials remaining after secondary treatments required for reuse application (Tchobanoglous *et al.*, 2003).

According to the cost of the treatment ecological and environmental considerations, treatment techniques can be classified as physicochemical and biological methods for removing contaminants. Physicochemical processes include screening, grit removal, sedimentation, ion exchange, filtration, adsorption, reverse osmosis, and ultrafiltration. Biological methods are broadly classified as aerobic and anaerobic. Aerobic methods are further divided as suspended growth (viz. activated sludge process, aerated lagoon, waste stabilization pond, etc.) and attached growth (viz. trickling filter, rotating biological contactor, constructed wetlands, etc.). Different

treatment technologies are adaptable for GW, as shown in Figure 2.2. Anaerobic treatments comprise contact beds, up-flow anaerobic sludge blanket reactors, sludge digesters, and anaerobic ponds (Ghaitidak and Yadav, 2013). On the other hand, commercial GWT systems can remove pollutants, bacteria, pharmaceuticals, and even viruses from GW.

### **2.5.1 Physical treatment**

Physical treatment comprises screening, sedimentation, floatation, and filtration, respectively.

#### ***Filtration***

Filtration is the process that removes the particulate, turbidity, and non-settleable type colloidal organic matter. The substance that is to pass through the filter media must be fluid. Methods of filtration vary depending on the location of the targeted material, i.e., whether it is dissolved in the fluid phase or suspended as a solid. Media filters are filters containing loose granular media such as sand or grit. Some filters have more than one type of media. The backwash is the process of removing the injected particles in the pores of the filter layer. Filters comprise media with different materials, uniformity coefficients ( $C_u$ ), and effective grain sizes ( $D_{10}$ ), as shown in Table 2.3. Filtration studies on the shower and washing machine GW from the household were conducted by Finley *et al.* (2009). Primary settled with an HRT of  $\pm 8$  h was treated by coarse filtration followed by slow sand filtration with an HRT of  $\pm 24$  h. Influent TS concentration 313–543 mg/L was changed to 330–633 mg/L. COD removal observed was from 278–435 to 161–348 mg/L. Ammonia–N was reduced from 1.2–6.2 to 4.1–5.1 mg/L. Reduction of total phosphorous (TP) was not observed.

Water drained freely from the upper to the lower reservoir container. A 2-cm thick layer of pebbles (crushed limestone and dolomite: average diameter 2.5 cm) was placed over the drain holes, followed by a middle layer containing 12 cm of plastic filter media with a high surface area ( $800 \text{ m}^2/\text{m}^3$ ) and large void volume. Each treatment container was topped with a 4-cm thick layer of peat. Anionic surfactant concentration 12.3 mg/L was reduced to 0.2 mg/L (removal 98.37 %). Suspended solids were removed by 93.48 % with an effluent concentration of 3 mg/L. Influent ammonia–

N, nitrite, nitrate and total P was reduced from 1.2, 1.3, 3.5 and 1.9 mg/L to 1.0, 0.04, 1.8 and 0.5 mg/L (removal 16.67, 96.92, 48.57 and 73.68 %), respectively (Gross *et al.* 2007).

Water drained freely from the upper to the lower reservoir container. A 2-cm thick layer of pebbles (crushed limestone and dolomite: average diameter 2.5 cm) was placed over the drain holes, followed by a middle layer containing 12 cm of plastic filter media with a high surface area ( $800 \text{ m}^2/\text{m}^3$ ) and large void volume. Each treatment container was topped with a 4-cm thick layer of peat. Anionic surfactant concentration 12.3 mg/L was reduced to 0.2 mg/L (removal 98.37 %). Suspended solids were removed by 93.48 % with an effluent concentration of 3 mg/L. Influent ammonia-N, nitrite, nitrate and total P was reduced from 1.2, 1.3, 3.5 and 1.9 mg/L to 1.0, 0.04, 1.8 and 0.5 mg/L (removal 16.67, 96.92, 48.57 and 73.68 %), respectively (Gross *et al.* 2007).

The introduction of the Mulch tower (MT) system for GWT in South Africa, assembled using mulch, coarse sand, and fine and coarse gravel, was done by Susilawati (2013). It consisted of a plastic column of the height of 650 mm and an overall diameter of 150 mm. A stainless-steel sieve with a 2-mm mesh was placed on the MT to remove large food particulates, plastics, and other large debris. Below this sieve, a 200-mm thick layer of mulch was placed with particle diameters from 10 to 35 mm. TSS removal was reported as 62 %. Reduction in ammonia nitrogen, nitrate, and  $\text{PO}_4\text{-P}$  was reported as 50, 39, and 33 %, respectively.

The COD/BOD ratio for GW ranged from 2:1 to 467:1 for the influent and that of 2:1 to 598:1 for effluent. This could be an indication influent BOD were retained in the MT, while at the same time readily biodegradable components of dead biofilm biomass, probably, released into the MT effluent, and COD removal was observed as 37 %. In addition, no systems, except bark and charcoal filters, could meet the BOD standards for reuse. Reduction rates of total P were high in the bark, charcoal, and sand filters (range 78–97 %). Evaluation of sodium, sodium adsorption rate, chloride, boron, and trace metal concentrations of the effluent water from these filters were not tackled in this study. A filtration study by Parjane and Sane (2011) used only bath and washbasin GW and did not investigate the reuse criteria parameters like Biological oxygen demand (BOD), turbidity, *E. coli*, etc. Hence, there is a need for further

investigations into filtration. In addition, other sources of GW like laundry, kitchen, and combined GW need research.

**Table 2.3** Various operating parameters for filtration

<b>Parameter</b>	<b>(Dalahmeh <i>et al.</i> 2012)</b>	<b>(Arias <i>et al.</i> 2001)</b>	<b>(Healy and Rodgers 2007)</b>	<b>EPA guidelines</b>
Filter materials	Pine bark, Activated charcoal, Polyurethane foam, and Sand	Gravel, Crushed lava rock, Silica Sand and Granular activated carbon (GAC 830W)	Stratified sand filter (Sand)	Single-layer filter (Sand)
Particle effective size ( $D_{10}$ ), mm	1.4	0.2-1.4	0.45	1- 1.5
Uniformity coefficient, $C_u$	2.2	1.7-4	3	< 4
Hydraulic loading rate (HLR) $m^3 m^{-2}day^{-1}$	0.032	0.2-0.4	0.0067	0.12-0.2
Organic loading rate, $kg m^{-2} day^{-1}$	0.014	0.07-0.496	0.023	0.034

### 2.5.2 Chemical Treatment

Chemical processes were reported for GW treatment and reused. The chemical processes applied to GWs include precipitation, coagulation, adsorption, and Ion-exchange processes. Coagulation and flocculation are used for the removal of solids. Negative electric charges on the finely dispersed particles (colloids) in the wastewater repel them from each other. Coagulation and rapid mixing can neutralize the colloid's negative charge (called zeta potential) by shear forces during rapid mixing. Colloidal particles can combine and form larger flocs. Flocculation, the action of polymers, enhances the floc formation process, which increases the floc size and its mass.

Flocculation is a process of bridging flocs by the activity of polymers. A slow mixing is required for forming a contact between flocs and agglomerates them further to form larger flocs. The larger the particle, the faster it will settle (Tchobanoglous *et al.*, 2003).

Pidou *et al.* (2008) performed coagulation-flocculation studies using jar test shower GW. The coagulant, either ferric sulfate (solution of  $\text{FeSO}_4$  (13 %), or aluminum sulfate (solution of  $\text{Al}_2(\text{SO}_4)_3 \cdot 14\text{H}_2\text{O}$  (48 %), was dosed in the jar and the pH adjusted to the chosen value (4.5, 6, and 7). The sample was flocculated for 15 min at 30 rpm and allowed to settle for an additional 15 min. The turbidity of shower GW was reduced from 46.6 to 4.28 and 5.2 NTU (removing 90.82 and 88.84 %) using alum and ferric sulfate coagulant. Comparison of the required doses showed that more ferric was required by mass to achieve a set level of removal. Conversion to molar concentrations indicates the minimum necessary amount was 0.79 mM for ferric and 0.89 mM for alum, indicating that proportionally more alum was required per unit of treatment. BOD of 205 mg/L for shower GW was reduced to 23 and 30 mg/L (removal by 88.28 and 85.37 %) using alum and ferric chloride coagulants, respectively. COD was reduced from 791 to 287 and 288 mg/L (63.72 and 63.59 %) using alum and ferric chloride coagulant, respectively. The concentration of Nitrate 6.7, TN 18, and  $\text{PO}_4\text{-P}$  1.66 mg/L was reduced to 5.7, 15.7, and 0.09 (removal 14.93, 12.78 and 94.58%), respectively, by using alum as a coagulant. The corresponding nitrate, TN, and  $\text{PO}_4\text{-P}$  removal were 8.96, 0.56, and 96.39 %, respectively, using ferric sulphate coagulant. Total coliforms were reduced from 56,500 to <1 and E. coli from 6,490 to <1 using alum coagulant, and similar removal was also observed by ferric sulfate coagulant.

Rock alum (aluminum sulfate) is used in a five-barrel GW treatment system consisting of five recycled polyethylene in flocculation (PE) (Kariuki *et al.*, 2011). pH decreased from 9.34 to 6.4 with an 8 h settling time. It was further reduced to 5.92 and 6.5 when passed through a filter (pore size 0.45 mm) and disinfected with sodium hypochlorite (NaOCl) and lemon juice, respectively. The pH of laundry GW decreased from 6.79 to 5.88 after flocculation and further changed to 6.3 and 6.5 when disinfected with NaOCl and lemon juice. pH was slightly acidic for both kitchen and laundry GW after flocculation and disinfection. EC of kitchen GW increased from 195 to 196.7



mS/m, and laundry GW increased from 32.6 to 49.5 mS/m using rock alum (aluminum sulfate) coagulant. There was no reduction in TC for the kitchen and laundry GW.

As a whole, Coagulation/ flocculation systems achieved BOD removal of 85 to 89 %. COD removal around 64 %, total N removal up to 13 %, TC removal >99 % and E. coli removal >99 %. Coagulation/flocculation system investigated for shower GW (Pidou *et al.* 2008) achieved good organics and coliforms removal levels, but found poor in the removal of total N. Further, this system provided better results in acidic pH, which attracts attention to readjust the pH after treatment. Adjusting pH before and after treatment would increase the cost of the system. Flocculation system using aluminum sulfate (Kariuki *et al.* 2011) did not affect pH, salinity, and electrical conductivity in both kitchen and laundry GW. Flocculated GW could not meet any of the reuse standards except pH. However, further disinfection with NaOCl could remove complete FC from laundry GW. Eight-hour hydraulic retention time (HRT) for flocculation/settling is not practically feasible. Hence, there is a need to investigate the performance of various coagulants in GW treatment at lower HRTs (preferably, 2 to 3 h). Coagulation/flocculation systems were not investigated with variation in intensity and duration of mixing at the rapid mix stage, velocity gradients applied during flocculation stage, flocculator retention time, type of stirring device used and flocculator geometry.

### **2.5.3 Biological Treatment**

In the biological treatment of GW, the removal and stabilization of dissolved and particulate organic materials in GW is accomplished by a variety of microorganisms. As a result, the biological treatment system is suitable for removing organic matter and nutrients.

#### **2.5.3.1 Constructed wetlands:**

This system consists of swamp plants, soils, and associated microorganisms, which remove contaminants from wastewater and provide a natural environment. It can remove impurities from wastewater, such as solids, metal, and other toxic organic compounds. Removal of pollutants by physical, chemical, and biological processes depends on surface loading rate and electron acceptor availability. The selected media

is generally a substrate rich in iron, calcium, and aluminum. For Subsurface horizontal flow constructed wetlands (SSHF CW), soil or gravel is recommended (Zhang *et al.* 2012). In Subsurface vertical flow constructed wetlands (SSVF CW), an active sand layer with a depth of 1.0 m (effective grain size,  $D_{10} = 0.25\text{--}1.2$  mm, the coefficient of uniformity,  $C_u < 3.5$ ) is recommended (Arias *et al.* 2001).

The GW from recycled vertical flow constructed wetland (RVFCW) had the following characteristics such as bed depth (0.5 m) and the recycling rate (390 L/h). A change in pH was observed from 6.3–7.0 to 7.0–8.0 and electrical conductivity raised from 120 to 130 mS/m. This experiment reduced the influent TSS of 158 mg/L to 3 mg/L (removal by 98.1 %). Similarly, influent BOD 466 mg/L and COD 839 mg/L was reduced to 0.7 and 157 mg/L (removal 99.85 and 81.29 %), respectively. Influent anionic surfactant concentration of 7.9 mg/L was reduced to 0.6 mg/L (removal by 92.41 %). Removal of nitrite, TN and TP from 0.3, 34.3 and 22.8 mg/L to 0.2, 10.8 and 6.6 mg/L (removal 33.33, 68.51 and 71.05 %), respectively was also observed. In this study, no removal was observed in the ammonia N and nitrate (Gross *et al.* 2007). Travis *et al.* (2010) studied artificial GW using RVFCW. GW comprises water, laundry powder, bar soap, pulverized vegetable oil, and raw dining hall/kitchen effluent. The set-up comprises two 500-L capacity stacked containers. Anionic surfactants concentration of 10 mg/L was removed by 94 %, and oil and grease concentration of 22 mg/L was removed by 95.45 %. Both bacterial and plant utilization of nitrate-nitrogen ( $\text{NO}_3\text{-N}$ ) in the RVFCW and the breakdown of organic nitrogen and subsequent release of ammonia into the air may account for the loss of N through the system. However, there was no removal in TP. Much of the removal of P in CWs is the result of absorption to the bed media. Moreover, the presence of organic matter (e.g., oils and surfactants) may inhibit the P adsorption through blockage of exchange sites. The relatively small size of the wetland bed of the RVFCW also reduces its ability to remove P from the GW stream. These increases might be due to loss of water from the system through evapotranspiration, resulting in an increase in the dissolved mineral content of the treated GW.

### **2.5.3.2 Rotating biological contactor**

Attached-growth biological process consists of one or more basins in which large, closely spaced circular disks mounted on horizontal shafts rotate slowly over wastewater. Disks are made up of high-density polystyrene, or polyvinyl chloride (PVC) is partially submerged in the wastewater so that a bacterial slime layer forms on their wet surfaces. As the disks rotate, the bacteria are exposed alternately to wastewater and to air from which they adsorb organic matter and oxygen. The rotary movement also allows excess bacteria to be removed from the surfaces of the disks and maintains a suspension of sloughed biological solids. A final clarifier is needed to remove sloughed solids. Organic matter is degraded, employing mechanisms similar to those operating in the trickling filters process. Generally, partially submerged RBCs are used for carbonaceous BOD removal, combined carbon oxidation, and nitrification. Completely submerged RBCs are also used for de-nitrification. Typically, treatment involves separation; degradation reduces solids, organic matter, nutrients, and pathogenic organisms improve after treatment. Organic matter decomposes and gets oxidized in the presence of oxygen by aerobic bacteria. When the free oxygen reduces in quantity, few bacteria continue the process by extracting oxygen from nitrates. When nitrates decrease, sulfates continue to supply oxygen to the bacteria during the oxidative process. The reduced sulfates give rise to hydrogen sulfide gas. The used-up sulfate provides a way for the anaerobic processes in which biogas consisting mainly of methane and carbon dioxide is produced (Revitt *et al.*, 2012).

A single-stage RBC was used to study GW by Pathan *et al.* (2011). The pH value of the untreated GW changed from  $6.23 \pm 0.05$  to  $6.48 \pm 0.08$ ,  $6.65 \pm 0.15$  and  $6.75 \pm 0.16$  mg/L when treated by using RBC at 0.5-, 1- and 1.5-h HRTs. The pH value increases with the increase of HRTs. The increase of pH value with the increase of HRTs indicates that volatile fatty acids oxidized due to increased aerobic conditions in the tank. No significant change in TDS removal was found. The TDS contents of the untreated and treated GW at 0.5, 1, and 1.5-h HRTs were found in the range of  $101.50 \pm 21$ ,  $102.50 \pm 21.61$ ,  $102 \pm 23$ , and  $103 \pm 24$  mg/L, respectively. The influent TSS of 154.63 was reduced to 140.75, 136.75 and 137.5 mg/L (removal 8.98, 11.56 and 11.08 %) at 0.5-, 1- and 1.5-h HRTs, respectively. The removal rate was not

increased with increased HRTs due to biomass growth during the aerobic treatment. The influent BOD of 55.61 mg/L was reduced to 40.43, 32.59 and 26.46 mg/L (removal 27.30, 41.40 and 52.42 %) at 0.5-, 1- and 1.5-h HRTs, respectively. An influent COD 146.05 mg/L was reduced to 114.68, 73.13 and 57.9 mg/L (removal 21.48, 49.93 and 60.36 %) at 0.5-, 1- and 1.5-h HRTs, respectively.

### **2.5.3.3 Membrane bioreactor**

A membrane bioreactor is a bioreactor that combines biological treatment (only aeration) with microfiltration (MF) or ultrafiltration (UF) systems. The membrane is used instead of a clarifier to separate the solids from the liquid. The membrane step provides a positive means of liquid, solid separation after biological treatment by preventing any loss of biological solids in the effluent and allowing a higher concentration of biomass to be held in the reactor (Ghaitidak and Yadav 2013b).

A laboratory-scale MBR for the treatment of shower GW had a 3-L capacity made up of a UF membrane. Turbidity was reduced from 29 to 0.5 NTU (removal 98.28 %), and the effluent was completely free from odors. The membrane retained the suspended and colloidal matter, and dissolved oxygen concentration (near saturation) in permeate indicated that bacterial activity in permeate was very low. Ammonia nitrogen, TN, and TP were reduced from 11.8, 15.2, 1, and 1.6 mg/L to 3.3, 5.7, and 1.3 mg/L in the effluent (removal 72.03, 62.50, and 18.75 %), respectively. Remarkably, despite the oxygen saturation and the high HRT, no complete nitrification was achieved in the MBR. Anionic surfactant concentration was reduced to 0.13 (removal 96.66 %). MBR reduced the COD load from 109 to 15 mg/L (removal 86.24 %). BOD removal was from 59 to 4 mg/L (removal 93.22 %). COD/BOD ratio in permeate reached values up to 25, indicating that the BOD was almost completely removed. During the reported period, the fraction of ammonium to total Kjeldahl nitrogen (TKN) in the influent increased from 44 to around 80 % and even reached 100 % on day 122. This is explained by the rising temperature, which allowed a faster degradation of organic nitrogen in the conveying pipe system (Merz *et al.*, 2007). Jong *et al.* (2010) treated GW using an anaerobic–anoxic-oxic (A2O) MBR. A submerged MF membrane of pore size 0.45  $\mu\text{m}$  was used in the MBR, and the volumes of the A2O reactors were 2, 2.5, and 8 L, respectively. Turbidity reduced from 2,131 to 1.63 NTU (removal 99.92 %). TSS were

reduced from 72.5–4,250 to 0–4.3 mg/L (removal 98.2–100 %). This high removal was obtained because the membrane achieved almost complete solid-liquid separation. COD was reduced from 807.7 to 6.57 mg/L (removal 99.19 %). The removal efficiency maintained to a satisfactory level due to the membrane that maintained high MLSS density (6,500–7,000 mg/L). A BOD of 23.5–392.4 mg/L was reduced to 7.8 mg/L (removal 93.7–99.6 %).

An overall MBR systems achieved removal of turbidity 98–99.9 %, TSS around 100 %, BOD 93–97 %, COD 86–99 %, ammonia N 6–72 %, total N 52–63 %, PO<sub>4</sub>-P 10–40 %, total P 19 % and FC 99.9 %. These systems could meet most of the standards for reuse about pH, turbidity, BOD (except in A2O reactor), COD, TSS, and NH<sub>4</sub><sup>+</sup>-N. Effluent FC was reported by (Merz *et al.* 2007). The nominal pore size of the membrane used was 0.1 µm and less, and it was found highly efficient in removing faecal coliforms.

**2.5.3.4 Sequencing batch reactor:** Special form of activated sludge process (ASP) in which all of the treatment processes take place in the single reactor tank (and separate clarifiers are not required). This process treats the wastewater in batch mode, and each batch is sequenced through a series of treatment stages. SBR performs equalization, biological treatment, and secondary clarification in a single tank using a time-controlled sequence. It is one of the technologies for removing conventional parameters in small communities. It offers great flexibility of operation for effective nutrient removal. The operation of SBR consists of five basic steps in sequence: fill, react, settle, draw, and idle, respectively. Lamine *et al.* (2007) studied the treatment of shower using SBR with reactor dimensions of diameter 19 cm, total volume 11 L, and working volume 5 L. A mechanical agitation (30 rpm) operated for complete mixing with airflow (5 L/min) through an air stone placed at the bottom of the reactor. SBR operations were divided into five phases: filling, reaction, settling, and effluent discharge. COD reduced from 102 to 12 and 20 mg/L (removal 88.24 and 80.29 %) at HRTs 0.6 and 2.5 days, respectively. BOD was reduced from 97 to 7 mg/L (removing 92.78 %) at both HRTs 0.6 and 2.5 days. The hydraulic retention time (HRT) variations affected the nitrification rate. Influent NH<sub>4</sub><sup>+</sup>-N concentration 6.7 mg/L was reduced to 6.2 and 0.3 mg/L at HRT of 0.6 and 2.5 days, respectively.

An investigation of dark GW using SBR in Malaysia was done, and findings are as follows: Turbidity of nutrient-deficient and nutrient-spiked dark GW with a COD/N/P ratio of 100:2.5:0.5; 100:3.5:0.75 and 100:5:1 resulted in outlet turbidity of 11, 9, 6, and 5 NTU, respectively, at 36-h HRT. Influent COD and BOD were 630 and 370 mg/L, respectively. The aerobic oxidation of nutrient-deficient and nutrient-spiked dark GW with a COD/N/P ratio of 100:2.5:0.5; 100:3.5:0.75 and 100:5:1, resulted in outlet COD values of 64, 35, 15 and 12 mg/L (removal of 89.90, 94.4, 97.6 and 98.1 %). The corresponding BOD value of 37, 22, 10 and 8 mg/L (removal 90, 94.1, 97.3 and 97.8 %) at 36-h HRT. In the case of nutrient-deficient and nutrient-spiked GW at a COD/N/P ratio of 100:2.5:0.5, the residual organic content in the treated GW was higher than the Malaysian water quality standard for agricultural activities (Krishnana *et al.* 2011). Similarly, studies on light GW consisted of bath products, eight kinds of shampoos, and three kinds of soaps. The research was carried out in thirteen lab-scale SBRs, which degraded 11 kinds of GW, a blank, and a reference compound, respectively. The working volumes of the SBRs were 2 L. Aeration pumps aerated the SBRs with a flow rate of 1.2 L/min. Biodegradability of eight kinds of shampoos and three kinds of soaps through 13 SBRs was reported. BOD/COD of all shampoos was less than 0.2. Their degradation reached more than 95 % in the experiments after 28 days. It demonstrated that the method BOD/COD for evaluation biodegradability had certain deficiencies (Erlangung and Weingärtner 2013).

Effluent from SBR treatment (Lamine *et al.* 2007) of shower GW meets the  $\text{NH}_4^+-\text{N}$ , BOD, and COD standards of wastewater reuse. HRT of the system (0.6 to 2.5 days) was relatively high. BOD removal varied from 80 to 98 %, and a similar range of COD removal was observed. BOD and COD of nutrient-spiked GW effluent from the SBR system by Krishnana *et al.* (2011) complied with the reuse standards. The HRT required (36 h) for achieving this efficiency was very high, which is not practically feasible.

#### **2.5.3.5 Upflow anaerobic sludge blanket reactor**

This is a high-rate anaerobic system preferred for several types of wastewaters. The UASB reactor can retain a high concentration of active, suspended biomass with simple and low-cost means. Moreover, the formation of granular sludge, which has a high

methanogenic activity and is better settleable than flocculent sludge, improves the maximum loading rate of the UASB system. Temmink *et al.* (2010) studied the treatment of GW using UASB with volumes 3.6 L and 5-L capacity, respectively. Removal of total N and total P was observed as  $15 \pm 33$  and  $11 \pm 28$  % leaving  $34 \pm 17$  and  $5.3 \pm 1.5$  mg/L in the effluent, respectively, and no  $\text{NH}_4^+$ -N removal was observed.

Anaerobic treatment of GW has been investigated using the UASB and a conventional anaerobic reactor. While the methanogenic activity was considered sufficient to perform the biodegradation process (Elmitwalli & Otterpohl 2007; Abu Ghunmi et al. 2010), anaerobic treatment can be slow and not very efficient at removing pollutants. Only 40% COD removal can be achieved at an HRT of 12–24 h with a UASB compared to 90% COD removal using an aerobic fed-batch reactor of similar volumetric size (3.6 L) (Hernandez Leal et al. 2007). Meanwhile, the removal of TN and TP was 21.7–29.8 and 15.2–20.6% respectively for the UASB and 17 and 10% respectively for the conventional anaerobic unit (Elmitwalli & Otterpohl 2007). The occurrence of a high concentration of surfactants can profoundly damage methane production during anaerobic treatment (Abu Ghunmi et al. 2010). However, the UASB is much more efficient at removing suspended COD rather than colloidal or dissolved COD (Hernandez Leal et al. 2010b), which makes it attractive along with its low cost and simplicity.

Nevertheless, good treatment can be achieved if anaerobic treatment is used pre-treatment or post-treatment combined with aerobic treatment (Abu Ghunmi et al. 2010); however, proper insulation and effluent disinfection are required. On the other hand, it has been argued that the limited energy gain from such a combined system renders the option unfeasible (Hernandez Leal et al. 2010b). Physical systems include filtration and sedimentation. Filtration is usually used as a pre-treatment stage before biological or chemical treatment or post-treatment before disinfection. The combinations of different treatment units and their performance have been represented in Table 2.4.

**Table 2.4** Comparison of organic matter and nutrient removal efficiencies of integrated or combined biological treatment systems for GW

Reference	Treatment Technology	Organic loading rate		HRT (h)	Removal efficiency (%)				
		Kg COD /m <sup>3</sup> *day	Kg BOD /m <sup>3</sup> *day		COD%	BOD%	NH <sub>4</sub> <sup>+</sup> -N%	TN%	TP%
(Priyanka <i>et al.</i> 2020)	SBR	-	-	24	96.2	97.38	81.68	-	72
(Abdel-Shafy <i>et al.</i> 2019)	Anaerobic/aerobic	1.93	1.1	24	98.4	98.3	95.3	94	90.5
(Tombola <i>et al.</i> 2019)	Sequencing batch biofilm reactor	-	-	24	86.5	-	98.4	71.4	-
(Eslami <i>et al.</i> 2017)	Integrated fixed-film activated sludge (IFAS)	0.11-1.3	-	8.1	93	85	-	90	87
(Saidi <i>et al.</i> 2017)	Multistage moving bed biofilm reactor	3.4	2.8	28.8-38.4	94.5	99.4	99.7	63	14
(Abdel-Shafy <i>et al.</i> 2015)	Anaerobic (UASB)/aerobic (MBR)	1.93	1.1	7.5-10.5	97.8	97.4	94.5	-	89.8
(Merz <i>et al.</i> 2007)	Membrane bioreactor technology	0.09- 0.21	-	9-18	85	94	72	-	19
(Hernández Leal <i>et al.</i> 2007)	Aerobic treatment	0.15-8	-	12-24	90	-	-	-	-
(Friedler <i>et al.</i> 2005)	Screening, Rotating biological contractors, Chlorination	-	-	-	75	96	96	-	58



#### **2.5.4 Integrated treatment systems**

Kuan-yeow-show et al. (2020) presented treatment of a high strength inhibitory acrylic acid wastewater by integrated anaerobic-aerobic processes. A novel scheme integrating an anaerobic granular sludge blanket (GSB) reactor, aerobic carrier biofilm (CBR) reactor, and activated sludge reactor (ASR) was examined. The pilot-scale implementation indicated comparable performance with overall removal up to 99% of COD removal.

Maria-Prihandrijanti et al. (2021) aimed to develop a model of an integrated system comprised of sedimentation, coagulation, flocculation, Upflow Anaerobic Sludge Blanket (UASB), and Modified Ludzack-Ettinger (MLE). The integrated system was achieved to remove 99% of BOD, 99% of oil and grease, 98% of TSS, and 87.8 % of total nitrogen (TN).

Sunil P Lohani et al. (2020) studied a full-scale pilot plant for decentralized domestic wastewater treatment installed and tested at Kathmandu University (KU), Nepal. The plant consists of three main steps, i.e., a septic tank, an anaerobic reactor (UASB), and a sand filter. It shows high removal efficiencies of COD, TSS, and FC of about 93%, 87%, and 93%, respectively.

#### **2.6 POLISHING TREATMENT**

The non-chemical disinfection acts as the primary post-treatment technique in the final drinking water, e.g., ultraviolet treatment for complete spectrum inactivation of pathogens. There are many advantages over chemical disinfectants, such as no disinfection by-products formation, no chemical residual, non-corrosive, no community safety risks, effective against active microorganisms, and the possibility of changing adequate regulations. So, photocatalysis can accelerate the chemical reaction using electronically excited species generated by absorption of UV or visible photons. Photocatalysis is a quickly growing field of research with a high potential for a wide range of applications, including degradation of organic pollutants, disinfection of water and air, production of renewable fuels, and organic synthesis. Fujishima and Honda demonstrated photocatalytic water splitting using  $\text{TiO}_2$  electrodes for the first time in 1972 (Fujishima *et al.* 2000; Styliidi *et al.* 2003). Catalysts can be classified into

homogeneous and heterogeneous catalysts. Homogeneous catalysis is a class of catalysis in which the catalyst occupies the same phase as the reactants. The most commonly used catalysts are ozone and Photo-Fenton systems. Whereas, Heterogeneous catalysis denotes processes in which the phase of the catalyst and reactants differs, e.g., a reaction involving gas-phase molecules adsorbing on a solid metal surface and forming a product.

### **2.6.1 Heterogeneous photocatalyst**

Heterogeneous photocatalysis is a process in which two active phases of solid (is a catalyst, usually a semiconductor) and liquid are present. The molecular orbitals of semiconductors used as a photocatalyst are of specific interest, mainly the filled valence band. It is primarily an empty conduction band and the gap between them, commonly characterized as bandgap energy ( $E_g$ ). When the semiconductor is illuminated with light ( $h\nu$ ) of an energy greater than the bandgap, an electron is excited from the valence band to the conducting band creating an electronic vacancy (also known as a hole) in the valence band and an electron in the conduction band (Ibhadon and Fitzpatrick 2013).

TiO<sub>2</sub> is a transition metal oxide that can be extracted from various naturally occurring ores containing ilmenite, rutile, anatase, and leucosene. Crystals of TiO<sub>2</sub> exist in rutile, anatase, or brookite forms. TiO<sub>2</sub> is a large band semiconductor, with band gaps of 3.2, 3.02, and 2.96 eV for the anatase, rutile, and brookite forms. TiO<sub>2</sub> absorbs light (ultraviolet-A region of the EMG spectrum) with energy higher than or equal to the energy gap ( $E \geq 3$  eV), which separates the valence band and the conduction band, electrons in the valence band are excited to the conduction band leaving behind holes. Photocatalyst attached with the migrated excited carrier charger. It got trapped at certain places of the crystal lattice, subsequently reacting with electron donor OH<sup>•</sup> or electron acceptor O<sub>2</sub> molecular species adsorbed at the photocatalyst surface. The holes react with either adsorbed H<sub>2</sub>O or surface OH<sup>-</sup> groups to form HO<sup>•</sup> radicals. Excess electrons in the conduction band react with molecular oxygen to form superoxide ions, which further disproportionate to form more HO<sup>•</sup> radicals (Herrmann 1999; Teoh *et al.* 2012). The valence band of TiO<sub>2</sub> is composed of 2p orbitals of oxygen, hybridized with the 3d orbitals of titanium, while the conduction band is only the 3d orbitals of titanium.

### 2.6.2 Homogeneous photocatalysis

The Fenton reaction defined the reaction of ferrous iron with hydrogen peroxide. It was named after H. H. Fenton (1894), who discovered the oxidation of tartaric acid by a mixture of iron sulfate and hydrogen peroxide. Fenton's reagent ( $\text{H}_2\text{O}_2$  with Fe (II)/Fe (III) ions) in water produces  $\bullet\text{OH}$  radicals and peroxy ( $\text{HOO}\bullet/\text{O}\bullet$ ) radicals. Those species, specifically  $\bullet\text{OH}$ , are potent oxidants used in various applications. The effect of light irradiation shows  $\text{Fe}^{2+}$  formation by photo-reduction of the aqua-Fe (III) complexes leading to additional production of  $\bullet\text{OH}$  radicals. In the presence of light  $\text{H}_2\text{O}_2$  breaks into two  $\bullet\text{OH}$ , and  $\text{Fe}^{2+}$  can be regenerated from  $\text{Fe}^{3+}$  in the presence of  $\text{H}_2\text{O}_2$ . In excess of  $\text{H}_2\text{O}_2$ , the  $\text{HO}\bullet$  will react with  $\text{H}_2\text{O}_2$  and form superoxide. The main advantage of the photo-Fenton process is the light absorption up to 580 nm comprising 35 % of the solar spectrum (Acidic *et al.* 2004; Spuhler *et al.* 2010).

### 2.6.3 Doping of semiconductors

Doped semiconductors are semiconductors that comprise impurities, foreign atoms incorporated into the crystal structure of the semiconductor. The pollutants generate free carriers in semiconductors that release electrons to the conduction band. They are called donors or provide holes to the valence band, in which case they are called acceptors. Donor impurities donate their extra valence electrons to a semiconductor's conduction band, providing excess electrons to the intrinsic semiconductor. These electrons increase the electron carrier concentration of the semiconductor, making it n-type. Acceptor impurity atoms have fewer valence electrons than the atoms they replace in the intrinsic semiconductor lattice. They accept electrons from the semiconductor's valence band. This provides excess holes to the intrinsic semiconductor. Excess holes increase the hole carrier concentration of the semiconductor, creating a p-type semiconductor (Bustarret 2015; Dayeh *et al.* 2017; Ye *et al.* 2017). The band structure of n-type and p-type is shown in Figure 2.2.

Fernández-ibáñez *et al.* (2015) studied solar photocatalysis disinfection with the  $\text{TiO}_2$ - (Reduced Graphene Oxide) RGO composite and compared it with  $\text{TiO}_2$  alone. The rate of inactivation of *F. solani* spores was similar for both the  $\text{TiO}_2$ -RGO and  $\text{TiO}_2$ . Similar studies were reported on solar photocatalysis disinfection to treat *E. coli* by using sunlight in a quartz reactor. *E. coli* concentration decreased to a safe level from

an initial concentration of 500–100,000 bacteria/ml during 4 h of photolysis using 350 nm light and solar light. The time taken for disinfection depends on bacterial concentration (Belapurkar *et al.* 2006). Different types of solution preparation methods do exist to synthesize the TiO<sub>2</sub> nanoparticles. Hydrothermal and solvothermal route methods provide good chemical homogeneity. The sol-gel method provides a good fixable thin film on surfaces as compared to other routes (Gupta and Tripathi 2012).

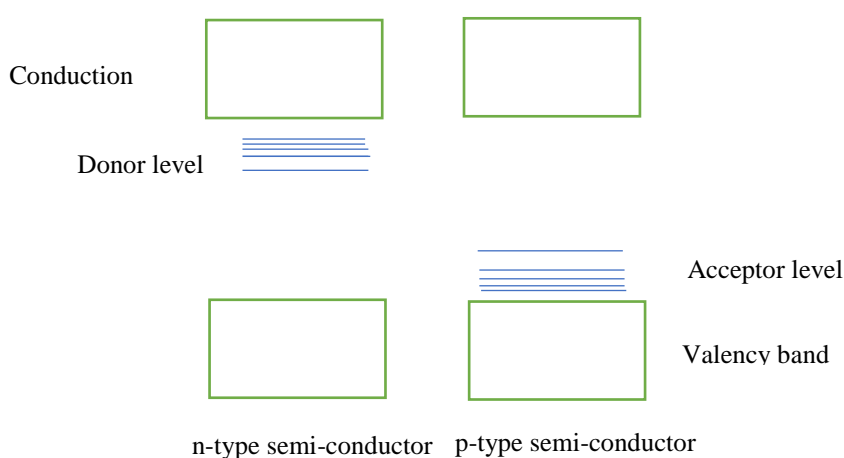


**Figure 2.2** Band structure of ‘n’ and ‘p-type semiconductors

In recent times, alien ion-based doping has been used to accomplish the main objectives and to enhance the activity of photocatalytic and the ability of absorption, namely self-based doping (Liu *et al.* 2014; Zau *et al.* 2012; Zing *et al.* 2014) non-metal doping (Liu *et al.* 2015; Marschall *et al.* 2014; Li *et al.* 2015), transitional metal doping (Song *et al.* 2013; Yu *et al.* 2012) and rare-earth metal-based doping (Borlaf *et al.* 2014; Angelis *et al.* 2007). Normally, the extra levels of energy are utilized for the doped ions in the structure of the band that can be attained to distribute the holes or track the electrons as of the bands. Therefore, it was permitted to surface more carriers. The concentration of the ion impurity otherwise the diffuse of oxygen emerges in TiO<sub>2</sub> can tend to shift the edge of the absorption. The doping of this function is simple in terms of high bandgap variation and the electronic scheme to maximize the visual properties for the production of an optical beam. This can enhance the wide recurrence of kinetics cost in the photo-developed carriers, and also the characteristics of surface and interface are also improved (Umezawa and Role 2012).

The  $\text{Ti}^{3+}$  has been self-doped with  $\text{TiO}_2$  in recent times, which consequences and predictions are estimated in both theoretical and experimental. This demonstrates that vacancies of intrinsic oxygen association increase in nonstoichiometric  $\text{TiO}_2$  crystals due to the chemical property of  $\text{TiO}_2$  that is enclosed with  $\text{Ti}^{3+}$ , which is completely different from the substance  $\text{TiO}_2$ . This method is varied from the conventional incorporation method like the self-doping of  $\text{Ti}^{3+}$  is indicated as the significant one to the absorption of the visible beam in  $\text{TiO}_2$  that the atomic distance mismatching may emit over the various nations (Cai *et al.* 2014; Huo *et al.* 2014; Zheng *et al.* 2013; Li *et al.* 2015;). During the synthesis process, the self-based doping can be easily achieved with the system's equilibrium charge via the chosen raw material, process regulation, and synthesis technique. Thus, the 1.23 eV towards 1.56 eV has been achieved in the interstitial Ti during the theoretical estimations below CB.

However, the VB has attained high impurity energy at the Ti vacant (Zuo *et al.* 2010; Justicia *et al.* 2002). The photocatalytic performance is improved by the two defects consequences such as absorption (Bromiley and Shiryaev 2006; Lu *et al.* 1994). The particle  $\text{Ti}^{3+}$  has been self-doped with the nanoparticles  $\text{TiO}_{2-x}$  that has been synthesized effectively by Liu *et al.* (2010) using the diffusion-redox of ion interface response. Thus, this approach has achieved superior crystalline activity, and the consequences are improved for the optimal photocatalytic oxidation for the beam-driven process (Liu *et al.*, 2014). The consequences of experimental and modeling show that the usage of reduction has significantly developed the ions of  $\text{Ti}^{3+}$  and vacancies of oxygen (Tian *et al.* 2016). Therefore, the adequate performance of this  $\text{Ti}^{3+}$  has been self-doped with the nanoparticles.  $\text{TiO}_{2-x}$  method has highly improved the function of a photocatalyst. Nevertheless, the compilation of  $\text{TiO}_2$  crystals and  $\text{Ti}^{3+}$  is complex in the real-time validation due to unstable species of  $\text{Ti}^{3+}$ , and the oxygen is suddenly oxidized. However, this compilation approach is main difficult in the future for the easy and regulated mode of synthesizing. Also, understanding this approach is essential to develop the models and the exploration monitoring of its characteristics. The highest electronegativity and ionization vitalities are obtained in the components of non-metals, namely, carbon (C) (El-Sheikh *et al.* 2014; Yu *et al.* 2011), nitrogen (N) (Bolokang *et al.* 2015; Zhang *et al.* 2013; Lynch *et al.* 2015), boron (B) (Štengl *et al.* 2010; Wang *et*

*al.* 2014; Patel *et al.* 2015), sulfur (S) (Li *et al.* 2012; Tipayarom *et al.* 2011), fluorine (F) (Senna *et al.* 2012; Kafizas *et al.* 2014; Qiao *et al.* 2012), and chlorine (Cl) (Ji *et al.* 2012; Xu *et al.* 2008). This method is more significant to the optimal band of photocatalytic activity that consequences in these activities are achieved as the narrowing region of bandgap and the edge absorption movement.

In a simplified fashion, it can be said that non-metal doping affects the VB by interacting with O<sub>2p</sub> electrons. Many impurity levels, particularly p states, in metallic doping, which can be positioned above VB, occur in several instances and therefore enhance the absorption edge of TiO<sub>2</sub>. At the same time, non-metal dopants can exist as individual atoms inside a surface rather than merely as clusters. That, together with the little excess of doped molecules, the doped state is more available than the VB optimum that has a greater chance of developing visible-based light photoactivity.

In the hydrothermal approach, the Fe-doped with TiO<sub>2</sub> nanocrystals was formed with varied atomic ratios over the use of a hydrothermal system (Manu and Khadar, 2015). They discovered that the quantity of Fe with dopants was greater towards the crystal structure as dopant particles were integrated hooked on the lattice at interstitial sites. The range of energy connected with the maximum at 2.63 eV was the high levels of achievement defect level. As a result, the electrocatalytic degradation was considerably increased. The team of Yan *et al.* established a quick hydrolysis technique for rutile TiO<sub>2</sub> and used it to produce a three-dimensional-based movement similar to Fe-doped rutile with TiO<sub>2</sub> nanostructure. They next examined the relationship involving Fe doping as well as crystal orientations (Yan *et al.*, 2015). Since the bandgap of Fe was relatively smaller than that of Ti, the correlating separation distance spacing of TiO<sub>2</sub> (110) decreased due to the removal of Ti atoms through Fe atoms. This result was the same as the reported findings of Liu and Zhang (2013). The difference in the position of the peak intensity in TiO<sub>2</sub> is consistent with this finding (Liu and Zhang 2013). The optical properties of rutile TiO<sub>2</sub> were improved by incorporating Fe classes hooked on the unpackaged stage, resulting in a significant bandgap narrowing. As the band gap decreases, the substrate improves the optical properties significantly.

Numerous studies have been carried out on the immobilization of TiO<sub>2</sub> in photocatalysis (Shan *et al.*, 2010). Several attempts have been made to utilize visible

light instead of UV light due to the challenges associated with UV light (Mukherjee et al., 2014). Qin et al. (2014) studied the modification of TiO<sub>2</sub> photocatalyst with a suitable co-catalyst to provide excellent photocatalytic activity for the degradation of organic contaminants. Liu et al. (2011) studied the bandgap of Fe<sub>2</sub>O<sub>3</sub>-TiO<sub>2</sub> composite, which exhibited stronger absorption in the ultraviolet region and adequate and strong absorption in the visible light region.

A few types of research have been only focused on the removal of TCS by photocatalyst via an immobilized catalyst. Fidelis et al. (2019) investigated the photocatalytic degradation of TCS in both ultra-pure and Cl<sup>-</sup>-containing water using an immobilized Fe/Nb<sub>2</sub>O<sub>5</sub> catalyst. Koseira et al. (2017) presented the utilization of ZnO immobilized in biopolymer as a photocatalyst for TCS degradation in ultra-pure water. Besides, Köwitsch and Mehring (2021) also studied the photocatalytic degradation of TCS using magnetic composites of iron oxide ( $\alpha$ -Fe<sub>2</sub>O<sub>3</sub> and Fe<sub>3</sub>O<sub>4</sub>) and carbon nitride materials (CN) synthesized via a microwave-assisted hydrothermal.

## 2.7. SUMMARY

In recent times, various researchers have investigated the treatment of GW using real-time application with numerous methods such as artificial wetlands, sequencing-based batch reactor, Membrane Bioreactor, and Rotating Biological based Contactor. There is an essential for low budget steady approaches for wastewater treatment with low energy contribution in emerging nations. A cost-effective, compact, and low-energy consumption pre-treatment method for wastewater was proven using the UASB in a laboratory setting. (Abdel-Shafy *et al.* 2015). Successively, the UASB scheme has been mostly utilized in tropical nations due to its great enactment in a warm environment (Oteng-Peprah *et al.*, 2018). Furthermore, the reduced organic substance is transformed into biogas.

Generally, any effluent treatment unit undergoes various intermittent organic and contaminant loading conditions when pollutant concentration changes abruptly. Shock loading occurs when a sudden change in the input wastewater concentration to the treatment plant can distort the flow and loading patterns. Therefore, shock loading

causes substrate growth and inhibits the treatment process. The magnitude of inhibition is based on total microbial activity, load shock expansion, and reactor type (Sahariah and Chakraborty 2015). The stability of the reactor undergoing shock loads is an essential design characteristic of wastewater treatment plants. Stability evaluation is vital to offer valued data to evaluate treatment unit performance and guide process design. Several biological techniques have been practically introduced for GW treatment, including constructed wetlands, RBC, UASB, membrane bioreactor, aerobic hybrid biofilm scheme, and aerobic sequential batch reactors (ASBR) (Oteng-Peprah *et al.* 2020; Wang *et al.* 2019). Among these, the sequential batch reactor (SBR) systems are advantageous due to the possibility to carry out the removal of substrates in a single unit, with a small footprint because of the lack of subordinate clarifiers.

SBR management of GW waste encounters most of the conventional pollutant values of wastewater reuse. SBR units are known for their high flexibility and time-controlled operation, and they are measured to be operative pollutant elimination knowledge. However, SBR systems are less efficient in eliminating total suspended solids (TSS) despite the high reduction in most other organic contaminants in the treatment of GW (Katukiza *et al.*, 2014; Boano *et al.* 2020). So, filtration is one of the low-cost techniques used as a post-treatment unit to eliminate colloidal particles and suspended solids. Furthermore, UASB is ideal for the anaerobic treatment of GW, and it ensures that organic loads are effectively removed (Abdel-Shafy *et al.*, 2019).

The SBR treatment is an effective process in sludge activation that can be used for the function and placed in a reactor tank. The time-regulated series are utilized for the SBR with the individual tank and carried out a different operation like treatment of biological, equalization, and clarification of the secondary process. Also, this method is mainly used for the elimination of contaminations from traditional small societies. The treatment of SBR for the waste removal from the GW has accomplished the limit of standard recycled wastewater such as BOD,  $\text{NH}_4^+\text{-N}$ , and COD (Lamine *et al.*, 2007). The eliminated COD has attained a similar range of BOD in the order of 80-90%. The high content of significance has been achieved using Hydraulic Retention Time (HRT); this process consumes 36 hours, but the process takes more computational time and is not applicable for real-time execution. The SBR function performance is



validated under various recycle constraints, such as not validated E. Coli TC, TSS, and FC (Ghaitidak and Yadav 2013).

In environmental circumstances, the TCS material creates a hazard to humans and other organisms. The approach of Photocatalysis can degrade the TCS. However, the photocatalytic significance is limited by the photocatalyst of photo-stability and photo-absorptivity. At the time of photocatalytic function, hazardous by-products will be produced. Thus, Au-coated based Cu<sub>2</sub>O nanowire of arrays (Au–Cu<sub>2</sub>O NWAs) is introduced by (Niu *et al.*, 2015), which is developed by the sputtering light of Au within the emerged nanowires of Cu<sub>2</sub>O commencing the foil of Cu. The observation shows that the developed Au–Cu<sub>2</sub>O NWAs method has significant merits. The TCS degradation of photocatalytic is obtained beneath the optimal beam in the range of radiation such as  $420 < \lambda < 780$  nm. The TCS degradation process reduces the electron and uses the reactive oxygen species for oxidation. Through radical trapping and various estimations methods, the process has been generated and improved its strength. The sandwich model of developed photostability and unusual function is denoted as Au-Cu<sub>2</sub>O-Cu. However, due to its significant advantages, such as long-term photostability, higher efficiency, and lower cost, TiO<sub>2</sub> material is the most effective in photodegradation (Mills and Lee 2002). The nanoparticle of TiO<sub>2</sub> plays an attractive part in various extensive applications in real-time systems, namely, lithography (MacFarlane *et al.*, 2011), photocatalysis, sterilization (Mills *et al.*, 2013), prevention of corrosion in metal (Vamathevan *et al.*, 2002; Zsilák *et al.*, 2014), organic mixtures degradation (Tatsuma *et al.*, 2002; Hashimoto *et al.*, 2005), anti-fogging resources (Mills *et al.* 2013) and nano-medicine (Sapizah *et al.*, 2012).

Kaur *et al.* (2020) enhanced the photocatalytic degradation of TCS after incorporation of reduced graphene oxide (rGO) in pristine TiO<sub>2</sub>. The scavenging experiment indicated the role of hydroxyl radical in the degradation mechanism. The composite displayed efficient degradation under natural sunlight attributed to the narrowing of the bandgap. The supreme oxidative species are developed by the semiconductor particles and the optimal use of a photocatalysis-based semiconductor approach to reduce the XOCs in organic water pollutions. It also performed effectively in secondary effluent containing TCS despite the matrix effect. Thus, the composite has

potential application as a promising photocatalyst in the tertiary handling of water and wastewater. Also, in the current study, the enhancement in the TCS photocatalytic degradation via immobilized TiO<sub>2</sub> after secondary treatment takes place.

## **2.8 RESEARCH GAP**

The various technologies have been designed to treat specific pollutants and do not offer a comprehensive GW treatment. Additionally, quality criteria vary according to the type of participatory design, and the composition and generation rate of GW vary significantly between points. Thus, systems should be built to detect and utilize a specific reuse option while considering geographical variations and complexity to ensure that wastewater from a treatment system complies with wastewater discharge regulations. Only treatment systems which can be applied on a massive scale were reviewed. In our view, this discourages community involvement in GW reuse projects. In the review, some natural materials were mentioned as having the potential to be used as media in GWT systems. These widely available raw materials can be used in almost all developing countries, and exploration should be done to see if they can be integrated entirely into conventional treatment systems. Designing simple GWT systems for household use that target a specific reuse option increases participation at the local level.

A high percentage of the population would use GW to deal with water scarcity. It means that different types of complex GWT systems are in use worldwide. As of now, it is impossible to say which GWT system is the best because each one has its strengths and weaknesses, and each country has a unique set of preferences and specializations. Various treatment systems, such as physical, biological, natural, and chemical, have been discussed where each is effective. Due to their hazardous nature and recalcitrant behaviour, hazardous XOCs have been rising in recent years. TCS is categorized under XOCs, and the TCS degradation studies have mostly been analyzed on the distilled water matrices. However, the efficiency of photocatalysis for TCS degradation on greywater and the effect of operational parameters have not been widely reported, which still is a research gap in this study field.

Because the traditional methods have proved ineffective in eliminating these same

micropollutants, potential treatment methods must be developed. In this way, new treatment methods, such as the photocatalytic oxidation method, are produced. The costlier AOPs named photocatalysis necessitate further research for these reasons. One aim of the study must be to lower the costs, which can be done, for example, by employing less expensive catalyst recovery and recycling and also by using solar radiation rather than UV light. Moreover, an efficient electron gatherer can be found to be an oxygen addition to the reactor due to the increased mass transfer brought on by oxygen. A higher quantum yield will be expected when oxygen is added to the immobilized system. However, oxygen added to the system in suspension showed a negligible effect, which is a research gap.

## **2.9 OBJECTIVES OF PROJECT WORK**

- Performance evaluation of the integrated anaerobic-aerobic-sand filter based greywater treatment system under variable organic and volumetric loads.
- To prepare a ternary composite ( $\text{Fe}_2\text{O}_3\text{-TiO}_2\text{/PVP}$ ) solution and develop optimum conditions for coating it on glass to act as catalyst in solar photocatalysis.
- To assess the performance of Immobilized  $\text{TiO}_2$  based photocatalysis for TCS removal in GW matrices.



## **CHAPTER 3**

### **MATERIALS AND METHODOLOGY**

#### **3.1 GENERAL**

All the laboratory experiments have been designed to study the performance of the combined anaerobic-aerobic-sand filter system to treat GW under various operating conditions. This treated GW is further treated using an immobilized solar photocatalytic reactor. The entire experiment work is done in two phases which are explained in successive sections.

Phase I (Biological treatment): Assessment of performance and stability of integrated anaerobic-aerobic-sand filter system under variable volumetric and organic loads.

Phase II (Polishing-treatment): Develop an appropriate coating technique to prepare the immobilized TiO<sub>2</sub> based catalyst for effective treatment of GW effluent by solar photocatalysis.

#### **3.2 MATERIALS & METHODOLOGY**

##### **3.2.1 Integrated anaerobic-aerobic-sand filter system**

###### **3.2.1.1 Composition of GW**

Synthetic GW was prepared by mixing the arrowroot powder (starch), detergent, urea (laboratory/analytical grade), liquid handwash, and milk powder to feed the pilot-scale plant. Phosphate buffer (KH<sub>2</sub>PO<sub>4</sub> 0.3 g/L) was used to maintain the pH value of the feed at around 7.5. This synthetic GW was made to represent the actual GW, and similar characteristics were observed by the study conducted by other authors, as shown in Table 3.1. The range of BOD: COD in GW was 0.74 to 0.76, and the average was 0.75, and thus, biological treatment could be a viable treatment option.

**Table 3.1** Physical and chemical characteristics of the synthetic GW

Parameter	Synthetic GW		* GW Range	
	Range	Average	Min-Max	Average
COD, mg/L	192-512	347.87±49	43.9-733	388
BOD, mg/L	64-400	260±30.1	17.10-290	244.2
pH	6.47-7.81	7.1±0.39	5.9-8.34	7.4
Surfactants, mg/L	27.5-89	46.44±18.19	12-22	17.42
TP, mg/L	3.72-9.56	6.53±1.89	3-12	7
NH <sub>4</sub> <sup>+</sup> – N, mg/L	14.45-33.75	24.26±2.3	3.7-8.3	6
TN, mg/L	24.12-53.64	40.73±7.3	17-28.82	17.8
Turbidity, NTU	29.5-68.5	39.5±5.9	14-27.4	20.7

\*(Boano *et al.* 2020; Priyanka *et al.* 2019)

### 3.2.1.2 Culture development in reactors

Seed sludge received from the anaerobic unit of Kavour sewage treatment plant, Mangalore, INDIA, was used as the inoculum in an anaerobic reactor. After the seed sludge was screened, the anaerobic reactor was filled with 100 L of anaerobic sludge at a mixed liquor volatile suspended solids (MLVSS) concentration of 1000-1500 mg/L. Coir fiber was used as a media in the anaerobic reactor to grow the biofilm. Coconut husk, the root source of coir fibre, was collected from a waste bunch of coconut fruit that is locally available. All the chemicals used to extract fibre are of analytical grade.

On the other hand, sludge (total solids 5.3 g/L and volatile solids 3.8 g/L) collected from the activated sludge process unit of the Kavour sewage treatment plant was used as inoculum for the experimental aerobic reactor. The aerobic reactor was filled with 100 L of diluted aerobic sludge at MLVSS concentration of 1500-2000 mg/L. Preventive measures were taken while collecting sludge from the effluent treatment plant to avoid bulk sludge. Reactors were allowed to acclimatize.

### 3.2.1.3 Sand filter media

The sand provided in sacks is sieved in standard sieve sizes (1-2 mm), followed by thorough washing in tap water to remove dirt. The gravel and sand materials provided in sacks are washed in tap water thoroughly before filling in the circular tank. The

empty volume (up to the outlet) of the tank is 70 L. There are two grades of gravel and one grade of sand provided. The 20L tank filled with an evenly spread a 20mm size of gravel at bottom topped with 10 -12.5 mm size of gravel. Finally, on top of it, for the volume of 10 L, the sand particles of 1-2 mm were spread. The filling of gravel and sand is carried out with constant tapping and spread evenly. Particle size distribution for sand filter media is shown in Table.3.2 & Figure 3.1.

### 3.2.1.4 Experimental setup

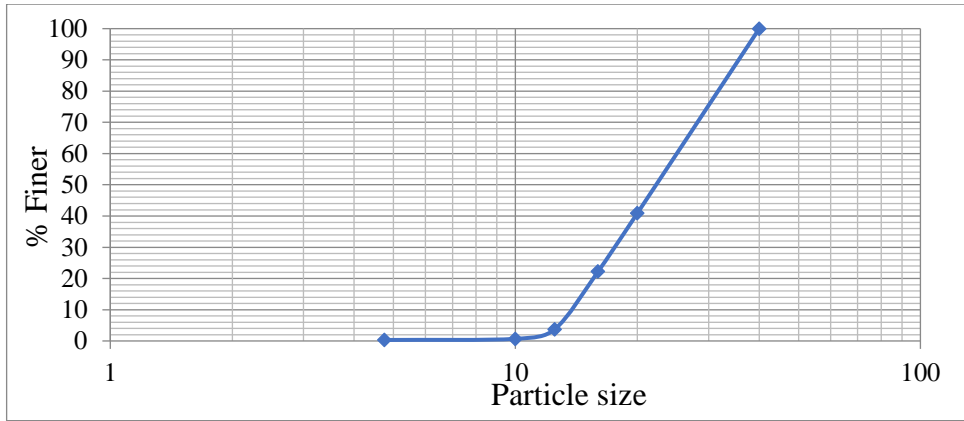
The integrated GW treatment plant consists of the following components: two same-size GW influent holding tanks, anaerobic sequential batch reactor (AnSBR, R<sub>1</sub>), as well as aerobic sequential batch reactor (ASBR, R<sub>2</sub>) followed by a sand filter (R<sub>3</sub>), as shown in Figure 3.2 (a). The entire setup is made of non-transparent PVC tanks. The holding tank's outlet is fixed with a delivery pump (P<sub>1</sub>), which pumps the feed to R<sub>1</sub> at the desired rate. The R<sub>1</sub> outlet is connected to the R<sub>2</sub> inlet by means of a hose so that the R<sub>1</sub> effluent passes as an input to R<sub>2</sub>. The effluent from R<sub>2</sub> flows to R<sub>3</sub>. The dimensions of each treatment unit are shown in Table 3.3.

**Table 3.2** Particle size distribution for sand filter media

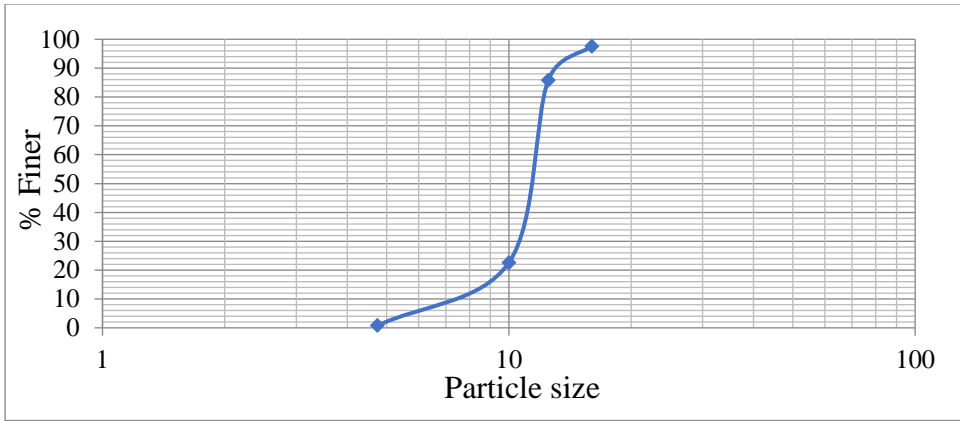
Particulars	Crushed stone (large)	Crushed stone (medium)	Coarse sand
D <sub>10</sub>	13.68683	6.975229	0.986667
D <sub>30</sub>	17.66524	10.2943	1.412131
D <sub>60</sub>	26.4682	11.48101	1.826651
C <sub>u</sub>	1.933845	1.645969	1.851336
C <sub>c</sub>	0.86185	1.323291	3.691775

**Table 3.3** Design of holding tank, AnSBR, ASBR, and sand filter

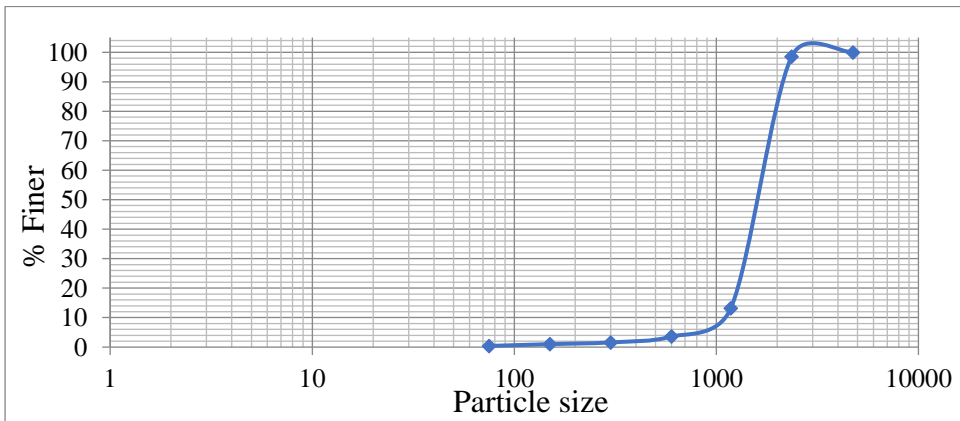
Operational Parameters	Diameter (m)	Height (m)	Total Volume (m <sup>3</sup> )
Holding tank #2 No.	0.4	0.77	0.2
AnSBR	0.55	0.87	0.2
ASBR	0.55	0.87	0.2
Sand Filter	0.30	0.53	0.04



a) Crushed stone (large size)



b) Crushed stone (medium size)



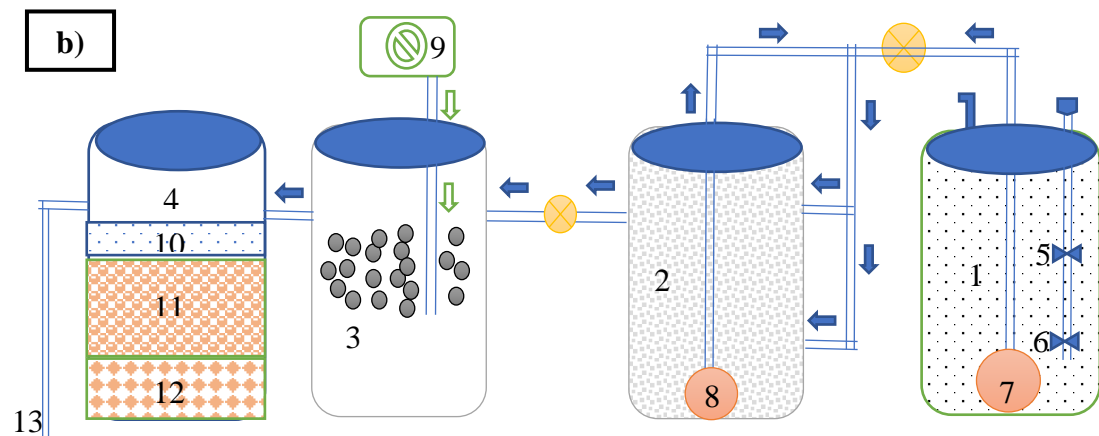
c) Coarse sand

**Figure 3.1** Particle Size Distribution Curve for a) Crushed stone (large size), b) Crushed stone (medium size), and c) Coarse sand



### 3.2.1.5 Reactor Operation

The integrated system mainly follows automation and data logging electronic operating systems. There are 24 segments (from 00 to 23) in each cycle. So overall time consumption for each cycle is 4 hours, and the total number of cycles per day is 6.



- |  |                         |
|--|-------------------------|
| 1. Holding tank (Influent collection and storage tank)   | 8. Recycle pump (P2)    |
| 2. Anaerobic reactor (R <sub>1</sub> )                   | 9. Air pump (P3)        |
| 3. Aerobic reactor (R <sub>2</sub> )                     | 10. Fine Sand media     |
| 4. Sand filter (R <sub>3</sub> )                         | 11. Medium gravel media |
| 5. Magnetic bead at level 1                              | 12. Large gravel media  |
| 6. Magnetic bead at level 2                              | 13. Effluent            |
| 7. Feed pump (P1) from holding tank to anaerobic reactor |                         |

**Figure 3.2** a) Experimental setup and b) Schematic diagram of Integrated anaerobic-aerobic-sand filter system

**Feed pump (P1):** The influent GW can flow into the anaerobic system from the holding tank once the water level reaches level 2. The feed pump runs for 20 minutes in two segments (i.e., 01, 02). Each segment runs for 10 minutes. Delay time (from segment 02 to 06) is around 40 minutes.

**Recycle pump (P2):** The recycle pump runs for 10 minutes at each segment 07,10,13 and 16, respectively.

**Air pump (P3):** The air pump runs continuously from segments 06 to 17, around 120 minutes. Delay time (from segment 18 to 23) is about 60 minutes.

The treatment unit has been operated with an automated configuration of 6 cycles. The typical duration of each cycle is 4h with 24 h of overall time in a day. It is then directed to an ASBR equipped with an aeration pump, where it is mixed for 12 h in a day for the desired final effluent quality. The operating procedure of the integrated system is shown in Table 3.4 & Figure 3.3.

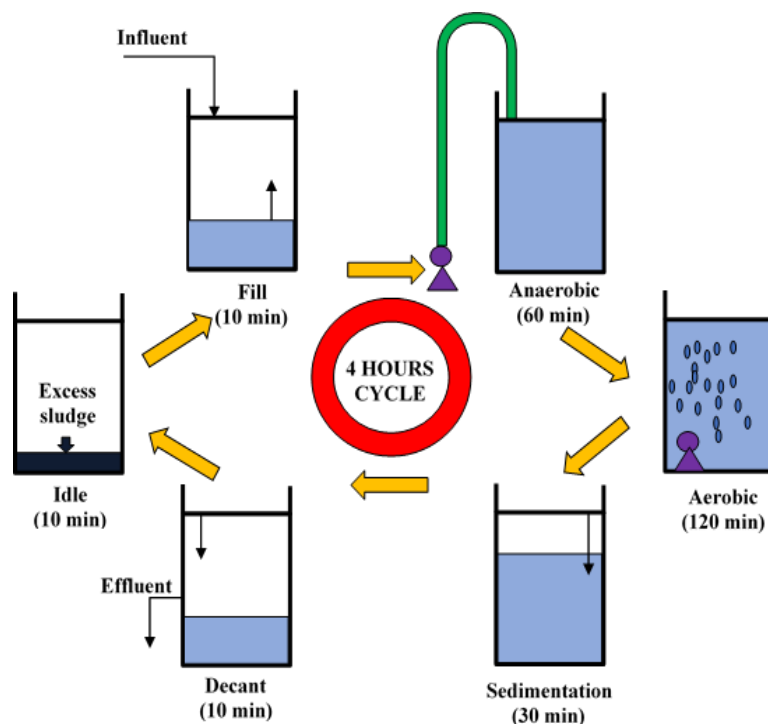


**Figure 3.3** Operation procedure for Integrated anaerobic-aerobic sequence batch reactors

**Table 3.4** Automation and data logging for the pilot-scale operation system

		<b>The time period of one complete Segment</b>																							
Segment divison No (S)	sub	00	01	02	03	04	05	06	07	08	09	10	11	12	13	14	15	16	17	18	19	20	21	22	23
Feed pump (P1)		■	■																						
Recycle pump (P2)									■			■			■			■							
Air pump (P3)								■	■	■	■	■	■	■	■	■	■	■	■						
Total complete segments per day – 6																									
Time period of one complete segment - 240 mins																									
Each segment has a time period of 10 minutes, which is further subdivided into 10 cycles (C). The time period of each cycle is 1 minute, starting from 0 to 9																									

■	Component running
Blank box	Idle/not on operation

### 3.2.1.6 Start-up and operation of the reactor

GW is supplied to AnSBR from the bottom of the reactor through a pipe of a diameter of 50 mm. It fills the reactor by a delivery pump placed at 30 cm above the feed tube in the holding tank. The AnSBR is designed with three compartments made of metallic mesh containers that hold the coconut coir media. The top chamber was set at 30 cm from the top of the reactor and 10 cm from the lowest. Coconut coir was used as substrate media to grow microorganisms, which plays an active role in decomposing organic contaminants. The details of the AnSBR reactor are shown in Table 3.5.

The sample outlet of the reactor is placed above the top compartment at 60 cm height from the digestion zone. The deposited solids in the digestion zone are uniformly utilized at a multistage level for effective treatment using a circulation pump fixed at the top compartment in the AnSBR. The effluent from the AnSBR is pumped into a circular aeration tank. The dimension of the ASBR is 0.55 m × 0.87 m, with a total capacity of 200 L. An aerator with a pressure capacity of 800 kPa is installed at the bottom for the air supply. The schematic flow of each reactor is shown in Figure 3.2 (b).

### 3.2.1.7 Shock loading application

Generally, when a sudden change in the wastewater flow and concentrations occur at the inlet of the treatment plant, it is said that the plant is under shock loading. This could drastically affect the performance of the plant.

Integrated GWT system is subjected to surfactant shock loading. In the initial stage, SSL is avoided, and the HRT of the reactor is maintained at 32 h. Then the HRT is changed to 24 h, 16 h, and then to 8 h. Each time the reactor is given time for stabilization after the change in HRT. The effects of SSL on the performance and stability of the reactor are assessed by increasing the anionic surfactant concentration to 2 to 5 times the average feed concentration (Seetha *et al.*, 2010). At SSL-I, the influent surfactant concentration was raised to 85.94 mg/L for 4 days in the integrated system, and after that, the normal feed was resumed. SSL-II of 121.2 mg/L is applied

to the integrated system for 4 days after 23 days of stable operation, followed by a steady feed supply. SSL-III and SSL-IV are further applied in a similar way as above.

**Table 3.5** The AnSBR dimensions and operation conditions

<b>Parameter</b>	<b>Value</b>
The Internal effective GW volume	100 L
The material of the piping scheme	PVC
Releasing as well as holding GW	via Valves
Interior AnSBR diameter	0.55 m
GW HRT	6 hours
BOD <sub>5</sub> organic loading rates (OLR) 2.6 kg BOD <sub>5</sub> /m <sup>3</sup> /day COD organic loading rates (OLR) 3.5 kg COD/m <sup>3</sup> /day Hydraulic loading rate (HLR): 0.1m <sup>3</sup> /day	

Surfactant concentration in the GW is increased by changing the amount of detergents, handwash, and milk powder. Changed values of surfactant concentration also mean a changed value of COD and BOD. The concentrate on the TP remains more or less the same in the influent at all shock loads. The characteristics of GW at various shock loads are shown in Table 3.6.

### 3.2.1.8 Analytical methods

GW samples were taken from four sampling locations, i.e., (1) inlet to GWT system (2) outlet of anaerobic reactor (3) outlet of the aerobic reactor and (4) outlet of sand filter on a daily basis. The various parameters were analyzed, and the procedures for analysis are shown in Table 3.7. For biofilm examination, the samples were taken in between each shock and examined using SEM and FTIR.

For SEM analysis, the sample has to be fixed and dehydrated. The following procedure is adopted.

- A tiny smear of biofilm was taken on a glass slide.
- The slide was then immersed in 2.5% glutaraldehyde for 10 h.
- After that, the slide was treated with 1% tannic acid and pounded with 70%, 30%, and 90% ethanol for 10 minutes each.

The slides were dried and examined under an SEM at various resolutions.

**Table 3.6** Characteristics of influent at various shock loads

Shock Load	Influent COD (mg/l)	Influent BOD (mg/l)	Influent Surfactant (mg/l)	Surfactant loading rate (g/m <sup>3</sup> /h)
SSL-I	640	414.7	85.94	10.74
SSL-II	800	512.5	121.2	15.15
SSL-III	960	625	155	19.38
SSL-IV	1104	928.5	180.5	22.56

**Table 3.7** Test Methods

S. No	Parameters	Instrument or Method used
1	COD	APHA 5220 C
2	BOD	APHA 5210 B (For DO modified Winkler's method)
3	TN	APHA 4500-N C. (Persulphate method)
4	TP	APHA 4500-P C.
5	NO <sub>3</sub> -N	USEPA 352.1 (Brucine method)
6	NH <sub>4</sub> <sup>+</sup> -N	USEPA 350.2
7	Surfactants	Simplified MBAS (Methylene Blue Active Substance)- S. Chitikela <i>et al.</i> ,1995
8	Triclosan	(Lu <i>et al.</i> 2009)
9	TSS	APHA 2540 D. TSS dried at 103-105° C method
10	Sulphates	4500-SO <sub>4</sub> <sup>2-</sup> E. Turbidimetric Method
11	Turbidity	APHA 2130 B. Nephelometric Method
12	MLSS	APHA 2540 D. TSS (MLSS) dried at 103-105° C method
13	MLVSS	APHA 2540 E. Fixed and Volatile Solids Ignited at 550°C
14	SVI	APHA 2540 D, 2710C, 2710 D. Sludge Volume Index
15	pH	HI11310: Digital pH electrode with integrated temperature sensor
16	EC	HI763100: Digital 4ring conductivity probe with integrated temperature sensor
17	Dissolved Oxygen	Or (Modified Winkler method)

### **3.2.2 Preparation of the immobilized TiO<sub>2</sub> based catalyst**

The effluent from an anaerobic-aerobic-sand filter system consists of pathogens and some recalcitrant (i.e., those left untreated). Therefore, an immobilized Fe<sub>2</sub>O<sub>3</sub>-TiO<sub>2</sub> composite-based solar photocatalytic reactor has been developed and used as post-treatment to handle triclosan (TCS), one of the recalcitrant.

#### **3.2.2.1 Preparation of ternary composite (Fe<sub>2</sub>O<sub>3</sub>-TiO<sub>2</sub>/PVP) solution and catalytic film Coating**

A ternary composite (Fe<sub>2</sub>O<sub>3</sub>-TiO<sub>2</sub>/PVP) solution was prepared by mixing 5-atomic weight percentages of Fe<sub>2</sub>O<sub>3</sub>, nanopowder of TiO<sub>2</sub>, and 3.5% (w/v) of polyvinyl pyrrolidone in 2-methoxy ethanol. The resulted solution was mixed using a magnetic stirrer (REMI-2MLH) at 350-450 rpm for 120-180 min. Then, it was homogenized with an ultrasonic bath (Skytron) for 30 minutes. The colloidal solution was further analyzed using TGA to fix the muffle furnace temperature needed to enhance the immobilization process. The detailed coating procedure is explained in Figure 3.4.

#### **3.2.2.2 Characterization of ternary composite (Fe<sub>2</sub>O<sub>3</sub>-TiO<sub>2</sub>/PVP) film**

Thermo Gravimetric Analysis (TGA, Seiko Exstar TG-DTA 6300) was used to determine the optimal annealing temperature for immobilized film formation on the glass pipe. The materials were tested with scratch hardness testers (ERICHSEN, LINEARTESTER 249). Tungsten carbide inserts with a 1 mm tip diameter were used to create a stylus tip. The stylus tip was then used to provide a continuous load of 20 N. Using the Field Emission Scanning Electron Microscope (FESEM, ZEISS GeminiSEM 300), the morphological study, coating thickness, and width measurement of the scratches on the samples were carried out. In addition, an Energy Dispersive X-ray (EDX) devoted to the FESEM was utilized to analyze each element's fundamental composition and uniform dispersion in the obtained film. In order to investigate the wear performance of the coated sample, sliding wear tests were conducted on the pin-

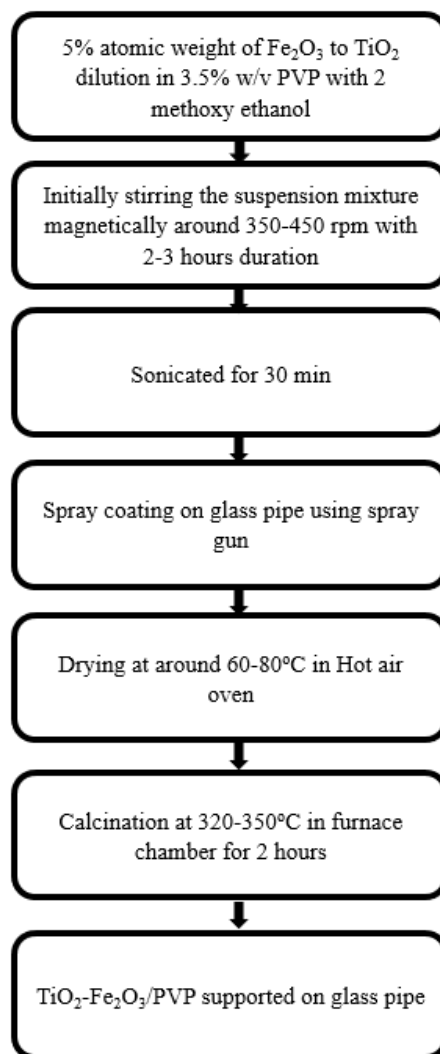


**Figure 3.4** Scheme of the thermal spray method for immobilization of (Fe<sub>2</sub>O<sub>3</sub>-TiO<sub>2</sub>/PVP) supported on a glass pipe

on the disc tribometer (TR-20LE-PHM 400-CHM 600) against EN 32 steel counter body. Besides, a 3D surface profilometer (NANOVEA ST400) was used to examine the wear mechanism. Furthermore, the adhesion strength of the catalytic film was analyzed by a Pull-off adhesion tester (POsiTest AT-A).

X-ray diffraction (XRD, JEOL-JPX 8) scan, with a scanning rate of 2°/min, was conducted using an X-ray source of Cu K $\alpha$  radiation ( $\lambda = 1.5418 \text{ \AA}$ ) to determine the composition of the ternary composite film. The sample scans were carried out with a diffraction angle range of  $2\theta = 10^\circ$  to  $90^\circ$ . Furthermore, Fourier Transform Infrared Spectroscopy (FTIR, Bruker Alpha 400) with an attenuated total reflection (ATR)



detector was utilized to examine the chemical functional groups present in the catalytic film.

### **3.2.2.3 Experimental set-up for photocatalytic treatment**

Since the rate of photocatalysis depends on the amount of irradiation, Parabolic Trough Concentrator (PTC) was developed to concentrate the solar radiation on the immobilized photocatalytic reactor and increase the removal efficiency of TCS. The PTC was made up of a 2 mm thick mirror-polished stainless-steel sheet along with stands to hold the coated glass tube. Moreover, the PTC orientation was also made to rotate the complete assembly to adjust the direction of solar irradiation.

A concentrically hollow cylindrical tube with a diameter of inner and outer cylinders of 30 mm and 50 mm, respectively, are used in the study. The coating is done on the surface of the outer cylindrical tube. This concentrically hollow cylindrical tube is mounted on the parabolic concentrator. Hence, providing about 12.5 mm space for the water flow. Provision for inlet and outlet is made. Figure 3.5 shows the solar photocatalytic reactor setup.

### **3.2.2.4 Operational procedure**

The photocatalytic activity of the immobilized  $\text{Fe}_2\text{O}_3\text{-TiO}_2\text{/PVP}$ -based PTC reactor was evaluated by conducting experiments under solar light irradiation. Three parameters, namely pH,  $\text{H}_2\text{O}_2$ , and contact time, were considered during the experimental work. After a preliminary physicochemical analysis, the effluent generated by the Integrated biological GWT system [anaerobic-aerobic] was used as an influent for the photocatalytic reactor treatment. The pH of the effluent was adjusted to the required range using 0.01 N NaOH (98%) and 0.01N  $\text{H}_2\text{SO}_4$  (98%). The flow rate was regulated using a peristaltic (MICLINS) pump. The treated water was then taken out from the reactor at 30 min intervals (such as 30 min, 60 min, 90 min, 120 min, 180 min, 150 min, 240 min, 210 min, 270 min, and 300 min irradiation time). Then, the water leaving the photocatalytic reactor was subjected to water quality analyses in triplicates. The washing procedure was carried out to clean the immobilized  $\text{Fe}_2\text{O}_3\text{-TiO}_2\text{/PVP}$  glass pipe from undesirable contaminants. This process was done by irradiating the immobilized glass pipe with deionized water for 30 min to attain zero contamination.

The amount of titanium (Ti) and iron (Fe) elements in GW effluent were determined using Inductively Coupled Plasma-Optical Emission Spectroscopy 5(ICP-OES) (5100 series; Agilent Technologies, USA) to study the leaching

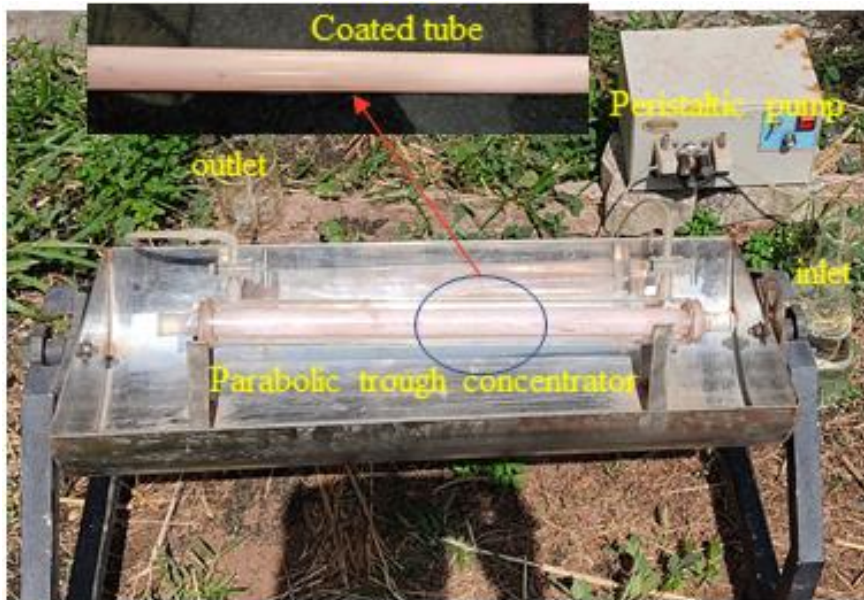


**Figure 3.5** Synthesis coated sample and solar photocatalysis reactor setup

### 3.2.2.5 Experimental design and Optimization

Many independent and influencing parameters were effective in treating greywater effluent using photocatalysis. Box Behnken Design (BBD) is one of the standard designs in the Response Surface Methodology (RSM), used to determine the independent variables. Accordingly, the total number of experiments obtained using the BBD, as given by Eq. (3.1).

$$\text{Number of experiments} = 2^k + 2k + n \quad (3.1)$$

Where k = no. of studied parameters; n = no. of central points

## CHAPTER 4

### RESULTS AND DISCUSSION

#### 4.1 PERFORMANCE OF INTEGRATED ANAEROBIC-AEROBIC-SAND FILTER SYSTEM

##### 4.1.1 Organic matter and Nutrient removal at steady-state condition

In the integrated GWT system, the influent COD concentration was maintained at  $347.87 \pm 49$  mg/L in the pilot plant. The operation conditions were HRT (24 h), biomass concentration ( $X=1-2$  g/L), and DO (3.5-4.5mg/L); Based on the inlet of the individual reactor and out concentrations, the percentage removal of COD from anaerobic, aerobic were 49.64% and 84.27% respectively. It is also noted that the removal efficiency increased with the increase in the influent COD concentration (Fig. 4.1a). The pilot plant showed an overall COD removal efficiency of 89.12% at a  $3.5$  kg/ COD/m<sup>3</sup>/day load rate.

In the present study, the influent's average BOD/COD ratio is 0.75, corresponding to the influent COD  $347.87 \pm 49$  mg/L, and BOD removal efficiencies in anaerobic and aerobic reactors 64.24% and 86.04%, respectively. Effluent from the sand filter showed a BOD concentration of 13.26 mg/L. Thus, the overall percentage removal of BOD by the complete integrated GWT system for the fixed loading rates ( $2.6$  kg BOD/m<sup>3</sup>/day and  $3.5$  kg/ COD/m<sup>3</sup>/day) is 94.9% (Fig. 4.1b).

The effluent of TN concentration decreased to 18.19 mg/L yielding a removal efficiency of 55.35% in UASB. The TN removal efficiency of aerobic effluent was obtained around 80.8% in ASBR. From the final effluent generated from the sand filter, the concentration of TN was reduced to 6.05 mg/L yielding a removal efficiency of 85.15% (Fig. 4.2). The secondary treatment of wastewater could be processed partially and still includes a matter of organic concentrations, particles of suspended, pathogens, nutrients exceeding the acceptable safety level. Effluent features of the AnSBR are given in Table 4.1.

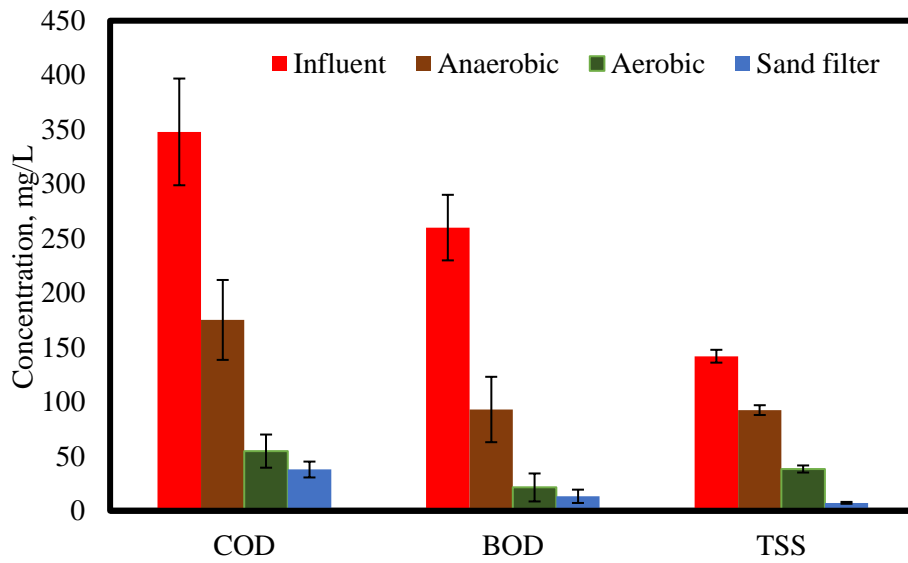


**Figure 4.1** Overall removal efficiencies of organic matter (a) COD (b) BOD in anaerobic, aerobic, and sand filter stages

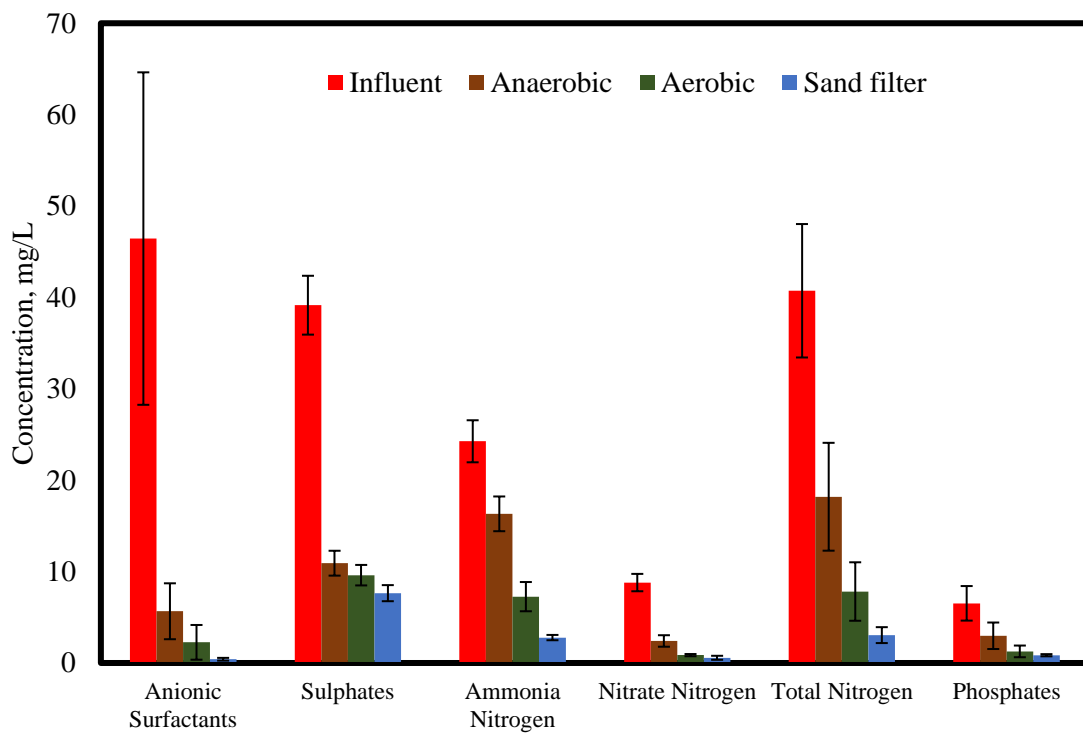


**Figure 4.2** Overall removal efficiencies of nutrients (a) TN (b) TP in anaerobic, aerobic, and sand filter stages.

Corresponding to the same trials, TSS, TN, and TP and anionic surfactants removals in anaerobic reactor was 19.6% (142 to 114.4 mg/L), 17.83% (39.94 to 32.82 mg/L), 30% (6.73 to 4.71 mg/L) and 84% (46.44 to 7.15 mg/L) respectively. Although the anaerobic reactor could remove anionic surfactants BOD<sub>5</sub> and COD to a considerable extent, but still weak in removing TSS, TN, and TP. The COD/TN/TP ratio of the effluent from an anaerobic reactor is 34.65/6.96/1, which correlates with Tchobanoglous *et al.* (2003).

So, to improve the efficiencies of various parameters, the effluent from an anaerobic reactor was treated in an aerobic unit.

The anaerobic reactor's efforts are treated in the aerobic reactor at different aeration times ranging from 15-120 min, as mentioned in Table 4.2. It can be seen that with the increase in aeration time, the efficiency of most of the parameters increased. However, the performance of the combined anaerobic-aerobic reactors was found to be limited as far as TSS removal was concerned. Although TSS limits comply with local standards, it needs to improve to meet international standards for recycling treated water prescribed for irrigation and reuse purposes, as shown in Table 4.3. As a result, to control this TSS, the eluent from the aerobic reactor is passed through a sand filtration unit, as discussed in Chapter 3 [ Section 3.2.1.5].

**Table 4.1** Effect of the anaerobic treatment

Parameters	Unit	N	Synthetic GW (average)	AnSBR overflow	
				Concentration	Efficiency
TSS	mg/L	10	142.3±6.09	114.4±5.5	19.60
Surfactants	mg/L	10	46.44±18.19	7.15±1.06	84.60
COD	mg/L	10	356±29.51	163.2±23.61	54.15
BOD <sub>5</sub>	mg/L	10	252.8±28.02	96±21.33	62.02
BOD <sub>5</sub> /COD	Ratio	10	0.71±0.09	0.59±0.13	-
TP	mg/L	10	6.73±0.69	4.71±0.47	30.00
TN	mg/L	10	39.94±3.23	32.82±1.8	17.83

*Each parameter value provided as the average ±SD value*

**Table 4.2** Aeration Effect at Dissimilar Times on the Characteristics of Chemical and Physical by AnSBR Effluent

Pollutants	N	AnSBR effluent (average)	Aeration time (min)									
			15		30		60		90		120	
			Conc.	%R	Conc.	%R	Conc.	%R	Conc.	%R	Conc.	%R
TSS, mg/L	10	94±3.40	~88.00	06.38	~79.00	15.96	~68.00	27.66	~53.00	43.62	~40.0	57.45
COD, mg/L	10	176±16.86	~159.80	09.24	~148.65	15.52	~135.34	24.10	~88.54	49.69	~44.8	74.50
BOD, mg/L	10	99.2±23.61	~83.00	16.33	~76.00	23.39	~70.00	29.44	~48.00	51.61	~22.0	77.82
BOD <sub>5</sub> /COD	10	-	51.94	-	51.13	-	51.72	-	54.21	-	0.49	-
TP, mg/L	10	3.11±0.33	-	-	-	-	-	-	-	-	~1.32	57.55
TN, mg/L	10	19.82±2.03	~16.80	15.24	~14.20	28.35	~11.60	41.47	~9.10	54.09	~7.48	62.26

The performance of the sand filter is shown in Table 4.3. COD, BOD<sub>5</sub>, TN, TP, anionic surfactants, and TSS concentrations varied from 30 to 45, 7 to 20, 2 to 4, 0.7 to 1, 0 to 1, and 6 to 8 mg/L, respectively.

**Table 4.3** Effect of up flow sand filter (UFSF) of GW on the chemical and physical characteristics

Parameters	Unit	N	Aerobic effluent (average)	UFSF effluent	
				Concentration	Efficiency
TSS	mg/L	10	38.34±3.25	7.25±0.87	81.09
Anionic Surfactant	mg/L	10	2.26±1.9	0.41±0.5	81.85
COD	mg/L	10	54.75±15.22	37.85±7.28	30.87
BOD <sub>5</sub>	mg/L	10	21.40±12.85	13.26±6.12	38.04
TP	mg/L	10	1.27±0.64	0.85±0.12	33.07
TN	mg/L	10	7.82±3.2	3.05±0.87	60.99

Each value of the parameter described as the mean value ± SD

The overall performance of the integrated system is shown in Table 4.4. Based on these results, treated GW can be reused for irrigation since it is satisfactory meeting the reusable limits for the same. Furthermore, the integrated aerobic-aerobic-sand filter treatment is practical, low-cost, and feasible.

## 4.2 PERFORMANCE EVALUATION OF INTEGRATED GWT UNDER SHOCK LOAD

According to some researchers, the surfactant had one of three fates in biological wastewater treatment: it either biodegraded completely, was metabolized into small molecules, or vanished entirely (Alina *et al.*, 2015). Surfactants, the specific chemicals used in cleaning solutions, activate or hinder microorganisms' activity based on their concentration. Surfactant concentrations that exceed 15 mg of dioctyl sodium sulfosuccinate per gram of sludge restrict the respiration of wastewater treatment bacteria, decreasing phosphorus removal. These changes also have an impact on the form of activated sludge, leading them to fragment and burst open the cell membranes of microorganisms.

**Table 4.4:** Effect of overall GW treatment of physical and chemical characteristics

Parameter	Unit	N	Feeding Tank	Anaerobic Effluent		Aerobic effluent		Sand filter effluent		Overall efficiency
				Concentration	% R	Concentration	% R	Concentration	% R	% R
pH	-	45	7.1±0.39	6.79±0.41	-	7.00±0.32	-	7.15±0.33	-	-
EC	µS/cm	45	262.35±48	584.58±157.3	-	533.97±94	-	551.15±88.7	-	-
D.O	mg/L	45	4.72±0.6	1.53±0.49	-	3.9±0.53	-	4.9±0.63	-	-
NH <sub>4</sub> <sup>+</sup> -N	mg/L	45	24.26±2.3	16.32±1.9	32.73	7.26±1.6	55.51	2.78±0.29	61.71	88.54
NO <sub>3</sub> <sup>-</sup> -N	mg/L	45	8.8±0.95	2.41±0.63	72.61	0.86±0.12	64.31	0.57±0.22	33.72	93.52
TN	mg/L	45	40.73±7.3	18.19±5.9	55.34	7.82±3.2	57	6.05±2.87	22.63	85.15
COD	mg/L	45	347.87±49	175.21±36.7	49.63	54.75±15.22	68.75	37.85±7.28	30.87	89.12
BOD	mg/L	45	260±30.1	92.98±30.02	64.23	21.40±12.85	76.98	13.26±6.12	38.04	94.9
TP	mg/L	45	6.53±1.89	2.98±1.45	54.36	1.27±0.64	57.38	0.85±0.12	33.07	86.98
TSS	mg/L	45	141.9±5.89	92.4±4.5	34.88	38.34±3.25	58.5	16.25±2.12	57.62	88.5
Surfactants	mg/L	45	46.44±18.19	5.66±3.06	87.81	2.26±1.9	60	0.41±0.15	81.8	99.11
Sulphates	mg/L	45	39.15±3.22	10.92±1.36	72.11	9.61±1.12	12	7.64±0.88	20.5	80.48

\*The parameter value is defined based on mean value ± SD



#### **4.2.1 Integrated GWT systems performance prior to surfactant shock loading**

As explained in section 3.2.1.7, the HRT was gradually reduced from 32 hours to 8 hours in steps of 8 hours. Table 4.5 shows the variations in performance with respect to the change in volumetric loading. It is clear from the results that when volumetric shock load occurs, the reactor efficiency decreases in the beginning but regains efficiency after some time. The overall efficiencies of COD, BOD, TN, anionic surfactants in the integrated system were found to be good. Thus, we can conclude that the pilot plant as a whole has a high tolerance to increase in volumetric loading rate. R<sub>1</sub> had a COD removal efficiency of about 59%, whereas the total COD removal by R<sub>1</sub> and R<sub>2</sub> combined is about 77%. As a result, R<sub>1</sub> and R<sub>2</sub> played a key role in removing most COD. This could be due to the abundant availability of active biomass in R<sub>1</sub> and R<sub>2</sub>. However, most of the readily biodegradable organic matter is oxidized in R<sub>1</sub>. In the current study, the overall removal of COD, BOD, TN, and surfactants by the anaerobic-aerobic-sand filter is found to be 95.45%, 96.15%, 90.26%, and 98.42%, respectively, at 8 h HRT. This also emphasizes that there is a significant improvement in the overall performance of the complete system by the addition of a sand filter.

#### **4.2.2 Performance of Integrated GWT system under organic shock loads**

The pilot plant was operated for 22 days at systematic feed concentration except for surfactant input. Further, the surfactants are introduced in the influent for 29 days before exposure to SSL-1. Feed parameters were maintained constant except COD, BOD, and surfactants during SSL1-1, SSL-2, SSL-3, and SSL-4. The Integrated system tackled SSL-1, SSL-2, SSL-3 with SSL-4 in terms of Surfactants and COD removal.

##### **4.2.2.1 Overall Performance of the integrated system during SSL**

Figure 4.3 shows the performance of three reactors operated at various loading rates. It was evident from the figures that the surfactant removal efficiency of R<sub>1</sub> increased at all times and then decreased due to prolonged loading. During SSL-I, R<sub>1</sub> had the maximum removal of 62.5%. During SSL-II, it was 68.2%. It followed the same pattern and had a maximum removal of 66.11% at SSL-III.

**Table 4.5** Comparison of reactor performance at various HRT

HRT (h)	Parameter	Removal efficiency (%)			
		Anaerobic (R <sub>1</sub> )	Aerobic (R <sub>2</sub> )	Sand filter (R <sub>3</sub> )	Overall
32	COD	31.2	48.31	55.74	84.26
	BOD	73.17	50	52.27	93.60
	TN	34.9	53.16	2.35	70.23
	Surfactants	74.34	72.62	43.30	96.02
24	COD	51.92	71.88	54.17	93.80
	BOD	70.04	64.53	51.96	94.90
	TN	54.22	59.55	40.06	88.90
	Surfactants	66.85	73.44	56.91	96.21
16	COD	51.86	79.54	50	95.08
	BOD	72.37	86.97	52.83	94.43
	TN	63.67	54.13	16.16	86.03
	Surfactants	71.5	62.96	50.45	94.81
8	COD	58.68	77	52.17	95.45
	BOD	73.91	62.12	61	96.15
	TN	63.78	60.84	31.3	90.26
	Surfactants	64.69	70.79	84.71	98.42

But, it decreases to 34.74% at SSL-IV. Prior to SSL-I, R<sub>1</sub>, R<sub>2</sub>, and R<sub>3</sub> released 15.04, 3.96, and 0.64 mg/L effluent surfactants with elimination efficiencies of 56%, 73.68%, and 83.83%, respectively. Immediately following the application of SSL-I (days 31-37), effluent anionic surfactants concentration increased from 46.62 to 67.34 mg/L. It started decreasing (38th day onwards) and reached a new steady-state condition in 5 days, and surfactants removal in R<sub>1</sub>, R<sub>2</sub>, and R<sub>3</sub> decreased to 41.87% (by 25.23% decrease), 63.95% (by 13.2% decrease), and 66.57% (by 23.71% decrease). In case of SSL-II, R<sub>1</sub>, R<sub>2</sub>, and R<sub>3</sub> released 17.76, 13.57 and 9.07 mg/L effluent surfactants with removal efficiencies declined to 42.63% (by 1.87% increase), 23.59% (by 63.11% decrease) and 33.16% (by 50.18% decrease), respectively. At SSL-III condition, R<sub>1</sub>, R<sub>2</sub>, and R<sub>3</sub> released 28.68, 21.45 and 17.02 mg/L effluent surfactants with removal efficiencies declined to 35.46% (by 16.81% decrease), 25.23% (by 6.9% increase) and 20.68% (by 37.64% decrease), respectively. Finally, in the case of SSL-IV, R<sub>1</sub>, R<sub>2</sub>, and R<sub>3</sub> released 23.35, 19.41.45 and 14.97 mg/L effluent surfactants with removal efficiencies declined to 23.82% (by 32.82% decrease), 25.23% (by 16.87% decrease)

and 22.87% (by 10.59% increase), respectively. The corresponding maximum values of overall efficiencies are 98.34%, 94.02%, 93.92% and 95.04% at SSL of 85.84, 121.2 and 180.56mg/l. Whereas, in the case of COD, maximum values of whole system efficiencies are 96.15%, 92.31%, 92.86%, and 75% at SSL of 85.84, 121.2, 155, and 180.5.

In the case of COD removal against shock load for 1104 mg/L, overall efficiency became less, and the steady-state was not attained for an extended period, as revealed in Figure 4.3b. However, the integrated system has not recovered pre-shock efficiency at SSL-IV for COD removal.

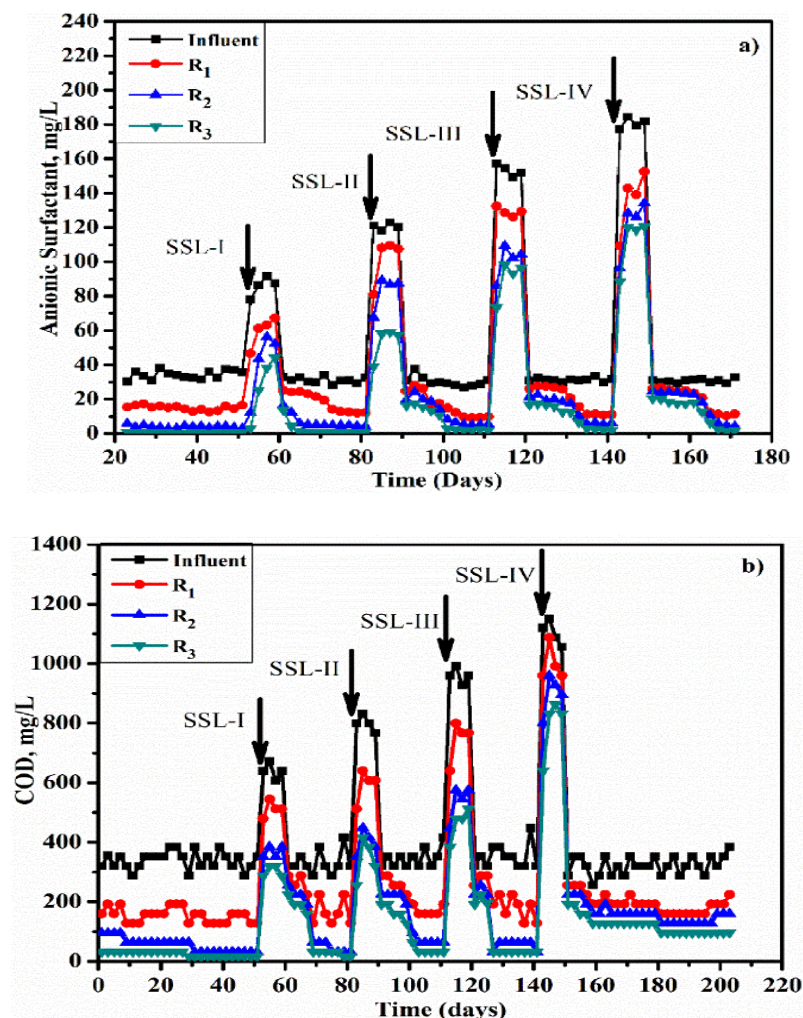


**Figure 4.3** Effects of SSL before and after the treatment on three-stage ( $R_1$ - $R_2$ - $R_3$ ) integrated system: (a) Surfactants and (b) COD

#### 4.2.2.2 Effect of Surfactant Shock Load (SSL) on Integrated Anaerobic-Aerobic-Sand Filter System

**(A) COD:** Figure 4.4 shows the COD variation in the effluent and influent under numerous shock tons. Here, the period of all shock loads, and the effluent COD concentrations of R<sub>1</sub>, R<sub>2</sub>, and R<sub>3</sub> increased. The concentration that has attained 256, 224, and 160 mg/L are the maximum COD effluent. Hence, maximum COD was gained for R<sub>1</sub>, R<sub>2</sub>, and R<sub>3</sub> at the 640 mg of COD/L load.

The consistent values are (320, 288, 224), (640, 448, 384) and (960, 800, 640) mg COD/L of shock loads, which are 800, 960, 1104 mg/L respectively. The effluent COD concentration starts decreasing while the usual loading conditions are restarted a load of shock afterward.

**(B) Surfactant:** The influent and overflow anionic surfactants variation under different shock loads, as shown in Figure 4.5. Effluent anionic surfactants concentration of R<sub>1</sub>, R<sub>2</sub>, and R<sub>3</sub> increased as various shock loads increased. The maximum effluent anionic surfactants concentration obtained was 67.34, 56.36, and 44.28mg/L, respectively, for R<sub>1</sub>, R<sub>2</sub>, and R<sub>3</sub> at the end of 85.94 mg/L. Also, the correspondent ideals are (109.67, 89.23, 59.12), (132.34, 86.28, 73.36) and (149.4, 96.34, 88.36) mg/L at SSL of 121.2, 155, 180.5 mg/L, respectively.

#### 4.2.2.3 Optimum loading rate

The integrated system process is not enough to execute the standard equations for various shock loads. Hereafter, the system's performance has been calculated by estimating the effective load discharge rate (ELDR) and effective loading rate (ELR) that denotes the normal influent and emission surfactants with the HRT. Moreover, ELR (g/m<sup>3</sup>/h) has represented the applied load (t-HRT) divided by HRT. Furthermore, the variance among ELDR and ELR is utilized to analyze the effect of ELR (g/m<sup>3</sup>/h) (Seetha *et al.*, 2010).

As the effective surfactant loading rate increased during SSL of 85.94 and 121.2 mg/L, the R<sub>1</sub> efficiency also raised until 6 h. At the SSL of 155 and 180.5 mg/L of anionic surfactant concentration, R<sub>1</sub> efficiency initially increased and decreased by increasing

the effective surfactant loading rate. At the SSL of 155 mg/L, the R<sub>1</sub> efficiency decreased after 4 h and 2 h of application of SSL of 155 and 180.5 mg/L, respectively, as an outcome of the high loading level. Meanwhile, in the circumstance of R<sub>2</sub>, anionic-based surfactant removal rate and competence increased up to 4 h with increasing effective surfactant loading rate at all SSL excluding at 180 mg/L, where the competence diminished after 2 h. In the case of R<sub>3</sub>, anionic surfactant efficiency increased up to 6 h with increasing effective surfactant loading rate at all SSL excluding at 180 mg/L. Here the efficiency rate was diminished after 4 h. By way of distance as the enactment of the overall plant is concerned, the whole competence has amplified with increasing surfactant loading rate for all SSL up to 4 h (shown as Figure 4.6 & Figure 4.7). Then the efficiency began to decline after reaching a specific value.

Figure 4.8 explains the competence of the whole arrangement with reverence to the real surfactant loading rate. The optimum effective surfactant loading rate of 22.56 g/m<sup>3</sup>/h in R<sub>1</sub> and the obtained maximum removal efficiency of anionic surfactant is around 67.6 %. As far as R<sub>2</sub> is concerned, anionic surfactant removal efficiency is around 70 % at an optimum loading rate of 12.5 g/m<sup>3</sup>/h. In reactor R<sub>3</sub>, anionic surfactant removal efficiency is around 59 %, which decreased after a certain surfactant loading rate.

The efficacy of the whole system increases with the effective surfactant loading rate; attains a maximum of 91.8 % at 19.38 g/m<sup>3</sup>/h and decreases with increasing surfactant loading rate. Although the anionic surfactant removal rate decreased with increasing effective surfactant loading degree after 4 h, the system was effective at eliminating additional substrate at advanced stacking rates.

The literature study has described that the attention of integrated systems (hybrid reactor) increases with increasing surfactant loading rate. When a higher portion of the biomass is attached to a coir fiber in the anaerobic reactor, the more significant portion of substrate will be degraded by the biofilm, and a small portion is left for the deferred biomass.

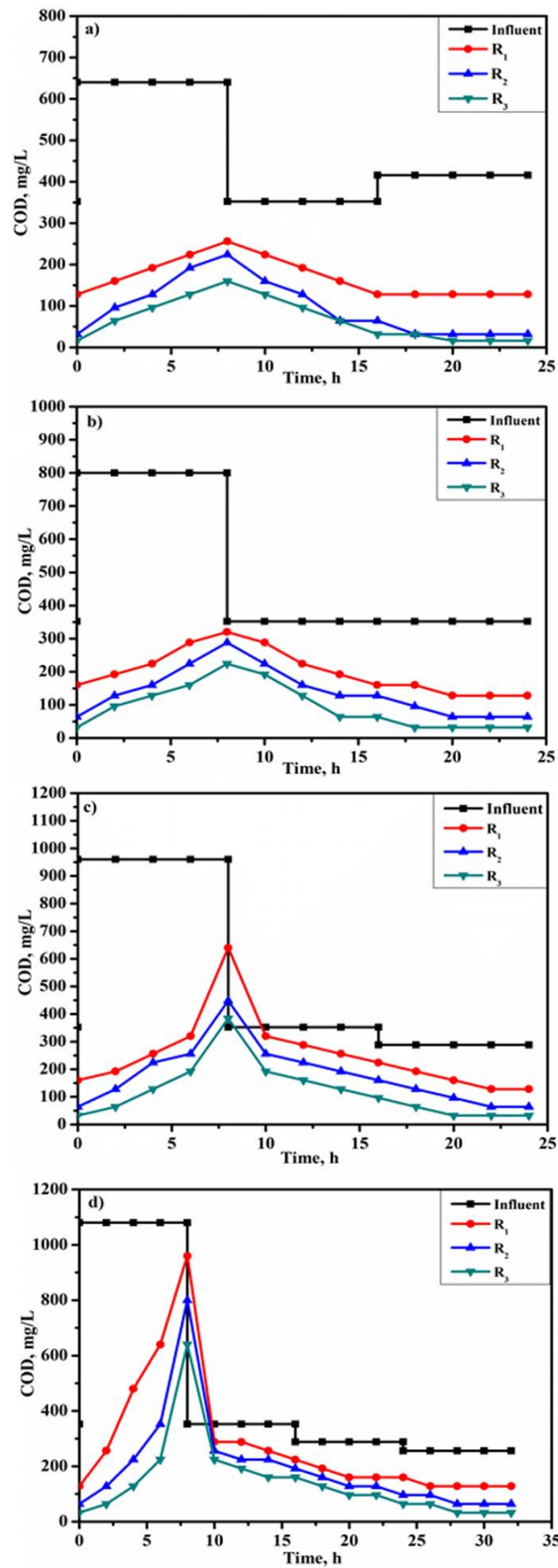


**Figure 4.4** COD variation in influent, R<sub>1</sub>, R<sub>2</sub> and R<sub>3</sub> at shock loads of (a) 640, (b) 800, (c) 960 and (d) 1104 mg/L

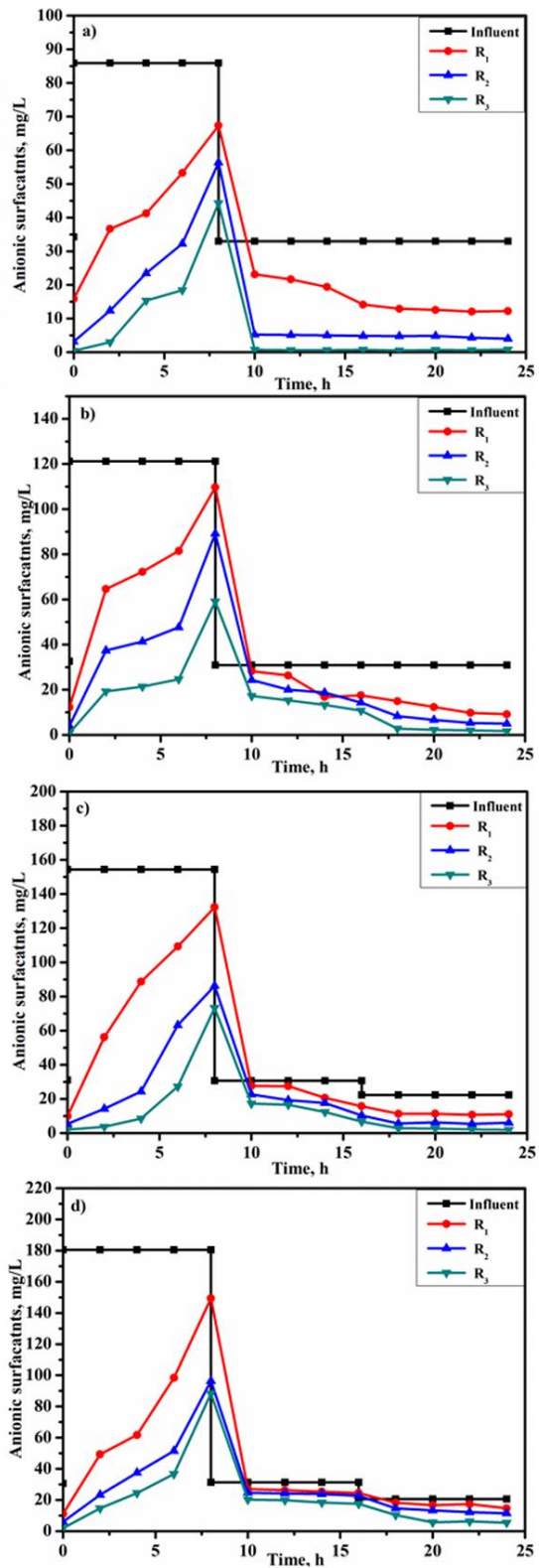


**Figure 4.5** Variation of anionic surfactants in influent, based on R<sub>1</sub>, R<sub>2</sub> and R<sub>3</sub> at shock loads of (a) 85.94, (b) 121.2, (c) 155 and (d) 180.5 mg /L.

This shows that the fixed biofilm would have prepared a greater influence for eliminating the anionic surfactant than the deferred biomass of aerobic reactor that is motivated to gain higher anionic surfactant removal measure at wide real surfactant loading rate in the anaerobic reactor.

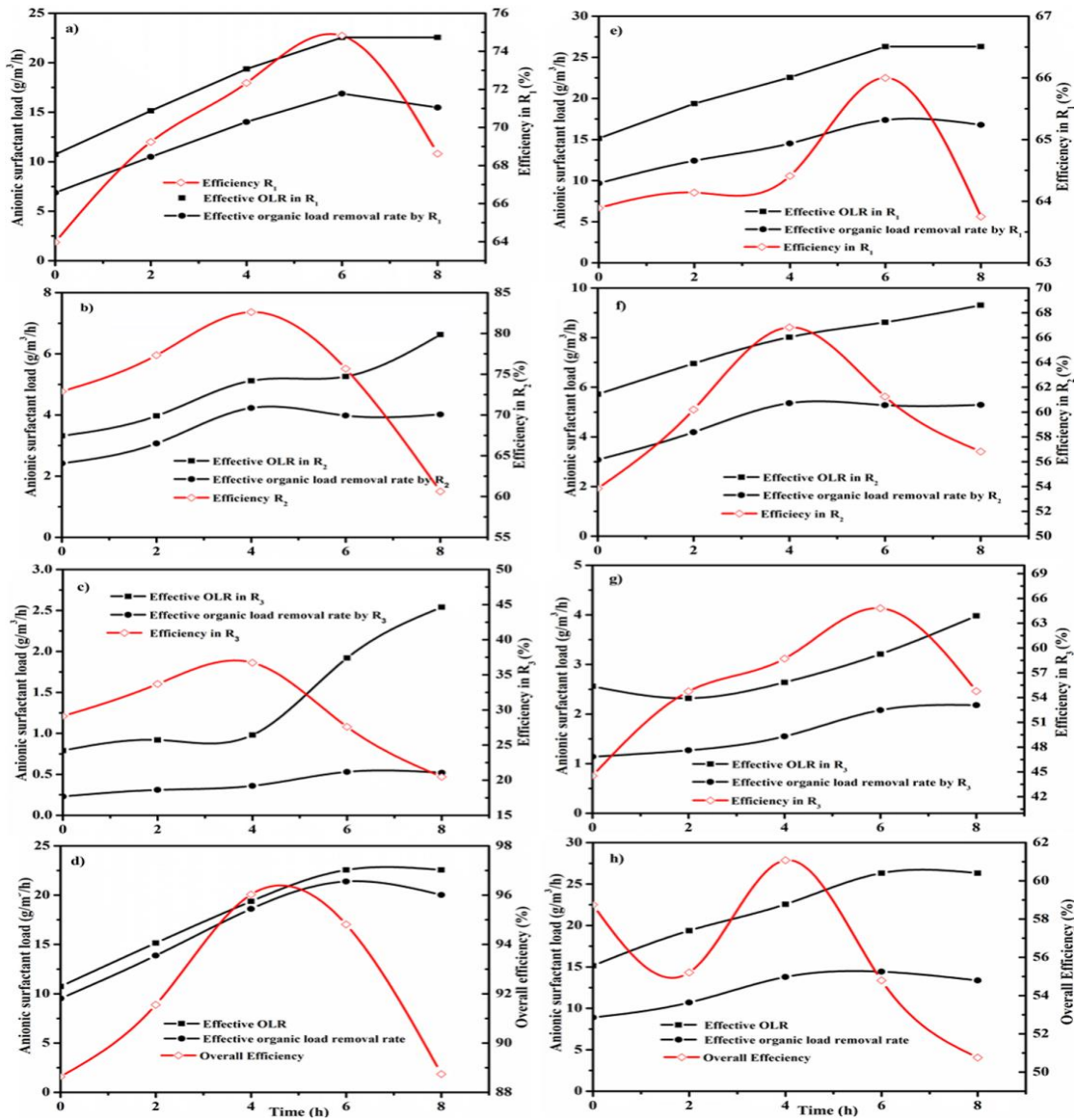


**Figure 4.6** Evaluation of a) R<sub>1</sub> at SSL of 85.94 mg/l, b) R<sub>2</sub> at SSL of 85.94 mg/l, c) R<sub>3</sub> at SSL of 85.94 mg/l, d) overall system at SSL of 85.94 mg/l, e) R<sub>1</sub> at SSL of 121.2 mg/l, f) R<sub>2</sub> at SSL of 121.2 mg/l, g) R<sub>3</sub> at SSL of 121.2 mg/l and h) whole system at SSL of 121.2 mg/l.



### 4.2.3 Characterization of sludge in an integrated system

#### 4.2.3.1 Fourier transformation infrared spectroscopy Analysis (FTIR)

Andrade *et al.* (2019) has investigated the natural and inorganic practical gatherings present in biomass from anaerobic and vigorous units that were recognized utilizing FTIR examination. It was additionally utilized in the separate chamber parts to portray germs dependent on the estimation of sub-atomic holding and pulsation compounds, invigorated through emission at a fitting recurrence. FTIR spectra of coconut coir fiber joined biofilm, anaerobic and high-impact biomass estimations in the scope of 500-5000  $\text{cm}^{-1}$  were considered to accomplish data on the bio-chemical arrangement of chambers. The most prominent components in raw coir fibre are cellulose (~40%) and lignin (~45%) constituents. The presence of lignin in the coir fibre is represented by characteristic peaks at 1210.80, 1361.27, 1699.86, and 2111.42  $\text{cm}^{-1}$ , as shown in Figure 4.9a.

The FTIR spectra of pure cellulose and hemicellulose are represented at the peaks 1210.80 and 1361.27  $\text{cm}^{-1}$ , respectively, according to the C-O stretching the sample (Adapa *et al.*, 2011). The presence of strong C=O linkage, a specific group of lignin, is responsible for the peak in the spectrum corresponding to raw fibres at 1699.86  $\text{cm}^{-1}$  (Abraham *et al.*, 2013). The peak at 2111.43  $\text{cm}^{-1}$  is appropriate to the combination for O-H and C-H stretching vibrations for hemicellulose, cellulose, and lignin (Li *et al.*, 2015; Raspolli Galletti *et al.* 2015). Lignin, cellulose, and hemicelluloses are the most abundant polymer in nature and are not composed of sugar. Anaerobic degradation of lignin is carried out by its depolymerization, oxidation of side chains, and demethylation. The depolymerization of lignin by extracellular enzymes requires oxygen; therefore, making this kind of lignin degradation cannot be possible. It is also efficient between pH values 4.6 to 7, and at a hotness range among the 25–50 °C, and the conditions are suitable for the growth of microorganisms using cellulose as a substrate (Čater *et al.*, 2014). Therefore, it was concluded that the raw coconut coir fibre would be considered as one of the most excellent media/materials for the substrate in the AnSBR. The FTIR spectrum of the attached biofilm (Figure 4.9b) showed that a broad absorption band among the 3669.50 to 3781.08  $\text{cm}^{-1}$  represents using alcohol (OH). In this range of 3275.21  $\text{cm}^{-1}$  to 3390.65  $\text{cm}^{-1}$ , the usual "polymeric" OH enlarge

atmospheres be the most significant practical group, mainly based on the breadth of the biofilm and longer strength (Manu and Thalla 2017).

#### 4.2.3.2 Effects of SSL on the microbial characteristics of biomass

Unprocessed GW recycled for garden irrigation stated an excellent threat for rotavirus. Afterward, GW management, the threat of contagion for rotavirus persisted (Ricardo *et al.*, 2021).

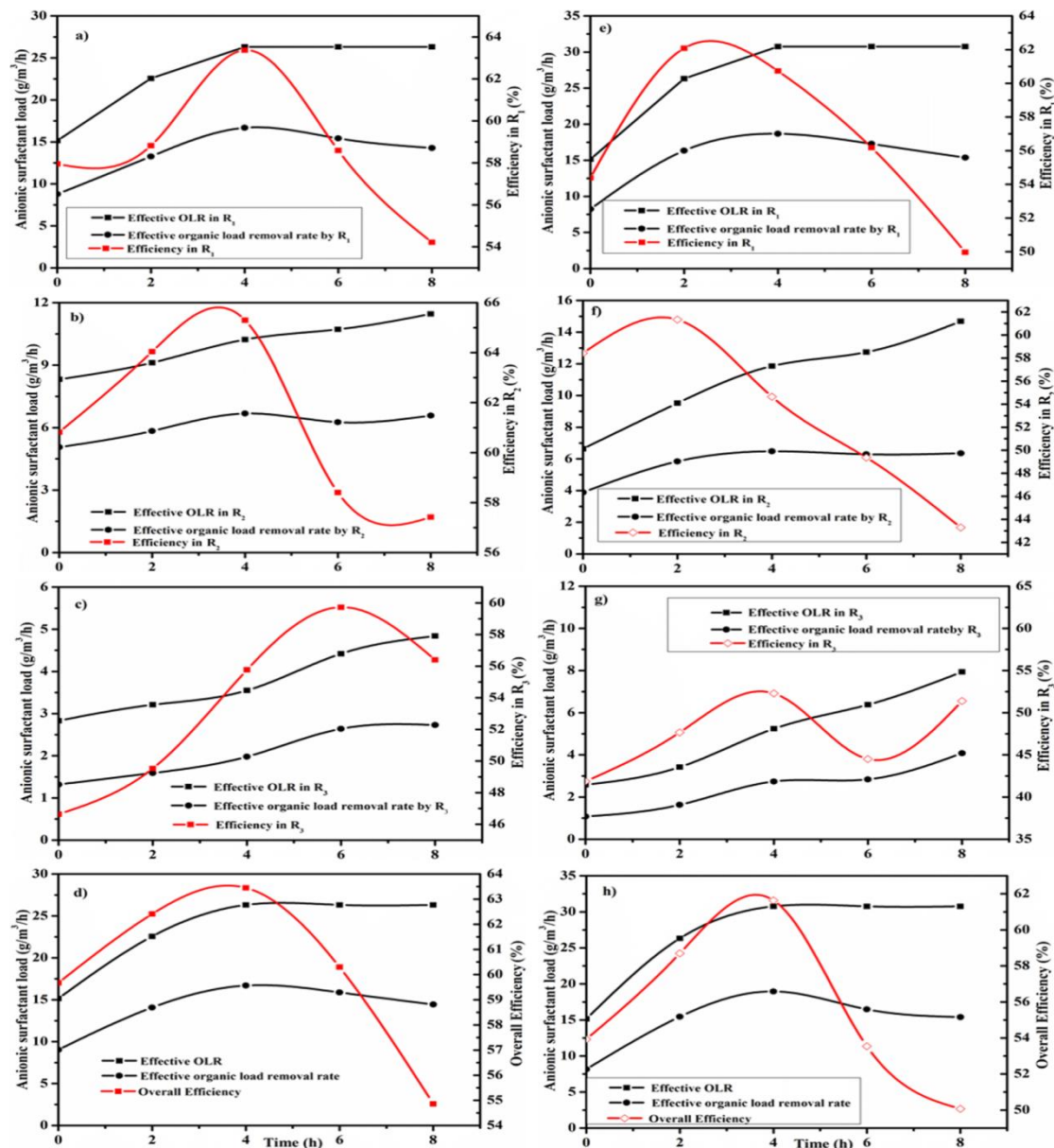


**Figure 4.7** Performance of a) R<sub>1</sub> at SSL of 155 mg/l, b) R<sub>2</sub> at SSL of 155 mg/l, c) R<sub>3</sub> at SSL of 155 mg/l, d) overall system at SSL of 155 mg/l, e) R<sub>1</sub> at SSL of 180.5 mg/l, f) R<sub>2</sub> at SSL of 180.5 mg/l, g) R<sub>3</sub> at SSL of 180.5 mg/l and h) SSL of 180.5 mg/l.

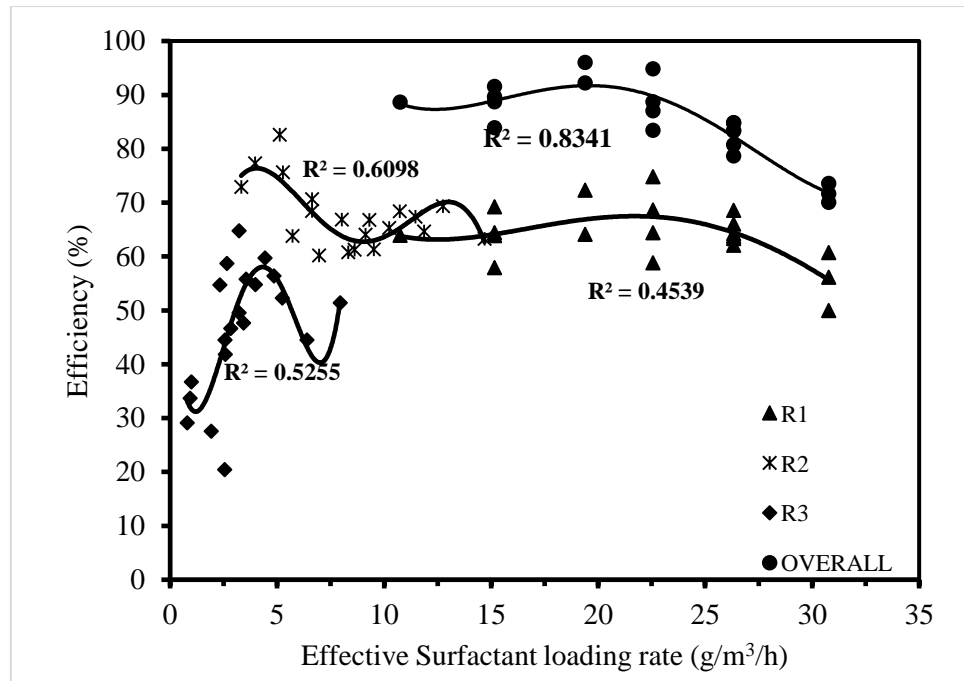


**Figure 4.8** Removal efficiency of the overall system and the effective surfactant loading rate

Post-treatment is essential to monitor the threat of infection by GW reuse. Hence it is essential to characterize microbial communities after GW treatment. Kamińska and Marszałek (2020) stated no change in *Escherichia coli* concentration during the biological purification process, whereas ultrafiltration succeeded in the total elimination of the determined pathogens. Sharaf and Liu (2021) stated that biodegradation was established to promote less than 26% to the whole treatment with  $178.71 \pm 14.12 \text{ mg g}^{-1}$  biomass density of biologically active granular activated carbon, where sorption usages were liable for the residual GW treatment. Hence it is necessary to characterize the biofilm formed and its composition during the treatment.

The surface structure and characters of the sludge generated under the anaerobic and aerobic conditions were determined using a different type of microscope, namely scanning electron microscope (SEM). This morphological action of microorganisms present in both anaerobic sludge and activated sludge is shown in Figure 4.10. The SEM

image of the anaerobic sludge, as shown in Figure 4.10a, was composed of microscale agglomerated fine powder-like particles and a heterogeneous morphology (Kobya *et al.*, 2017).

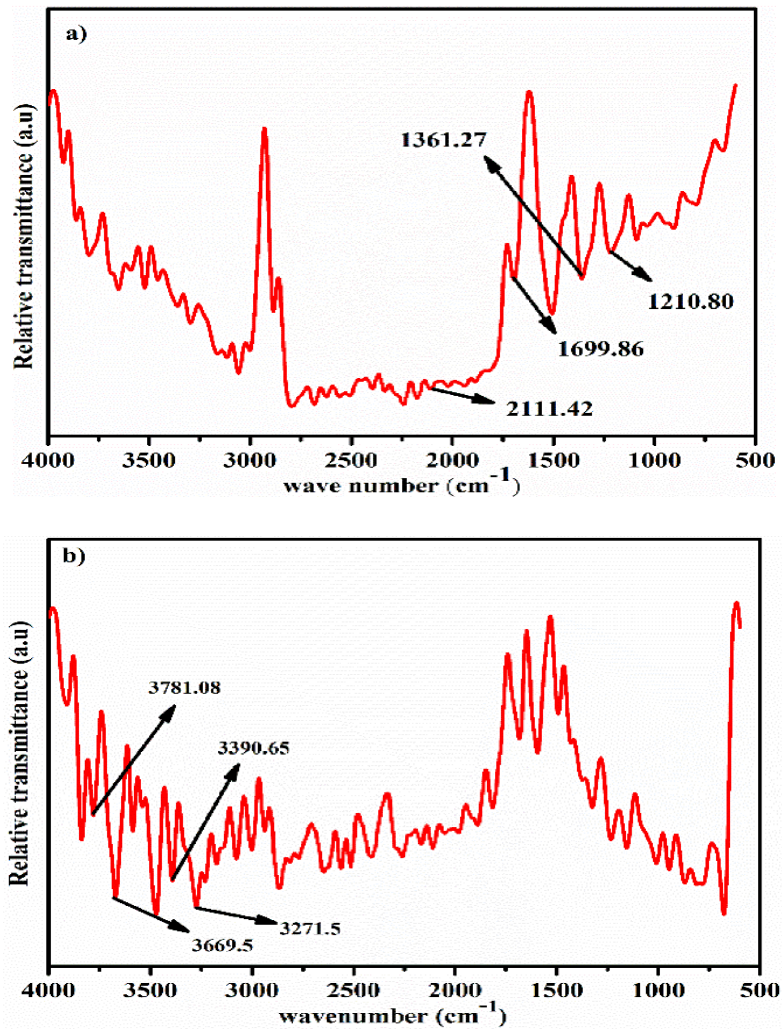


**Figure 4.9** Fourier transformation infrared spectroscopy (FTIR) analysis for a) Coir fibre, b) attached biofilm in anaerobic sludge

The microstructure presented in Figure 4.10b is represented as activated sludge to display the gel layer based on the microporous as well as a dotted declaration of microbes such as streptococcus sp. Bacilli (rod-shaped) and Cocci (spherical shaped) have grown pairs, chains, or clusters over the surface of suspended biomass in the aerobic reactor.

So, the finished occurrence due to the gram-negative bacteria (*E. coli*) is confirmed in the activated sludge. Figure 4.10c to 4.10f show the SEM results of bacterial biofilm.

The figures showed similarity with SEM images of filamentous bacteria (Han *et al.*, 2018). Thus, we can understand that biofilm predominantly consisted of filamentous bacteria before and after the load.

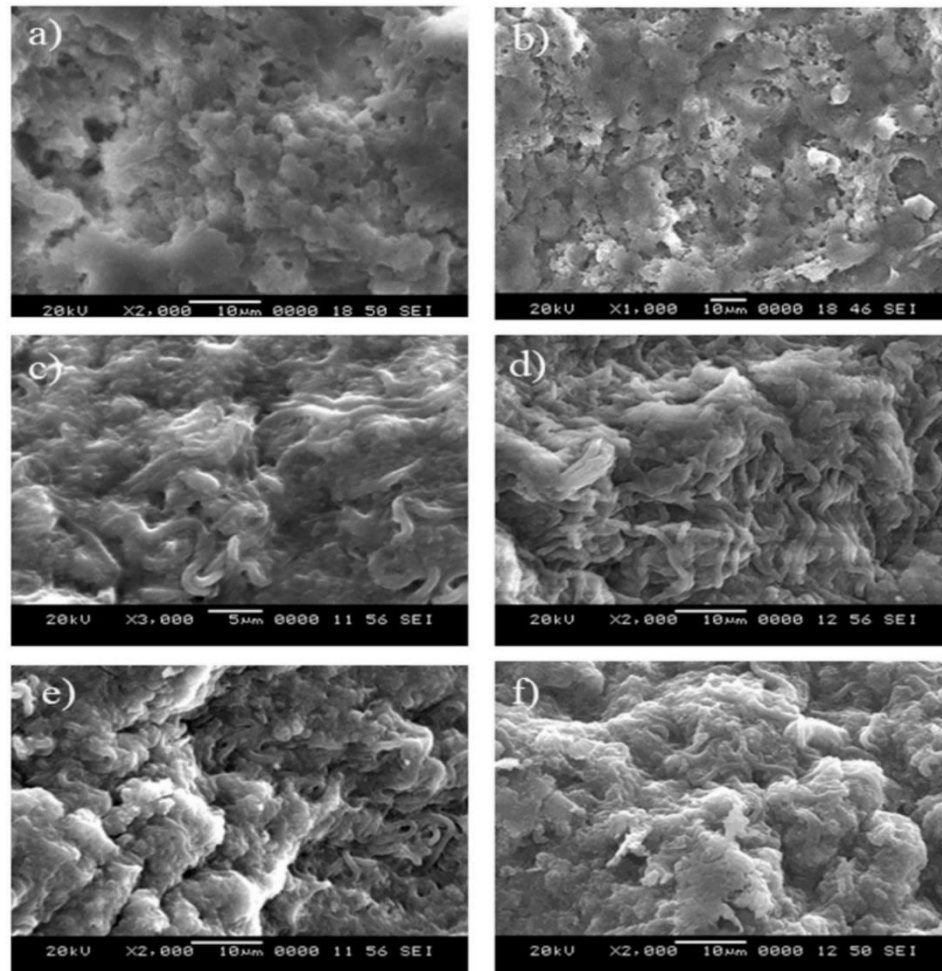


**Figure 4.10** Surface morphology studies for (a) initial seed of anaerobic sludge, (b) initial seed of activated sludge, (c) Biofilm after the application of shock load-1, (d) Biofilm after the application of shock load-2, (e) Biofilm after the application of shock load-3 and (f) Biofilm after the application of shock load-4

### 4.3 IMMOBILIZATION PHOTOCATALYST PREPARATION AND APPLICATION FOR TCS TREATMENT IN GW

#### 4.3.1 Structures and surface morphologies of Immobilized ternary composite ( $\text{Fe}_2\text{O}_3\text{-TiO}_2\text{/PVP}$ ) coated film

It is significant to know the temperature at which the composite solution is altered into the proper coating film at the required temperature. To achieve this, the precursor solution's thermal analysis is performed. Figure 4.11 (a) displays the TGA thermogram of the ternary composite solution.

For 'A' (at 60-80 °C) and 'B' (at 320-350 °C), the two significant weight losses, and the corresponding differential analysis (DTA) responses (A' and B'; Figure 4.11 (b)) suggest that the loss of weight around 60-80°C is due to solvent evaporation; similarly, the drastic loss of weight at 320-350°C, since the degradation of the precursor solution. The initial phase of degradation occurs at 320 °C. More specifically, the weight loss at 350 °C has an intense other exothermic reaction in the DTA counterpart, indicating that the degradation occurs at a fixed temperature of 350 °C.

The Fe<sub>2</sub>O<sub>3</sub>-TiO<sub>2</sub>/PVP coated substrate is scratched in the inconsistency of the stylus tip during the scratch hardness test, which results in the shearing of binding atoms. As the bond strength value gets high, the scratch hardness is most likely at its maximum. Cohesive detailed integrated of the catalytic film is indirectly gauged by scratching hardness. The compressive strength of the coated film is improved with greater cohesive bond strength. The scratch hardness values (Hs) are calculated using the formula below. (4.1)(Augustin *et al.*, 2016).

$$H_s = 8F_N/\pi b^2 \quad (4.1)$$

Where  $F_N$  is the normal force used, and  $b$  is the average scratch width.

Figure 4.13 (c) demonstrates the top interpretation of the scratches imprinted on the coated film with different Fe<sub>2</sub>O<sub>3</sub>/TiO<sub>2</sub> compositions. All the films deposited with the coating have been formed with a thickness of 15.84 μm and a surface roughness of 2.93 μm. It is observed that the 5% Fe<sub>2</sub>O<sub>3</sub>/TiO<sub>2</sub> composition catalytic film is the optimum coating with higher scratch hardness 7.984 GPa compared to other Fe<sub>2</sub>O<sub>3</sub>/TiO<sub>2</sub> composition catalysts (Table 4.6).

The XRD patterns of PVP, Fe<sub>2</sub>O<sub>3</sub>, TiO<sub>2</sub>, the binary composite (TiO<sub>2</sub>/PVP), and the ternary composites (Fe<sub>2</sub>O<sub>3</sub>-TiO<sub>2</sub>/PVP) are shown in Figure 4.12 (a). The XRD analysis for the composite samples is carried out at an angle ranging from 10° to 90°.

Diffraction peaks are identified as too broad and shallow for PVP. This broad curve and low intensity indicate that the PVP is amorphous or very poor crystalline in nature.

**Table 4.6** Scratch hardness at different ratio Fe<sub>2</sub>O<sub>3</sub>-TiO<sub>2</sub> coated samples

Fe <sub>2</sub> O <sub>3</sub> /TiO <sub>2</sub> compositio n	Scratch width (μm)				Scratch hardness (GPa)
	Position1	Position 2	Position 3	Average	
1%	108.3	107.7	114.8	110.27	4.186
3%	108.3	91.8	141.6	113.9	3.924
5%	79.3	74.38	85.86	79.85	7.984
7%	102.3	100.6	101.2	101.37	4.954
9%	109.9	106.6	109.9	108.8	4.3

The compounds that the distinct peaks have identified are shown in Table 4.7; it indicates the presence of TiO<sub>2</sub> and Fe<sub>2</sub>O<sub>3</sub> in the composite samples. Pure Fe<sub>2</sub>O<sub>3</sub> shows diffraction peaks having corresponding values such as 24.2°, 33.1°, 35.7°, 40.9°, 49.4°, 54.2°, 57.6°, 62.4°, 64.0°, 69.6°, 72.0°, 75.5°, are assigned to the (012), (1 04), (110), (113), (024), (116), (122), (214), (300), (208), (101), and (220) diffraction based on the planes, respectively (JCPDS file No.33-0664). The distinct peaks of the TiO<sub>2</sub> (JCPDS file No. 84-1286), for both Pure TiO<sub>2</sub> and TiO<sub>2</sub>/PVP at 2θ values of 25.38°, 37.88°, 48.11°, 53.94°, 55.14°, 62.75°, 68.88°, 70.35°, 75.15°, and 82.92°, corresponds to the (1 0 1), (0 0 4), (2 0 0), (1 0 5), (2 1 1), (2 0 4), (1 1 6), (2 2 0), (2 1 5), and (2 2 4) diffraction planes, respectively. The XRD peaks of Fe<sub>2</sub>O<sub>3</sub> (JCPDS file No. 33-0664) in Fe<sub>2</sub>O<sub>3</sub>-TiO<sub>2</sub>/PVP (high temp at 320°C) are found at 35.71°, 57.39°, and 82.92°, assigned to the (1 1 0), (1 2 2), and (0 2 10) reflections, respectively, whereas, in Fe<sub>2</sub>O<sub>3</sub>-TiO<sub>2</sub>/PVP (low temp at 60 °C), no peak that belongs to Fe<sub>2</sub>O<sub>3</sub> due to the low amount of (only 5 wt.%) Fe<sub>2</sub>O<sub>3</sub>; its amorphous phase (small size of crystallites). Hence, the high-temperature treatments improve the crystallinity of the coated film (Banisharif *et al.*, 2015).

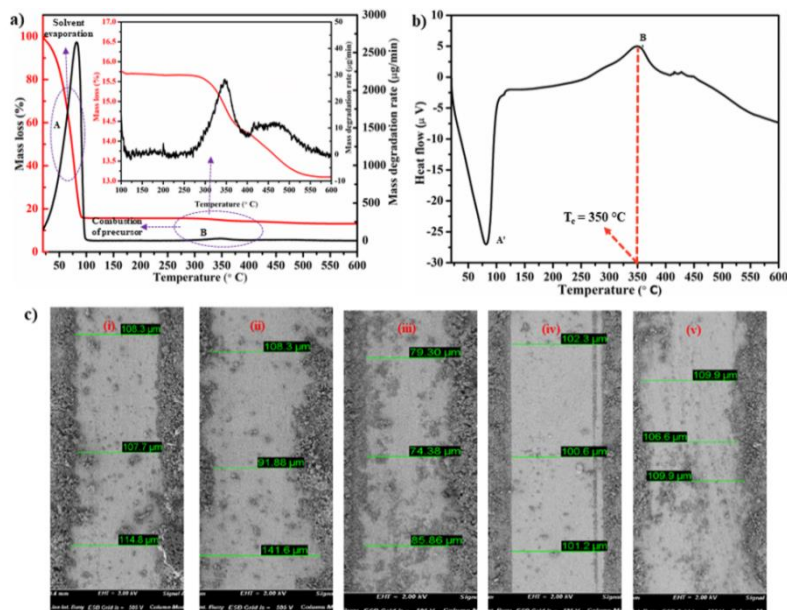


**Figure 4.11** (a) TGA thermogram (b) DTA trace for  $\text{Fe}_2\text{O}_3\text{-TiO}_2/\text{PVP}$  composite solution and (c) FESEM micrographs of scratches on coated samples with scratch width dimensions at different ratios of  $\text{Fe}_2\text{O}_3/\text{TiO}_2$  compositions of (i) 1 atomic wt.%, (ii) 3 atomic wt.%, (iii) 5 atomic wt.%, (iv) 7 atomic wt.% and (v) 9 atomic wt.%.

In the FTIR spectrum, the C=O units of PVP show a maximum of  $1659.4\text{ cm}^{-1}$ . This unique peak is being studied to investigate the effect of metals on PVP. PVP titanium-iron complexes offer a range of apparent peaks, starting around 1403, 1287, and  $1630\text{ cm}^{-1}$ , respectively corresponding to C–N–C, N–C, and C=O (K V 2014). It is shown from Figure 4.12 (b) the frequencies of C–NC, NC, and C=C group movement have shifted in the samples.

The peak positions of both the C=O and N–C polymer chains have shifted. The movement of the peaks from the higher wavenumber zone to the higher wavenumber region indicates a weakening of the C–N–C bond. The titanium ions, ferrous ions, and PVP engage with the oxygen, including its C=O molecule of the polymer, resulting in a complex. The creation of C–N–C, =O, and –NC bonds from oxidized PVP is displayed here as an example of boosting photoactivity via an electron donor. The surface morphology of  $\text{Fe}_2\text{O}_3\text{-TiO}_2/\text{PVP}$  composites is examined by FESEM, as shown in Figure 4.12 (c). It is observed that the  $\text{TiO}_2$  and  $\text{Fe}_2\text{O}_3$  are in a spherical-like structure with a smooth surface (obtained by annellation at  $320\text{ }^\circ\text{C}$ ). This homogeneity helps in the uniform coating of this ternary composite on the surface of the glass pipe.



**Table 4.7** Compounds identified in the different composite samples using XRD

S. No	Composite	Compounds	Peaks identified
A	PVP		No peaks identified
B	Pure Fe <sub>2</sub> O <sub>3</sub>	Fe <sub>2</sub> O <sub>3</sub>	24.2°, 33.1°, 35.7°, 40.9°, 49.4°, 54.2°, 57.6°, 62.4°, 64.0°, 69.6°, 72.0°, 75.5°
C	Pure TiO <sub>2</sub>	TiO <sub>2</sub>	25.4°, 37.0°, 37.9°, 38.7°, 48.1°, 53.9°, 55.1°, 62.7°, 68.9°, 70.4°, 75.1°, 76.1°, 82.9°
D	TiO <sub>2</sub> /PVP	TiO <sub>2</sub>	25.4°, 37.0°, 37.9°, 38.7°, 48.1°, 53.9°, 55.1°, 62.7°, 68.9°, 70.4°, 75.1°, 76.1°, 82.9°
E	Fe <sub>2</sub> O <sub>3</sub> -TiO <sub>2</sub> /PVP (low temp)	TiO <sub>2</sub>	25.3°, 37.0°, 37.7°, 38.5°, 48.0°, 53.8°, 55.0°, 62.6°, 68.7°, 70.2°, 75.0°, 82.6°
		Fe <sub>2</sub> O <sub>3</sub>	No peaks identified
F	Fe <sub>2</sub> O <sub>3</sub> -TiO <sub>2</sub> /PVP (high temp)	TiO <sub>2</sub>	25.4°, 37.0°, 37.9°, 38.7°, 48.1°, 53.9°, 55.1°, 62.7°, 68.9°, 70.4°, 75.1°, 76.1°, 82.9°
		Fe <sub>2</sub> O <sub>3</sub>	35.7°, 57.4°, 82.9°

The uniform distribution of elements on the surface of the ternary composites is seen in the surface elemental mapping (see Figure 4.12 d). The EDAX spectrum confirms Fe<sub>2</sub>O<sub>3</sub>-TiO<sub>2</sub>/PVP ternary composite elements, as it exhibits the characteristic peaks of Ti, Fe, O, N and C. The obtained film thickness of the Fe<sub>2</sub>O<sub>3</sub>-TiO<sub>2</sub>/PVP ternary composite film is in the range of 13.8 to 16.4 μm (Figure 4.12 e) for the ternary composite obtained after calcination at 320 °C. The elemental composition of the Fe<sub>2</sub>O<sub>3</sub>-TiO<sub>2</sub>/PVP ternary composite film is shown in Figure 4.13.

It is also observed that the film obtained is more uniform and has a low thickness. The immobilized catalytic film thickness varies in a range, from 6.9 to 34.1 μm, and is practically suitable for photocatalysis (Han and Bai 2011). The R-profile is determined by a surface roughness meter for the coated film of Fe<sub>2</sub>O<sub>3</sub>-TiO<sub>2</sub>/PVP (Hajduk 2018), whose thickness is found to be 15.84 μm (shown in Figure 4.14).

### ***Surface roughness analysis***

The average arithmetic deviation of the profile  $R_a$ :

$$R_a = \frac{1}{N} \sum_{i=1}^N |Y_i| = 2.93 \mu\text{m} \quad (4.2)$$

The average square deviation of the profile  $R_q$ :

$$R_q = \sqrt{\frac{1}{N} \sum_{i=1}^N Y_i^2} = 3.61 \mu\text{m} \quad (4.3)$$

The maximum height of the profile  $R_z$ :

$$R_z = \frac{1}{N} \sum_{i=1}^N R_{zi} = 15.84 \mu\text{m} \quad (4.4)$$

### **4.3.2 BET analysis**

The two key factors for  $\text{Fe}_2\text{O}_3\text{-TiO}_2$  heterojunction production are the appropriate porosity and high porosity (small particle size). Brunauer–Emmett–Teller (BET) investigation finds that when  $\text{N}_2$  is adsorbed and desorbed at 77K, the produced  $\text{Fe}_2\text{O}_3\text{-TiO}_2$  nanomaterial exhibits type IV isotherm. This suggests that the composite has a well-developed mesoporous nanostructure (shown in Figure 4.15).

The area of surface and quantity of volume based on BET is obtained from the Value for  $\text{Fe}_2\text{O}_3\text{-TiO}_2$  at high temperature due to the following values  $56.532 \text{ m}^2/\text{g}$  and  $0.2677 \text{ cm}^3/\text{g}$ , correspondingly. Moreover, the area of the surface volume is  $\text{Fe}_2\text{O}_3\text{-TiO}_2$  at high temperature is established to greatly advanced qualified to  $\text{Fe}_2\text{O}_3\text{-TiO}_2$  at low temperature, which verifies the position of saturated  $\text{Fe}_2\text{O}_3$  and temperature in the improvement based on the detailed exterior region. From the corresponding Barrett–Joyner–Halenda (BJH) pore size, the attained indicated aperture width is  $\text{Fe}_2\text{O}_3\text{-TiO}_2$  was established to be  $18.943 \text{ nm}$  (Table 4.8).

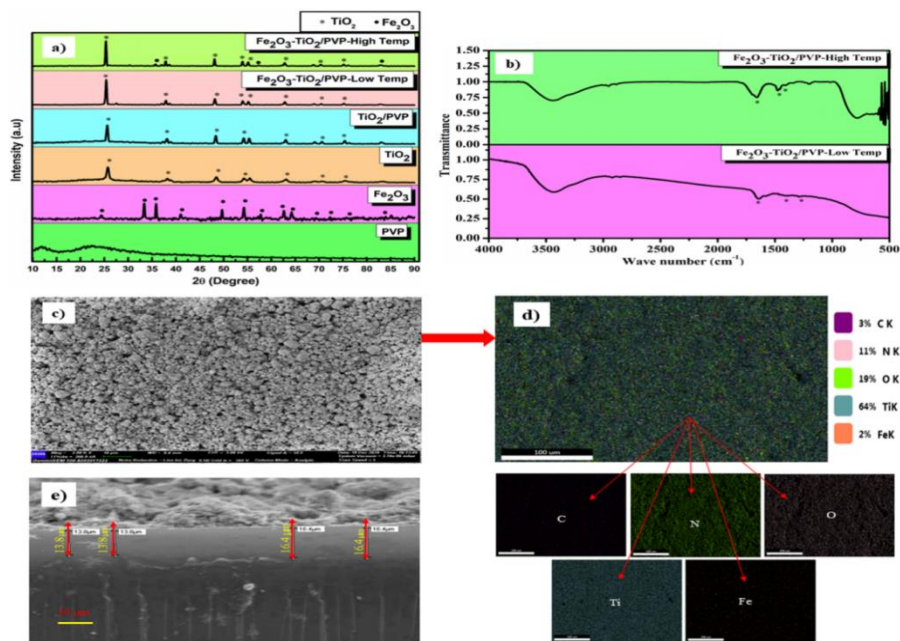


**Figure 4.12** (a) XRD patterns, (b) FTIR spectra, (c) FESEM image, (d) EDAX mapping, and (e) Thickness of coated samples.

### 4.3.3 Mechanical stability of Fe<sub>2</sub>O<sub>3</sub>-TiO<sub>2</sub>/PVP catalyst

In order to investigate the wear performance of Fe<sub>2</sub>O<sub>3</sub>-TiO<sub>2</sub>/PVP coating, sliding wear tests were conducted on the pin on the disc tribometer against EN 32 steel counter body. The wear tests were performed at dry and ambient temperature conditions under different loads (5N, 10N). The sliding distance of 12 m was kept constant. At 5N load, wear of the coating is noted as 5 μm. As increasing load to 10N, it is observed that the wear is increased to 11 μm. The stable friction coefficients of the coatings under 5N and 10N are noted as 0.155 and 0.216, respectively (Figure 4.17).

The friction coefficient increased to some extent as increasing load from 5N to 10N. The removed coating particles again acted as third bodies and influenced the frictional forces. Comparatively, deep grooves are observed at 10N load. The coating delamination observed at some locations was attributed to the formation of micro-cracks during sliding wear operation. These cracks progress and reach critical length as increasing loads. b) Fe<sub>2</sub>O<sub>3</sub>-TiO<sub>2</sub>/PVP after drying @ 60<sup>0</sup> - 80<sup>0</sup>C.

In order to understand the wear mechanism, 3d Profilometer studies were performed. The 3d surface profiles of the worn surfaces are shown in Figure 4.16. The

profile curves of the coatings are shown in Figure 4.16 b, d. The Ra values are noted as 1.580 and 2.065, respectively. From 3d Profilometer studies, maximum wear depth at 5N and 10N are observed as 7.28 and 12.56  $\mu\text{m}$ .

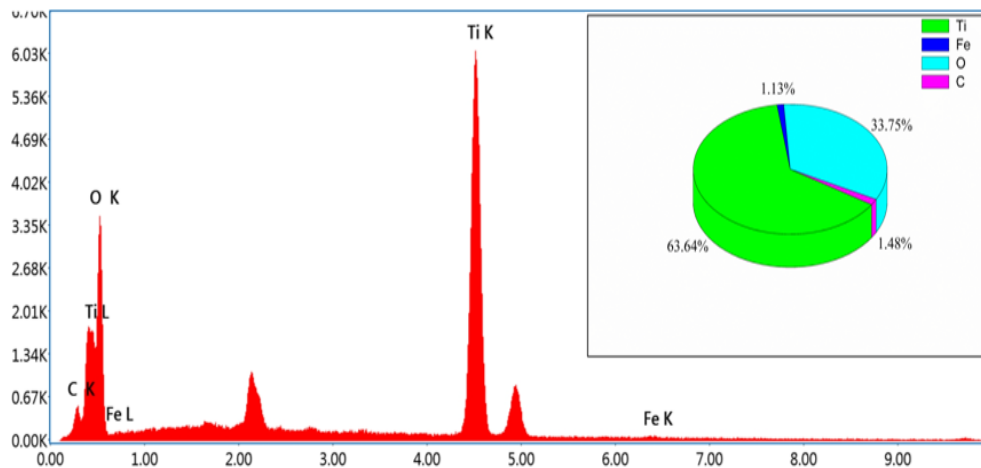


**Figure 4.13** Elemental compositions of Ternary composite annealed at 320°C

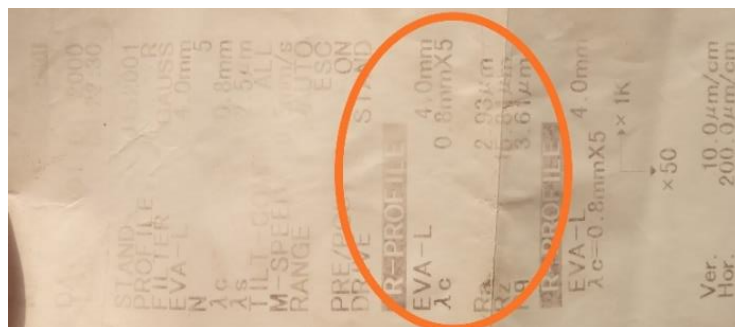


**Figure 4.14** Surface roughness R-profile of ternary composite annealed at 320°C

### 4.3.4 Immobilized photocatalytic degradation of TCS

#### 4.3.4.1 Kinetics of Photodegradation

The photocatalytic performance of immobilized catalytic solar concentrated reactor, under the sunlight for TCS elimination, is examined based on the kinetics energy theorems using a Langmuir-Hinshelwood kinetic representation (Priyanka *et al.*, 2019). The precision of the model fitting is measured by  $R^2$  (Eqn. 4.5):

$$\frac{dC_t}{dt} = k_1(C_0 - C_t) \quad (4.5)$$

Integrating and rearranging the Eqn. (3) gives the linear representation based on pseudo-first-order replica, as represented in Eqn. (4.6):

$$\ln \frac{C_t}{C_0} = -k_1 \times t \quad (4.6)$$

Where  $k_1$  is represented as pseudo first order reaction rate that is the steady-state of photocatalytic degradation ( $\text{min}^{-1}$ ),  $t$  is denoted as irradiation time of the reaction rate (min),  $C_0$  is denoted to as initial final TCS concentration, and  $C_t$  is referred to as final TCS concentration ( $\text{mg L}^{-1}$ ).

Moreover, experiments are obtained that mean  $k_1$  for the photocatalytic formation attained starting of the plot of  $\ln (C_t/C_0)$  against the form of  $t$  for an immobilized catalytic solar concentrated reactor, as shown in Figure 4.18a. The  $\text{Fe}_2\text{O}_3\text{-TiO}_2/\text{PVP}$  catalyst confirms that the photocatalysis process involves  $k_1$  of  $0.105 \text{ min}^{-1}$  and  $k_2$  of  $0.015 \text{ min}^{-1}$  under sunlight. The Langmuir-Hinshel wood kinetic model exhibits the best suitable for photodegradation of TCS since the  $R^2$  value is 0.95 (shown in Figure 4.18b). The best fit model is the 1<sup>st</sup> order kinetic model from this analysis, as can be seen by comparing it with the pseudo-second-order kinetic ideal ( $R^2 = 0.88$ ) is exposed in Figure 4.19.

**Table 4.8** The BET summary of prepared samples

	<b>Area of surface(<math>\text{m}^2/\text{g}</math>)</b>	<b>dimension of pore (nm)</b>	<b>Pore quantity (<math>\text{cm}^3/\text{g}</math>)</b>
<b><math>\text{Fe}_2\text{O}_3\text{-TiO}_2</math> at high temp.</b>	56.532	18.943	0.2677
<b><math>\text{Fe}_2\text{O}_3\text{-TiO}_2</math> at low temp.</b>	15.773	28.234	0.1113

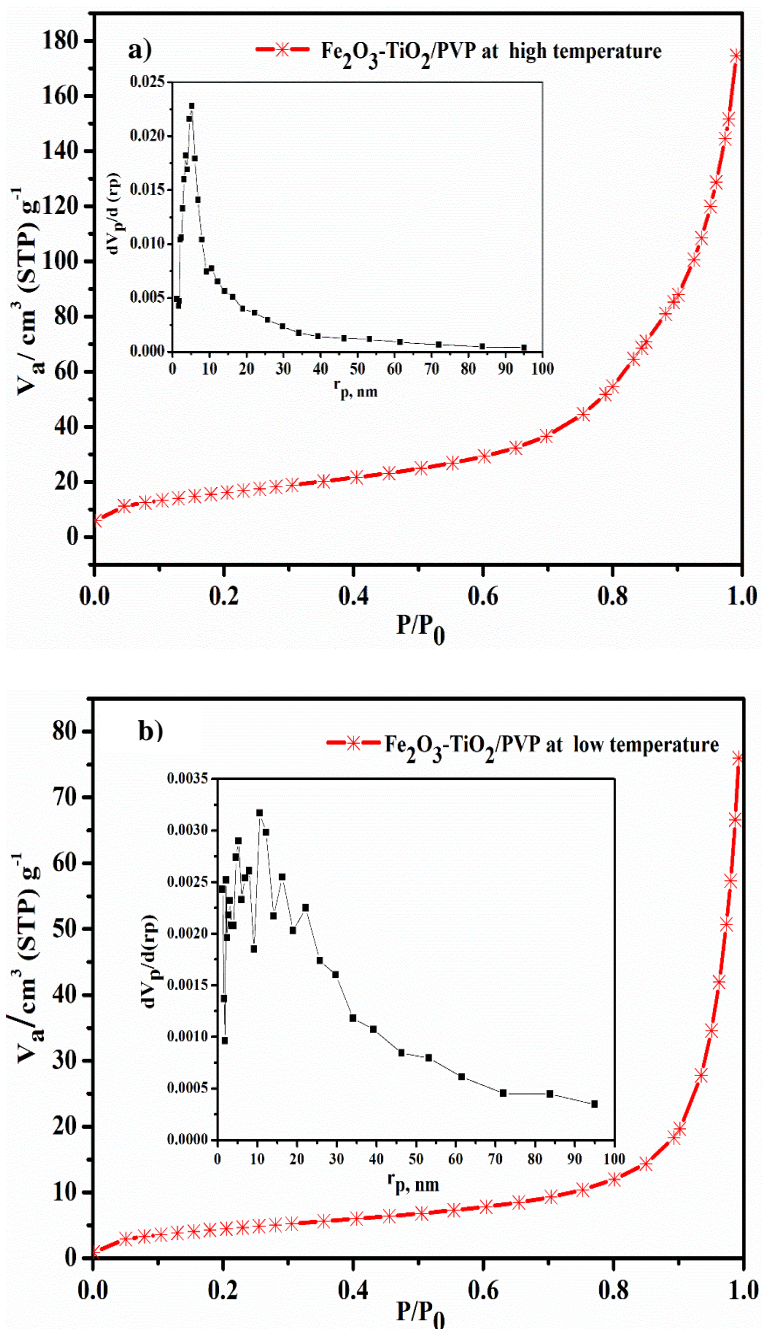


**Figure 4.15** BET surface area: a)  $\text{Fe}_2\text{O}_3$ - $\text{TiO}_2$ /PVP after annealing @  $320^\circ\text{C}$ ,

Further,  $k_{TCS}$  has been compared with different photocatalytic treatment systems of TCS in the present study. Through a kinetic model, the kinetics of the procedure, using 1 to 10  $\text{mg L}^{-1}$  TCS, demonstrates that the observed rate is constant ( $k_{TCS}$ ) and ranges from 0.3405 to 0.0687  $\text{min}^{-1}$  under UV light. Hence, the  $k_{TCS}$  (i.e.,  $k_I = 0.105 \text{ min}^{-1}$ ) for

this present study has been observed in the adequate range, under sunlight, with the immobilized  $\text{Fe}_2\text{O}_3\text{-TiO}_2\text{/PVP}$  catalysts (Azarpira *et al.*, 2019).

#### 4.3.4.2 Response Surface Methodology (RSM)

The surface response is based on the effect of operational considerations based on the TCS degradation output is optimized using a BBD. The BBD has allowed the most important parameters and their communications to be studied, specifically, the contact instance based on the initial level concentration of  $\text{H}_2\text{O}_2$  and the pH. Response surface and contour plots have led to the best situations for the degradation of the TCS, subsequent in 83.27% of TCS removal.

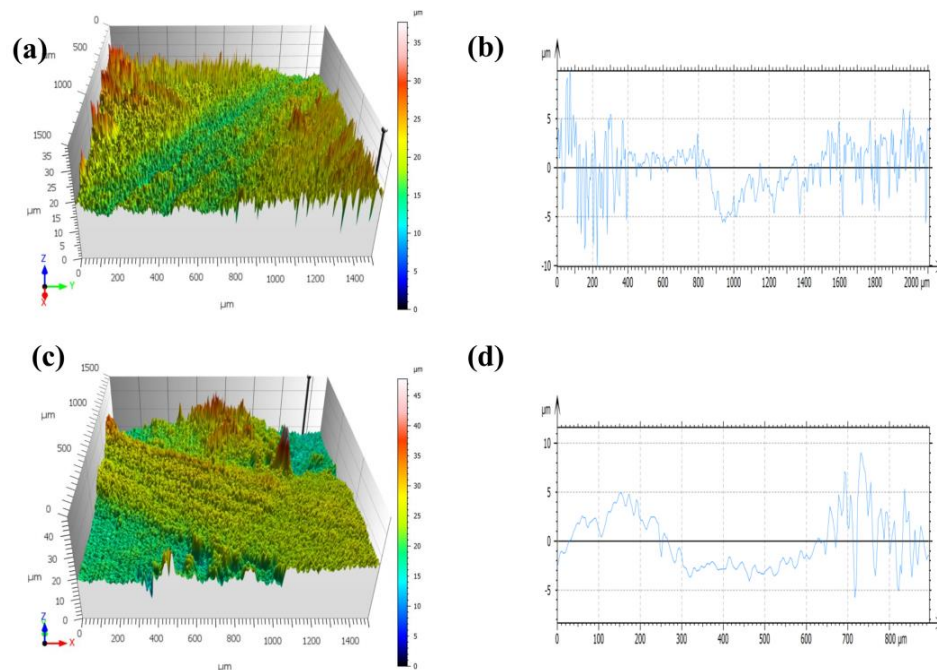


**Figure 4.16** Surface topography of the worn surfaces after pin on disc wear test (a) coating at 5N load (b) coating at 10N load.

The lab-scale continuous photocatalytic reactor has exhibited good performance. Table 4.9 summarizes the efficacy of 17 sets of BBD-based tests.

#### 4.3.4.3 RSM Results

The model equation for the TCS degradation yield, attained using statistical tests after 17 experiments and clearance the negligible effects, is as follows (Eqn. 4.7):

$$Y = 43.33 + 17.33 x_1 - 4.15 x_2 + 17.43 x_3 - 3.01 x_1 x_3 + 6.86 x_1^2 \quad (4.7)$$

The statistical model makes it possible to predict the contact time ( $x_1$ ), the preliminary concentration of  $H_2O_2$  ( $x_2$ ), and the pH ( $x_3$ ) with upright accuracy (the correlation coefficient is found to be  $R^2 = 0.99$ ).

This comparison between experimental and calculated responses shows that an explicit agreement between the values observed and those anticipated by the statistical model is in place (see Figure 4.21a). It is apparent from the residual plot in Figure 4.21b that the mathematical model used in the calculation is appropriate; moreover, it is verified that all experimental and measured response values are consistent. According to the equation of regression (Eq. 4.7), the contact time ( $x_1$ ) and pH solution ( $x_3$ ) have the greatest impact on the response ( $b_1 = +17.33$  and  $b_3 = +17.43$ ).

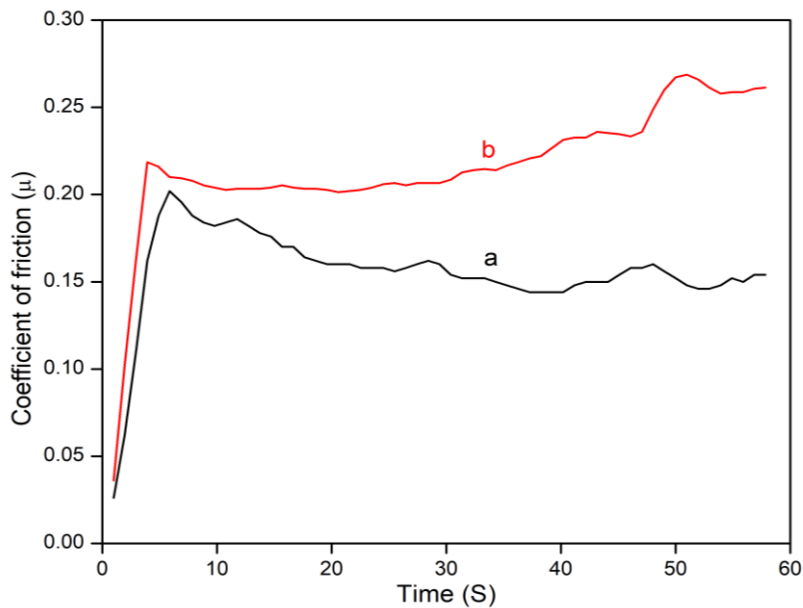


**Figure 4.17** Variation in friction coefficient with respect to sliding time under (a) 5N (b) 10N load

The positive effect of these variables specifies that TCS degradation has improved for increasing the contact time and pH solution. TCS has a pKa of 7.9-8.1 (a weak base) and readily ionizes at environmental pH (Quan *et al.*, 2019). For the pH effect study, the elimination efficiency for TCS at  $pH > pKa$  is about 79.21 %, and it decreases marginally (to~72.6%) because pH is neutral.  $Fe_2O_3-TiO_2/PVP$  has a point of zero charges at  $pH=6.8$  (Figure 4.20), indicating that its surface has a positive



protonation charge at pH lower than 6.8 and deprotonation unenthusiastic charge in the pH superior to the 6.8. The substantial removal of TCS from a fundamental solution is, therefore, due to other adsorption processes, such as hydrogen bonding and precipitation. Dissociation of TCS occurs at  $\text{pH} < \text{pK}_a$ , resulting in a positive charge.

Pseudo first order

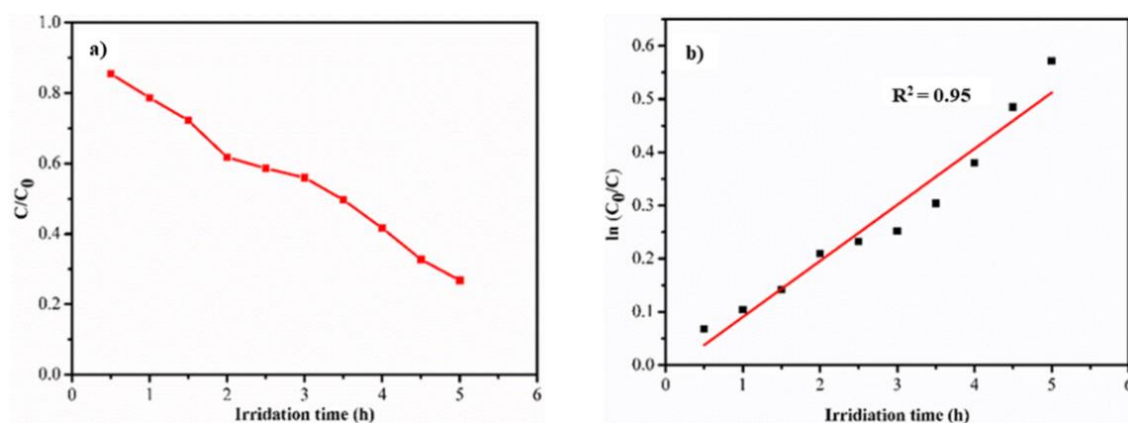


**Figure 4.18** Pseudo first-order kinetics for TCS removal (under natural GW pH)

Pseudo second order

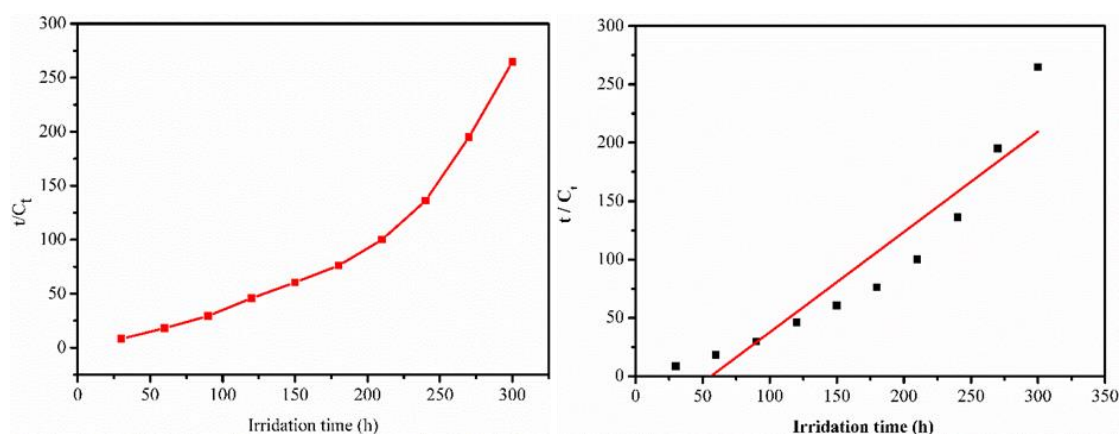


**Figure 4.19** Pseudo second-order kinetics for TCS removal

Thus, between 6.8 (PZC of  $\text{Fe}_2\text{O}_3\text{-TiO}_2/\text{PVP}$ ) and 7.9-8.1 ( $\text{pK}_a$  of TCS), electrostatic attraction is the significant scope in the attachment of TCS to the positively charged  $\text{Fe}_2\text{O}_3\text{-TiO}_2/\text{PVP}$  surface.  $\text{Fe}_2\text{O}_3\text{-TiO}_2/\text{PVP}$  become positively charged at  $\text{pH} < 6.8$ , resulting in a decrease in TCS removal ( $\sim 51\%$ ) as electrostatic repulsion (among the TCS absolutely stimulating and the catalyst exterior positively charged) is dominant. However, the reduction of TCS is significant between pH 7 and 10

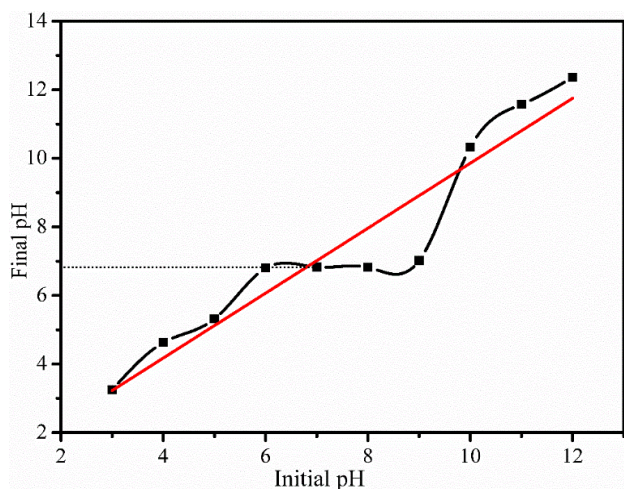


**Figure 4.20** The point zero charges (PZC) of the  $\text{Fe}_2\text{O}_3\text{-TiO}_2/\text{PVP}$  show the final pH as a function of initial pH.

**Table 4.9** Box Behnken Design matrix in the photocatalyst process

<b>Irradiation time (min)</b>	<b>H<sub>2</sub>O<sub>2</sub> (mM)</b>	<b>pH</b>	<b>Actual response (TCS removal efficiency, %)</b>
180	25.5	07	45.81
60	01.0	07	31.28
180	50.0	10	54.35
180	01.0	10	61.65
300	50.0	07	62.69
300	25.5	04	51.03
300	01.0	07	72.59
180	25.5	07	41.22
180	25.5	07	46.25
300	25.5	10	79.21
60	25.5	10	51.46
180	01.0	04	29.69
60	25.5	04	11.26
180	25.5	07	42.13
60	50.0	07	29.69
180	50.0	04	15.29
180	25.5	07	41.25

-(increasing from ~ 72.6 to 79.21 %), and the target TCS is more accomplished of photocatalytic degradation in strongly alkaline conditions.

The other significant parameter is the initial concentration of H<sub>2</sub>O<sub>2</sub>. The negative sign of this coefficient ( $b_2 = -4.15$ ) shows an indirect relationship between the preliminary concentration of H<sub>2</sub>O<sub>2</sub> and the degradation of TCS, which decreases due to an increase in H<sub>2</sub>O<sub>2</sub> concentrations. When the concentration of H<sub>2</sub>O<sub>2</sub> is higher, the excess H<sub>2</sub>O<sub>2</sub> entraps the OH• radicals to form weaker oxidant H<sub>2</sub>O• radicals (Reza *et al.*, 2017; Tseng *et al.*, 2012). This undesirable reaction retards TCS removal efficiency.

#### **4.3.4.4 Model Validation**

Model validation is mainly based on the Analysis of Variance (ANOVA) to confirm based on the capability of second-order replica, showing the importance of the affects on individual parameters. Moreover, the outcomes are enclosed in Table 4.10.

The F-value in the model of photocatalysis is 93.55, which indicates that the model is significant. As the P-value is below 0.05, the model parameters are vital in predicting the TCS removal efficiency.

The calculated R<sup>2</sup> of 0.9346 is insensible contract using an attuned R<sup>2</sup> of 0.9812, which means the difference is fewer than 0.2. The closer the R<sup>2</sup> to 1, the better the connection among the independent variables is expressed, and the reaction becomes more precise.

The Adjusted R<sup>2</sup> = 0.98 is very close to the R<sup>2</sup> value for photocatalysis, indicating no additional terms in the model. Pred-R<sup>2</sup> for the process is equal to 0.93, which shows the ability of the model to predict TCS removal. The COV value of the presented model in the photocatalysis process is 5.59%, which is less than 10%; the model proposed is reliable and accurate (Hassanshahi and Karimi-Jashni 2018).

#### **4.3.4.5 Optimization**

Moreover, to find out the optimal charge is independent considerations, the pH is initially maximized to be similar to the pH of raw GW for the highest removal efficiency of TCS in the photocatalytic process; to minimize the cost of chemicals required for pH adjustment.

**Table 4.10** ANOVA of Quadratic model for TCS degradation rate

Source	Sum of Squares	D F	Mean Square	F-value	p-value	
<b>Model</b>	5359.35	9	595.5	93.55	< 0.0001	<b>Large</b>
<b>A-Contact time</b>	2514.47	1	2514	395.00	< 0.0001	
<b>B-H<sub>2</sub>O<sub>2</sub></b>	137.70	1	137.7	21.63	0.0023	
<b>C-Ph</b>	2429.04	1	2429	381.58	< 0.0001	
<b>AB</b>	17.26	1	17.26	2.71	0.1436	
<b>AC</b>	36.12	1	36.12	5.67	0.0487	
<b>BC</b>	12.60	1	12.60	1.98	0.2022	
<b>A<sup>2</sup></b>	198.30	1	198.3	31.15	0.0008	
<b>B<sup>2</sup></b>	5.40	1	5.40	0.8480	0.3878	
<b>C<sup>2</sup></b>	16.09	1	16.09	2.53	0.1559	
<b>Residual</b>	44.56	7	6.37			
<b>Lack of Fit</b>	19.66	3	6.55	1.05	0.4611	<b>not significant</b>
<b>Pure Error</b>	24.90	4	6.22			
<b>C or Total</b>	5403.91	16				
<b>Std. Dev.:2.52; R<sup>2</sup>:0.992; Mean: 45.11; Adj. R<sup>2</sup>: 0.9812; C.V: 5.59%; Pred. R<sup>2</sup>:0.9346; Adeq. Precision: 36.33.</b>						

In addition, the use of metal oxide concentration is minimized to be economical in the immobilized coating technique. Finally, to reduce the use of the UV lamp, the reaction time is moderate with solar light absorption. After performing trials of the various operating parameters by BBD, the response surface and contour plot have been drawn using Design-Expert 11 software (see Figure 4.21c and 4.21d). This plot analysis allows the following optimal conditions to be deduced for the TCS degradation  $9 \leq \text{pH} \leq 10$ , a contact time of 300 min of stream rate of 50 mL/min, and an initial H<sub>2</sub>O<sub>2</sub> concentration is 1mM, resulting in TCS degradation of 83.27%. The performance of the present study is compared with previous studies, as shown in Table 4.11.

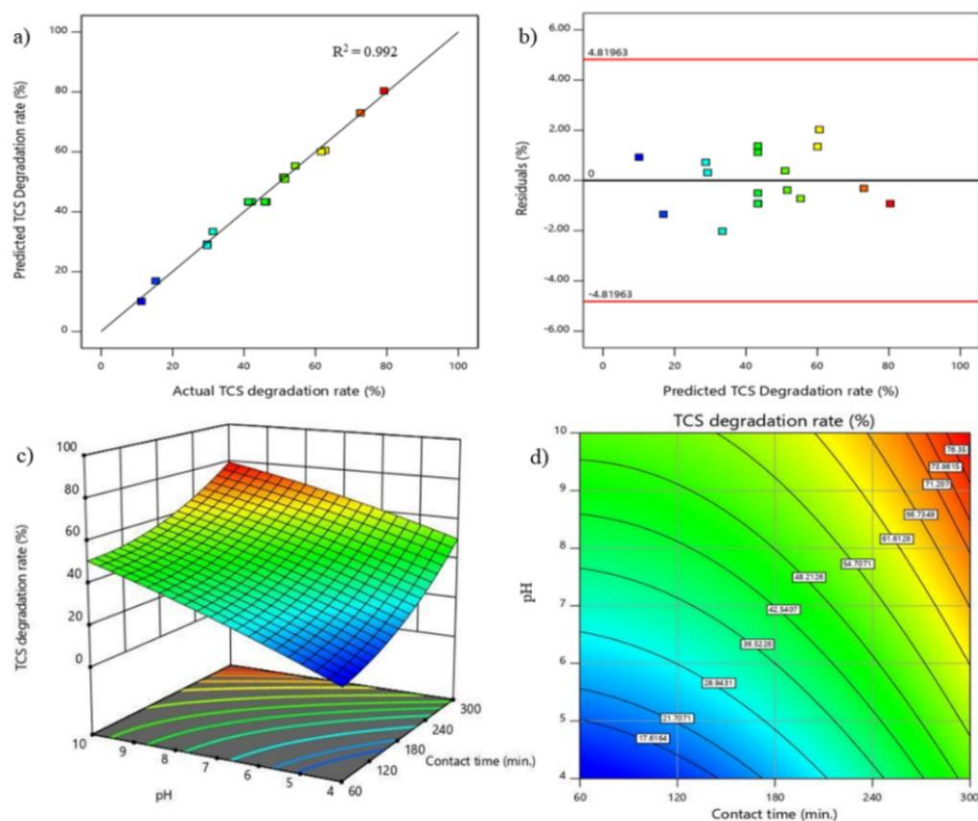


**Figure 4.21** Response surface analysis (a) experimental and theoretical responses, (b) predictable model's residual analysis, (c) Response surfaces, and (d) contour plots showing the effect of the contact occasion and the value of pH solution of the TCS degradation

#### 4.3.5 Plausible Degradation pathway of TCS

From the preliminary studies, it is observed that TCS is not completely degraded in the photocatalysis process. It is also made possible that the photocatalytic process could result in some intermediates derived from the parent compound. To find these intermediate compounds, further experiments are carried out. The final irradiated sample is analyzed using LC-MS to identify the intermediate compounds formed during photocatalysis. Since the photocatalytic degradation of TCS is carried out on the synthetic GW effluent, different noise peaks and interference of other constituents present in GW are possible.

**Table 4.11** Comparison of the present study with other photocatalytic treatments of TCS from the aqueous medium

S. No.	PPCPs	Catalysts combination	Light source	Optimal conditions	Efficiency	References
1	TCS	ZnO powder	UV light	pH 10, Time 90 min	90%	Arifin <i>et al.</i> (2021)
2	TCS	TiO <sub>2</sub> nano tubes	UV light	pH 5.8, Time>30 min	62.2%	Arifin <i>et al.</i> (2021)
3	TCS	immobilized catalyst Fe/Nb <sub>2</sub> O <sub>5</sub>	UV light	pH 8.5, Time 80 min	91%	Michel Z. Fidelis <i>et al.</i> (2019)
4	TCS	TiO <sub>2</sub> films on porous Tezontle stone	UV light	pH = 5	65.9%	Sandra Martínez <i>et al.</i> (2014)
				pH = 7	58.5%	
				pH = 9	74.7%	
5	TCS	TiO <sub>2</sub> Nanotubes	UV light	Time >30 min	67.2%	Liu <i>et al.</i> (2013)
6	TCS	TiO <sub>2</sub>	UV-A LED	pH 6.5, Time 4 h	100%	Sophie Schröder <i>et al.</i> (2020)
7	TCS	ZnO powder	UV light	Time 90 min	90%	Kosera <i>et al.</i> (2017)
8	TCS	Ag <sup>0</sup> -Ag <sub>2</sub> O@nanocomposite hydrogel	photocatalysis	pH 6, time 180 min	89%	Sharma <i>et al.</i> (2020)
9	TCS	TiO <sub>2</sub> & Fe <sub>2</sub> O <sub>3</sub>	Sun light	pH 10, Time 300 min	83.27 %	Present study

Majorly, TCS undergoes three different reaction mechanisms to produce different intermediates through hydroxylation, OH radical attack on the aromatic ring, and de-chlorination reactions. These intermediates subsequently degrade to other smaller organic intermediates, which can further be mineralized to CO<sub>2</sub> and water. Based on these LC-MS data and comparison with the available literature, the plausible degradation pathway of TCS is elucidated. Eleven intermediate products have been identified, and their molecular structures are inferred m/z 318, m/z 306, m/z 255, m/z 248, m/z 235, m/z 199, m/z 163, m/z 147, m/z 142, m/z 113, m/z 109 and m/z 94. Figure 4.22 displays the photocatalytic degradation pathway of TCS. Firstly, the attack of the h<sup>+</sup> and •OH radicals, produced from the solar irradiation of the immobilized Fe<sub>2</sub>O<sub>3</sub>-TiO<sub>2</sub>/PVP catalyst has led to the formation of the chlorophenol intermediates I1 (m/z

306) by hydroxylation reaction and disproportionation mechanism. The chlorophenol intermediates are unstable. Therefore, they are further oxidized to quinone, I2 (m/z 318), and finally mineralized into insignificant molecular inorganic acids (Li *et al.*, 2019). The intermediate I2 sequentially undergo C-O bond cleavage due to the •OH radical attack and another product at m/z 142 (I3). Secondly, •OH radicals and h<sup>+</sup> attack on the ether bond of TCS; another intermediate I4; identified as m-Dichlorobenzene (m/z 147), which is generated by OH radical attack and aromatic ring cleavage. Further, intermediate I4 is reduced to another intermediate (I5), identified as chlorobenzene (m/z 113), through de-chlorination reaction (Xie *et al.*, 2019). Through hydroxylation reaction, the intermediate I4 further transforms into another product with m/z 163 (I6). And it is also reduced to another compound, I7, through successive de-chlorination reactions, which are identified as phenol (m/z 94).

On the other hand, the intermediate, (I8) 4-chlororesorcinol (m/z 143) is derived from TCS due to C-O cleavage (Chen *et al.* 2015); further, it is reduced to another intermediate, (I9); resorcinol (m/z 109) can also be formed by the de-chlorination reaction from 4-chlororesorcinol. Similarly, in another reaction mechanism, 5-chloro-2-(2chlorophenoxy) phenol, I10 (m/z 255) is generated from TCS by a de-chlorination reaction since the C-Cl bond cleavage is formed in the effluent treatment. The same compound has also been identified in the literature of other works. Further, I10 undergo Cl substitution by OH and results in another intermediate I11, identified as 5-(4-Chlorobenzyl)-2-furoic acid, with them/z of 235 and release of HCl. The intermediate I11 can result in two more transformation products with hydroxylation and de-chlorination reactions.

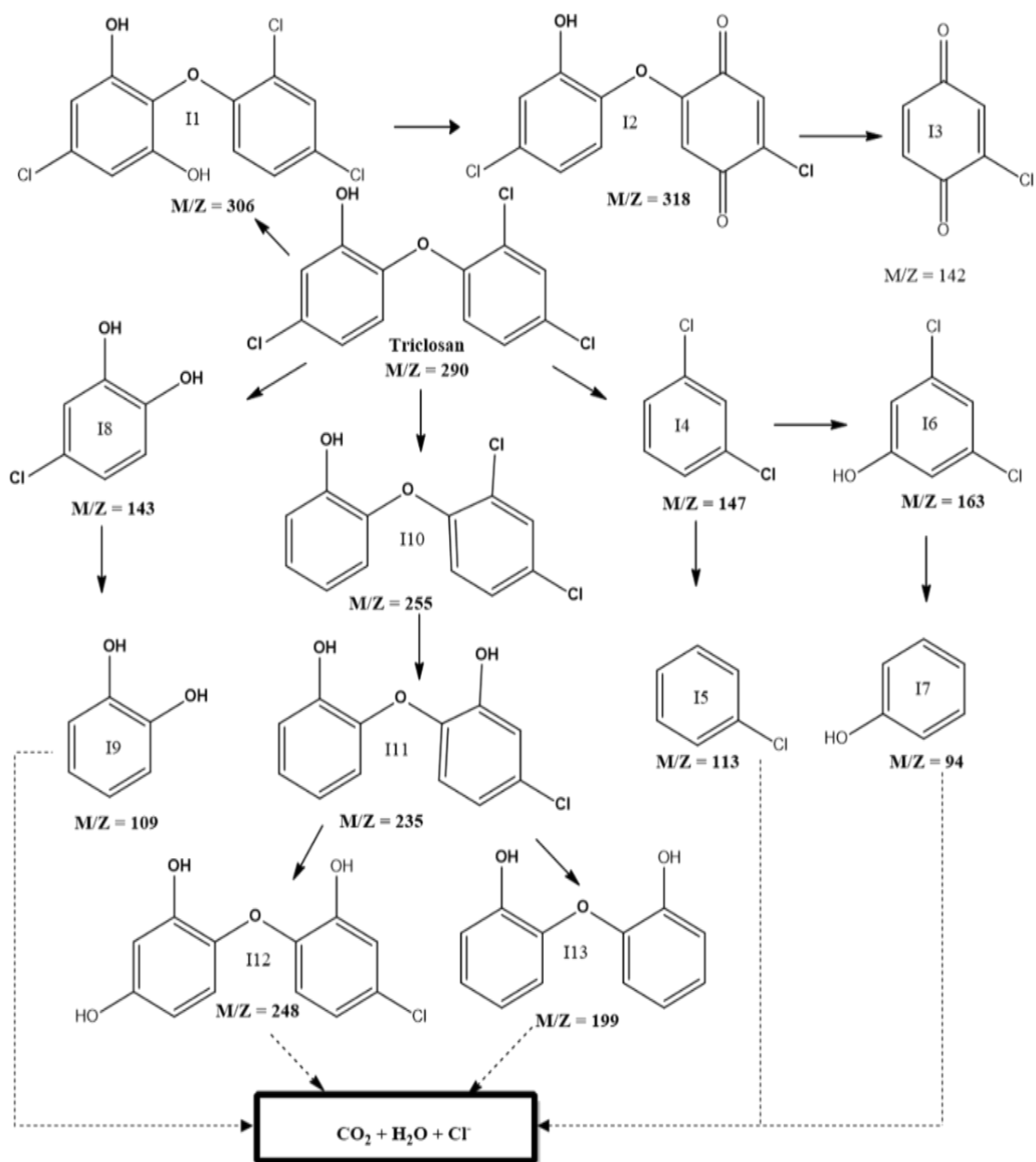


**Figure. 4.22** Plausible degradation pathway of TCS by immobilized ternary composite ( $\text{Fe}_2\text{O}_3\text{-TiO}_2\text{/PVP}$ ) coating catalyst



**Table 4.12** Concentration of metal ions released from the coated catalyst into solar photocatalysis outlet as determined by ICP-OES

Catalyst exposure	Exposure time	The concentration of metal ions released (ppm)	
		Ti (337.280 nm)	Fe (259.940 nm)
Natural sun light	After 1 h	0.01	0.06
	After 2 h	ND	ND
	After 3 h	0.02	0.08
	After 4 h	ND	0.01
	After 5 h	0.02	ND
Dark conditions	6 months	0.01	0.06

(ND = Not detected)

First, the intermediate I12 with  $m/z$  248 resulted from hydroxylation reaction on the side chain of the intermediate I10. Second, the same intermediate I10 endures a de-chlorination reaction and produces another intermediate I13 at  $m/z$  199. All the formed intermediates are possibly mineralized to simpler inorganic compounds by a ring-opening mechanism.

#### 4.3.6 Toxicity studies

The developed  $\text{Fe}_2\text{O}_3\text{-TiO}_2/\text{PVP}$  catalyst has applications in tertiary treatments such as photocatalysis that are exposed to aquatic environments. So, it is important to investigate the stability, shelf life, and toxicity of any metals leached out of the coated film into the aquatic environment. Leaching of metals from the  $\text{Fe}_2\text{O}_3\text{-TiO}_2/\text{PVP}$  catalyst causes metals bioaccumulation in aquatic animals and biomagnification through the food chain, which may have short and long-term effects on aquatic life and human health.

The immersion GW effluent of the  $\text{Fe}_2\text{O}_3\text{-TiO}_2/\text{PVP}$  catalyst contains trace amounts of Ti and Fe. Both Ti and Fe concentrations are very low in the leached metals (almost  $< 0.1$  ppm in all conditions), as observed from Table 4.12. The rate of Ti release is almost negligible, which has been influenced by the addition of  $\text{Fe}_2\text{O}_3$  to the catalyst (Wahyuningsih *et al.*, 2018). So, the catalytic film provides a stable surface that prevents the peel out of metals from the coating layer beneath and delivers the highest TCS degradation rate.

#### 4.3.7 Cost implications/energy consumption

The power consumption of the present study is compared with other studies, shown in Table 4.13.

Total power consumed (kWh) = Power utilized (kW) × response instant (h)

Entire power used /COD elimination (kWhkg<sup>-1</sup>) =  $\frac{\text{Total power consumed ,kWh}}{(C_0 - C_f) \times \text{working volume, L}}$

**Table 4.13 Comparison of power consumption of present system with other systems**

<b>Treatment</b>	<b>Initial level of COD value, (mg/L)</b>	<b>Elimination efficiency based on COD, (%)</b>	<b>operating level, l</b>	<b>Power consumption, (W)</b>	<b>Reaction time (h)</b>	<b>entire level of power utilization, (kWh)</b>	<b>Power consumed at the COD elimination (kWhkg<sup>-1</sup>)</b>	<b>References</b>
<b>UV/TiO<sub>2</sub></b>	53.8	62	1	150	2.5	0.375	1124.23	(Priyanka et al. 2019)
<b>UVC/H<sub>2</sub>O<sub>2</sub></b>	225	87	0.5	30	3	0.09	923.08	Chin et.al. (2009)
<b>Immobilized Fe<sub>2</sub>O<sub>3</sub>-TiO<sub>2</sub>/PVP Solar photocatalysis</b>	54.75	62.64	15	50	3	0.15	291.55	Present study



## CHAPTER 5

### CONCLUSIONS

In this study, an integrated anaerobic-aerobic-sand filter treatment system was investigated to remove organic and nitrogen compounds from synthetic GW. The pilot plant achieved an effective treatment of GW to a good quality that meets the standards of reuse for irrigation. In order to check the stability, the integrated system was applied to the volumetric and organic shock loads. The direct stand trial was completed by means of the integrated anaerobic-aerobic-sand filter system, and the research revealed that it could deal with shock loads of up to 4 times the base loading. So, the integrated aerobic-aerobic-sand filter explored for GWT is practical, less energy, and feasible. Meanwhile, the post-treatment was carried out to effectively treat GW effluent generated by pilot-plant using solar photocatalysis.

In Phase I experiments, the removal capacity of the pilot plant for COD, BOD, anionic surfactants, TN, TSS, and TP is 89%, 95%, 99%, 85%, 88.5, and 87%, respectively, under steady-state conditions at a constant load of 3.5 kg COD/m<sup>3</sup>/day. Under volumetric shock load conditions, the overall efficiency of COD, BOD, TN, anionic surfactants in the integrated system was found to increase at 8 h HRT compared to the previous HRT conditions. R<sub>1</sub> could handle the higher surfactant loading rate of 22.56 g/m<sup>3</sup>/h due to the coir fiber used as media for attached biofilm growth. Furthermore, the efficiency of the entire system peaks at 91.8 %, with the optimum effective surfactant loading rate at 19.38 g/m<sup>3</sup>/h. Based on these findings, it is evident that the integrated anaerobic-aerobic system coupled with the sand filter process achieves efficiency.

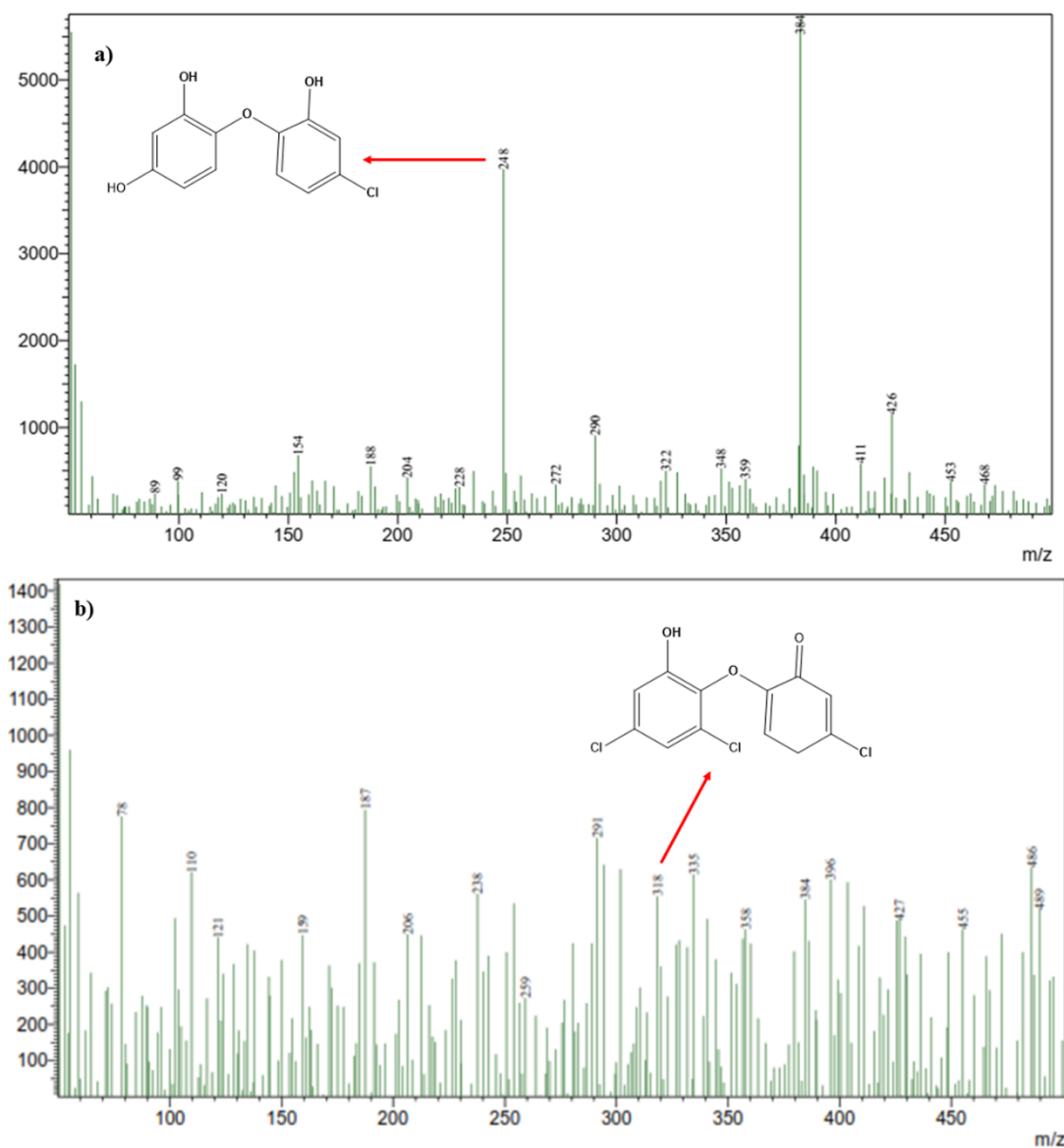
During Phase II of the study, an efficient photocatalytic degradation process for TCS was discovered using immobilized Fe<sub>2</sub>O<sub>3</sub>-TiO<sub>2</sub>/PVP as a spray pyrolysis coating. In addition to these advantages, the immobilization strategy used in this example displayed several properties that made it particularly attractive for large-scale use: rapid surface layer formation, no extreme temperatures (> 400 °C) system requirement, and

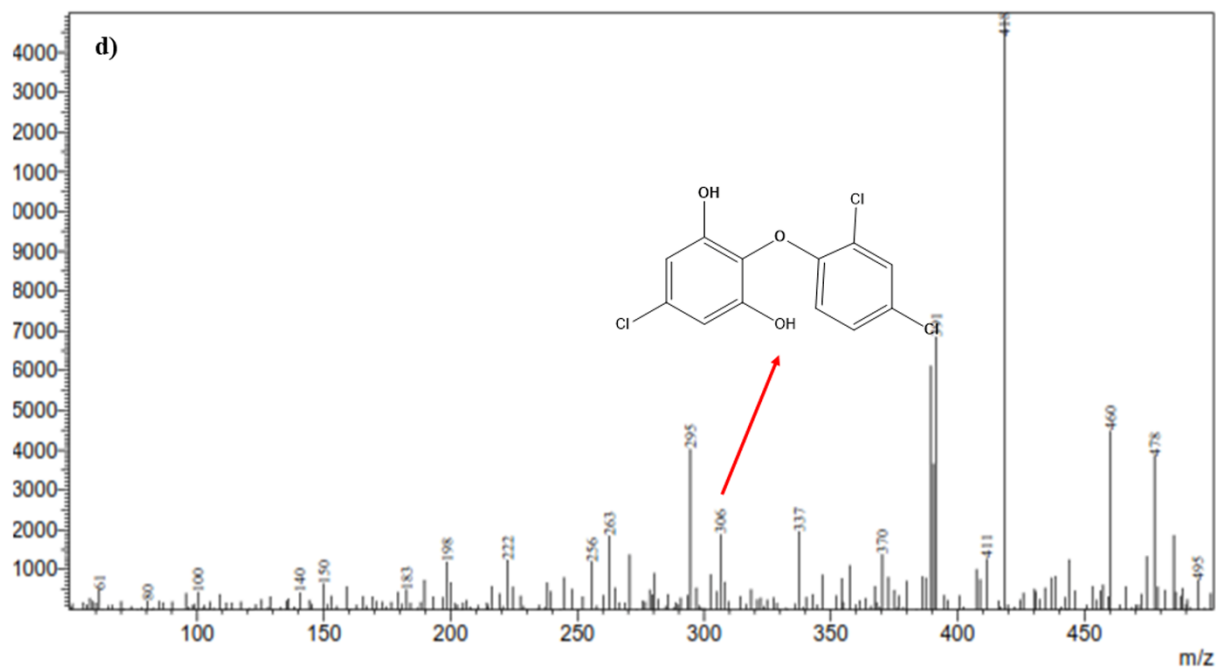
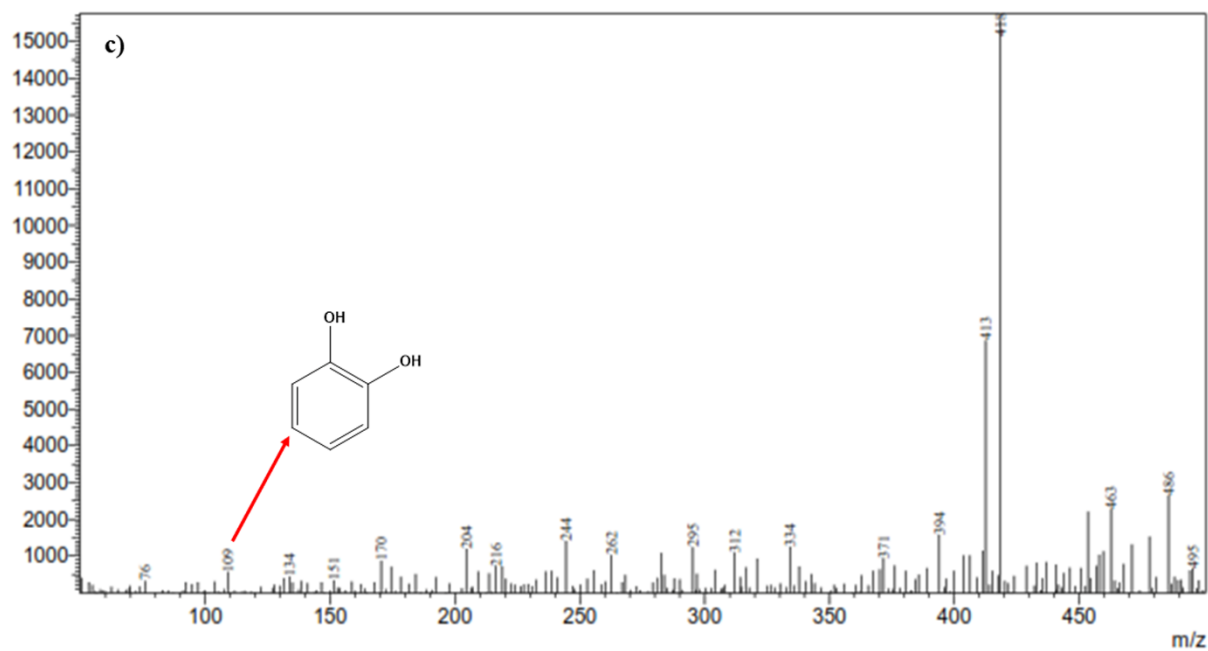
the ability to scale up for an extensive range of applications. Additionally, the generation of C–O, C–N–C, and –N–C may explain the effectiveness of the therapy since these molecules worked as electron donors to improve photoactivity. The composite catalyst developed for this 5% Fe<sub>2</sub>O<sub>3</sub>-TiO<sub>2</sub> composite had higher scratching hardness (7.984 GPa), greater homogeneity, and a smoother and more consistent surface shape with a coating structure. While the ternary composite proved capable of producing an acceptable film thickness, the film formed was 15.84 μm thick. The pseudo-first-order kinetic prototypical fitted well ( $R^2=0.95$ ) and the  $k_{TCS}$  ( $k_I=0.105 \text{ min}^{-1}$ ) observed for this study in the appropriate range for photodegradation of TCS under sun irradiation. Using surface response analyses and contour plots, GW successfully removed 83.27% of TCS in the effluent. According to LC-MS results, a hypothesized pathway for TCS breakdown suggested that 5-chloro-2-(2-chlorophenoxy) phenol, chlorobenzene, 5-(4-chlorobenzyl)-2-furoic acid, and other unidentified chemicals were formed as intermediate photoproducts in the GW wastewater treatment process. Intermediates generated during hydroxylation, oxidation, and dichlorination could have been mineralized through hydroxylation, oxidation, and dichlorination to generate simpler inorganic compounds.

Eventually, the Integrated anaerobic-aerobic-sand filter has proved that it can regenerate industrial interest in technology. A hybrid optimization must be implemented in this GWT model to optimize the GW treatment parameters and time consumption. Hence, the GWT design could be enhanced and will get an optimized result. In Immobilized photocatalysis, most of the studies have been so far focused on materials design, with only a few focusing on system design, which should be addressed in future research.

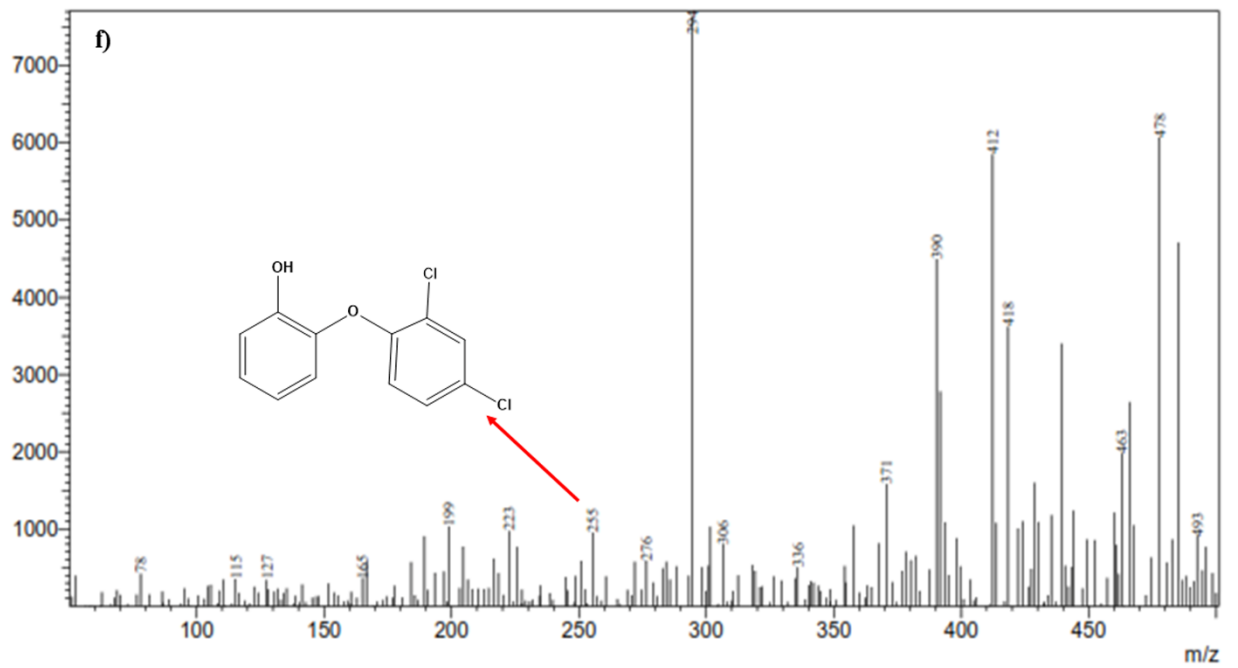
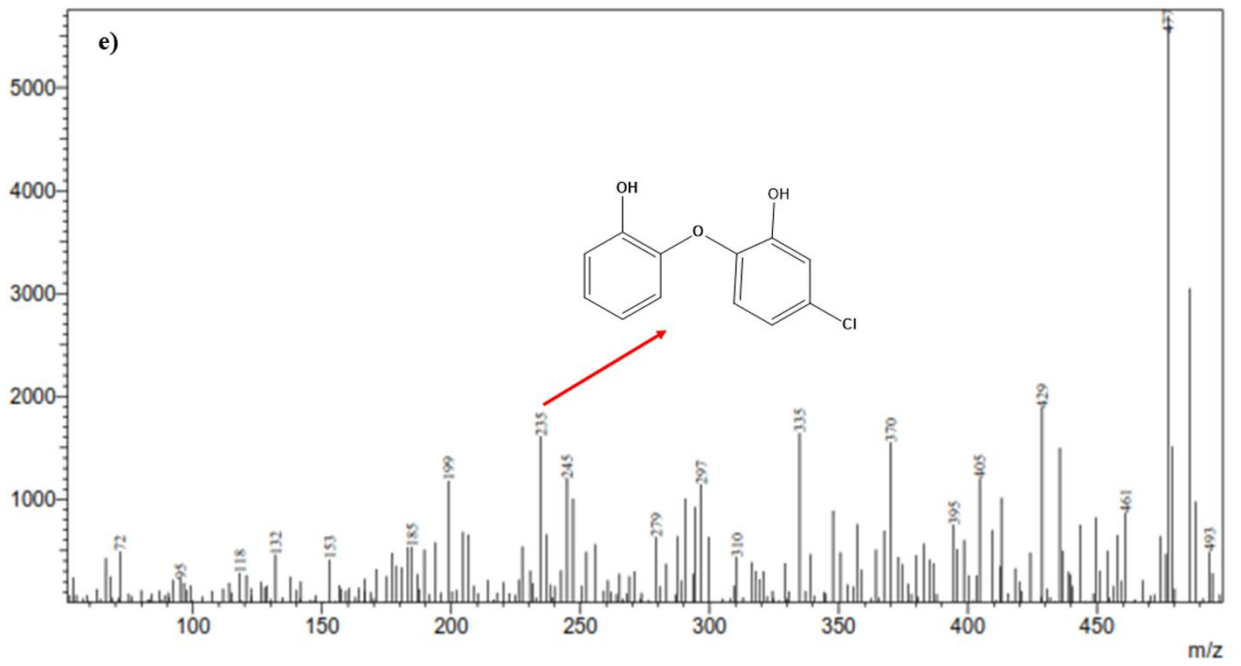
## APPENDIX

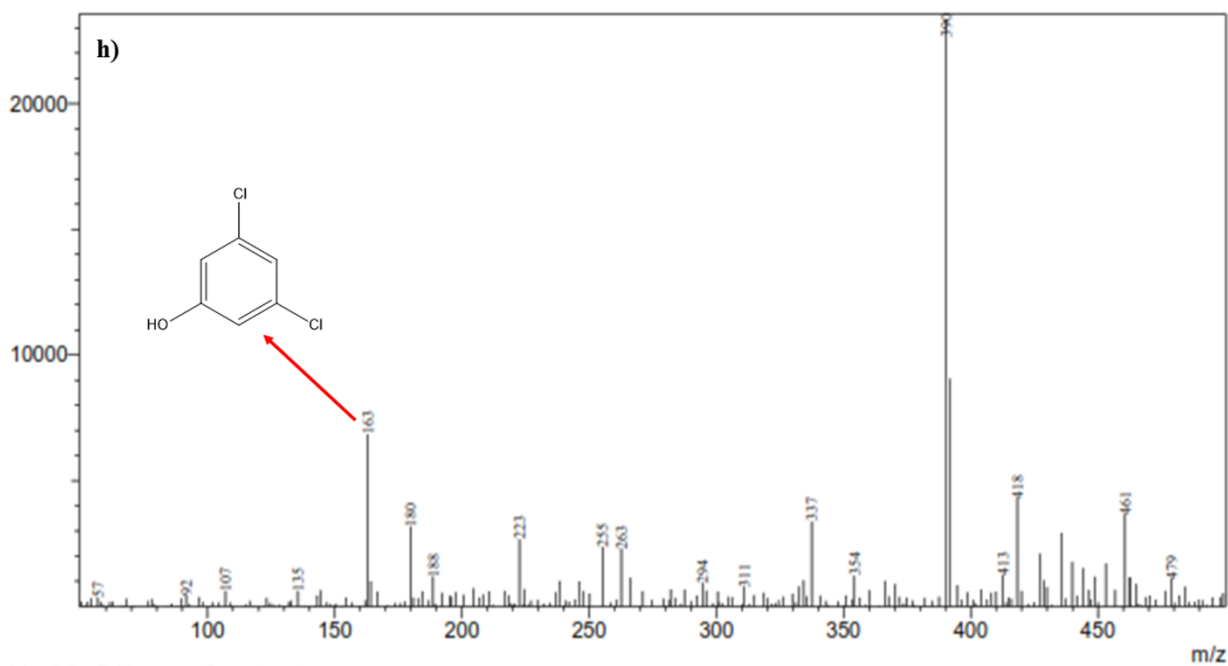
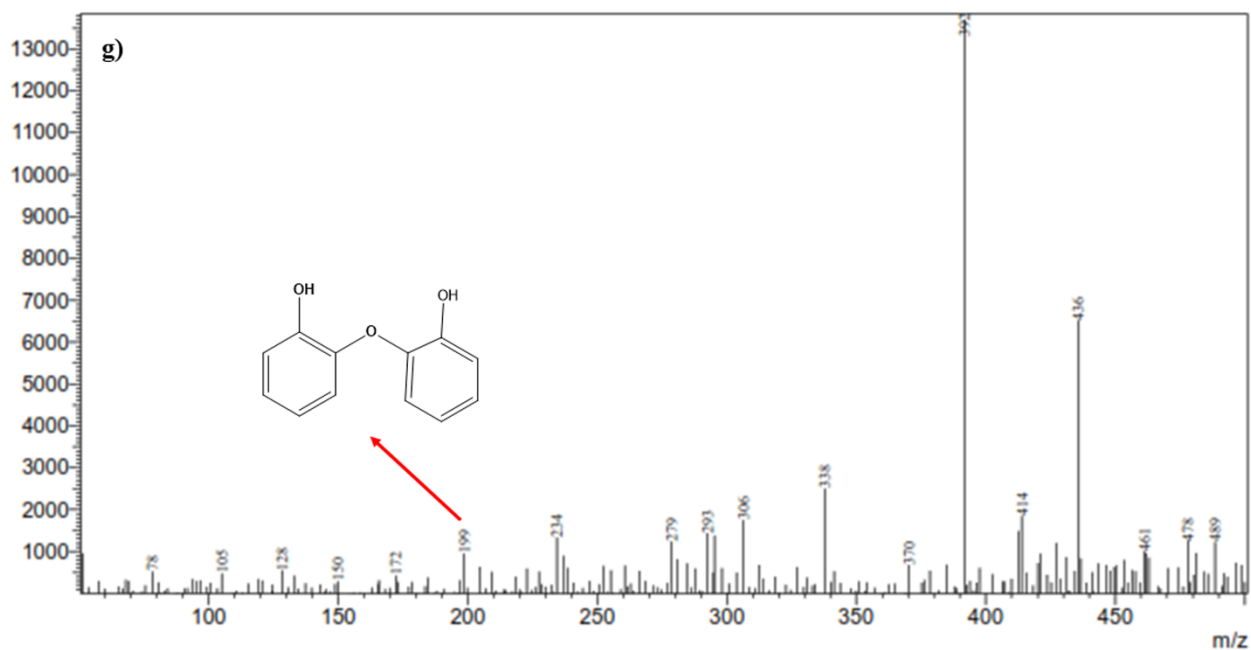
During the degradation of TCS in greywater effluent, the intermediate products were tentatively identified, using Liquid Chromatograph Mass Spectrometer (LCMS-2020, Shimadzu, USA); a C18 reversed-phase liquid chromatography column; single quadrupole mass spectrometer; coupled with Electron Spray Ionisation (ESI) operating in positive mode. The sample injection volume was 20 L, and the UV-Vis detector wavelength was set to 280 nm. The other conditions were oven temperature of 40 °C, N<sub>2</sub> as a carrier gas, and pump pressure of 79 bars (Wang and Wang 2019).

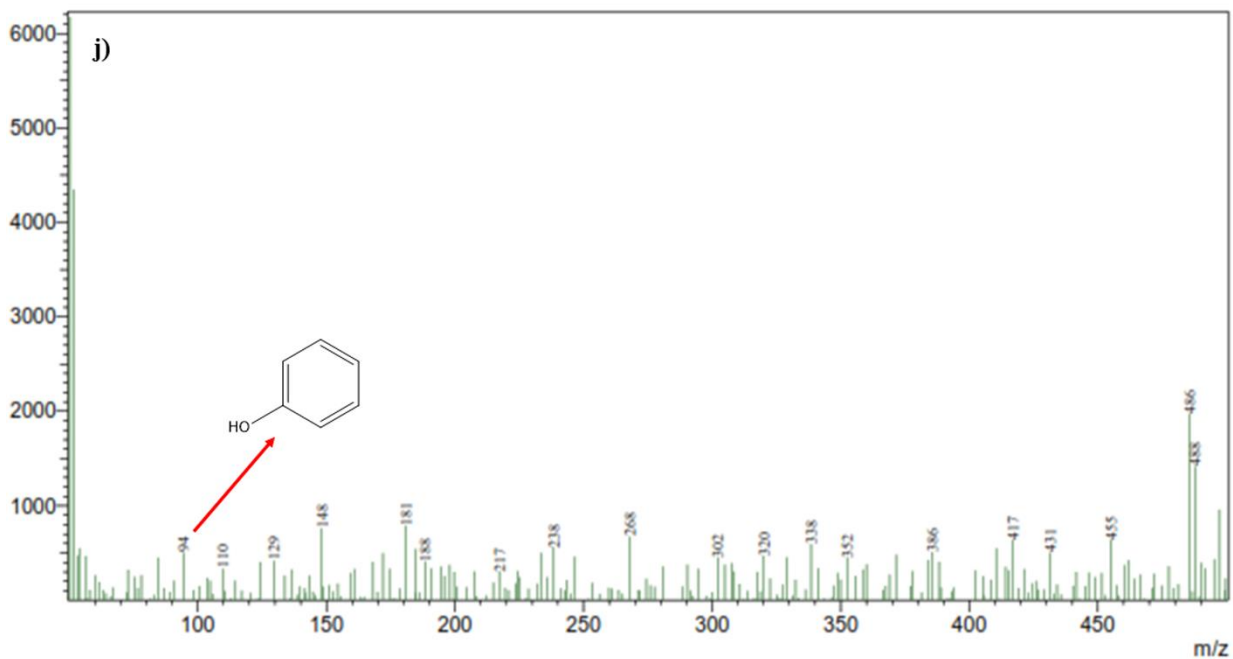
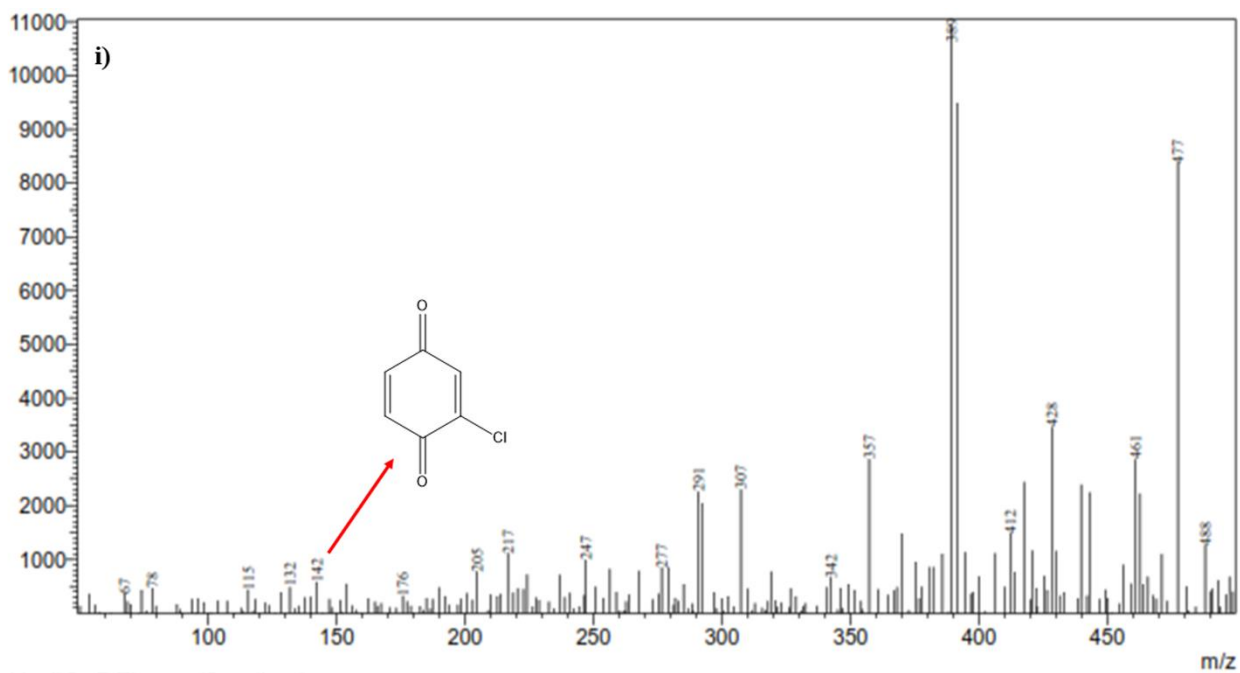












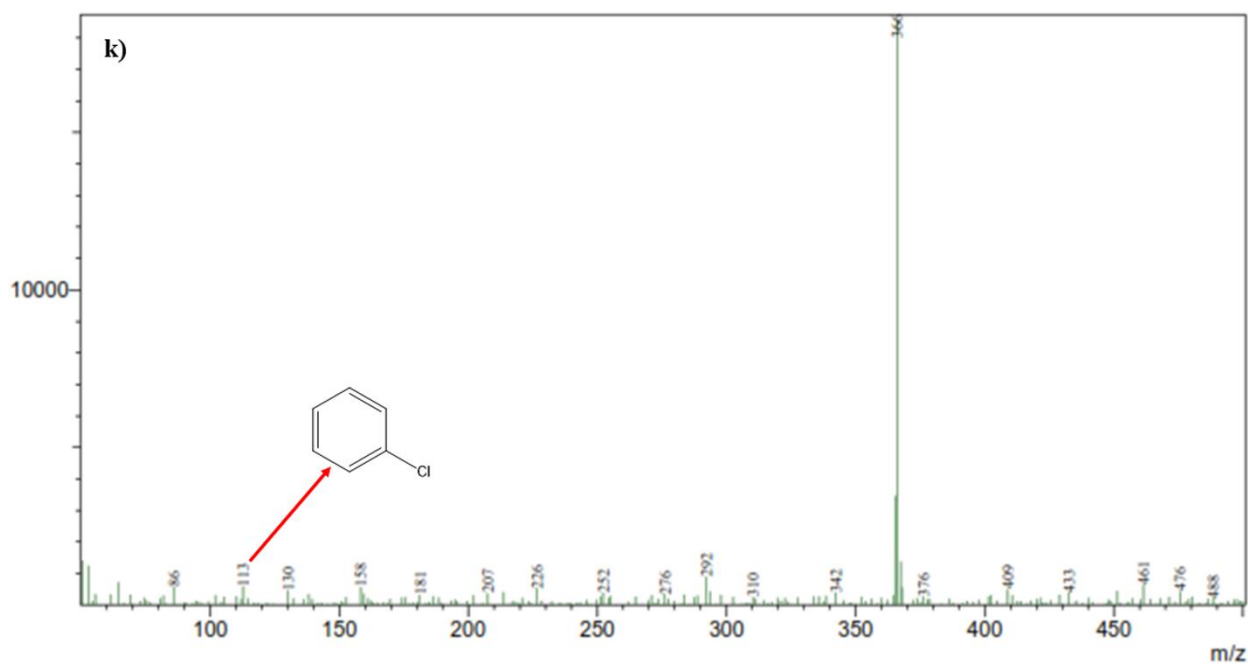


**Figure:** Total Liquid Chromatograph Mass Spectrometer of eleven main intermediates or reaction products

## REFERENCES

- Abdel-Shafy, H. I., Al-Sulaiman, A. M. and Mansour, M. S. M. (2015). "Anaerobic/aerobic treatment of greywater via UASB and MBR for unrestricted reuse." *Water Sci. Technol.*, 71(4), 630–637.
- Abdel-Shafy, H. I., Mansour, M. S. M. and Al-Sulaiman, A. M. (2019). "Anaerobic/aerobic integration via UASB/enhanced aeration for greywater treatment and unrestricted reuse." *Water Pract. Technol.*, 14(4), 1–14.
- Abraham, E., Deepa, B., Pothan, L. A., Cintil, J., Thomas, S., John, M. J., Anandjiwala, R. and Narine, S. S. (2013). "Environmental friendly method for the extraction of coir fibre and isolation of nanofibre." *Carbohydr. Polym.*, 92(2), 1477–1483.
- Acidic, S., Cho, M., Lee, Y., Chung, H. and Yoon, J. (2004). "Inactivation of Escherichia coli by Photochemical Reaction of Ferrioxalate at Inactivation of Escherichia coli by Photochemical Reaction of Ferrioxalate at Slightly Acidic and Near-Neutral pHs." *Appl. Environ. Microbiol.*, 70(2), 1128–1134.
- Adapa, P. K., Schonenaus, L. G., Canam, T. and Dumonceaux, T. (2011). "Quantitative Analysis of Lignocellulosic Components of Non-Treated and Steam Exploded Barley, Canola, Oat and Wheat Straw Using Fourier Transform Infrared Spectroscopy." *J. Agric. Sci. Technol.*, 1(May 2014), 177–188.
- Aguiar, E. De, Calijuri, M. L., Assemany, P. P., Santiago, F. and Lopes, L. S. (2014). "Greywater treatment in airports using anaerobic filter followed by UV disinfection : an efficient and low cost alternative." *J. Clean. Prod.*, 1–8.
- Albalawneh, A. and Chang, T. K. (2015). "Review of the greywater and proposed greywater recycling scheme for agricultural irrigation reuses." *International Journal of Research- Granthaalayah*, 3(12), 16-35.
- Al-Gheethi, A. A., Radin Mohamed, R. M. S., Efaq, A. N. and Amir Hashim, M. K. (2016). "Reduction of microbial risk associated with greywater by disinfection processes for irrigation." *Journal of water and health*, 14(3), 379-398.
- Al-Hamaiedeh, H. and Bino, M. (2010). "Effect of treated grey water reuse in irrigation on soil and plants." *Desalination*, 256(1-3), 115-119.
- Ali, F., Omar, R. and Amin, M. (2013). "An examination of the relationships between physical environment, perceived value, image and behavioural Intentions: A SEM approach towards Malaysian resort hotels." *Journal of Hotel and Tourism Management*, 27(2), 9-26.
- Alqam, M., Jamrah, A. and Daghlas, H. (2011). "Utilization of cement incorporated with water treatment sludge." *Jordan Journal of Civil Engineering*, 5(2), 268-277.
- Andrade, J., Pereira, C. G., Almeida Junior, J. C. de, Viana, C. C. R., Neves, L. N.

de O., Silva, P. H. F. da, Bell, M. J. V. and Anjos, V. de C. dos. (2019). “FTIR-ATR determination of protein content to evaluate whey protein concentrate adulteration.” *Lwt*, 99, 166–172.

Aonghusa, C. N. and Gray, N. F. (2002). “Laundry detergents as a source of heavy metals in Irish domestic wastewater.” *Journal of Environmental Science and Health, Part A*, 37(1), 1-6.

Arias, C. A., Bubba, M. D. E. L. and Brix, H. (2001). “Phosphorus Removal By Sands For Use As Media In Subsurface Flow Constructed Reed Beds.” *Water Res.*, 35(5), 1159–1168.

Arias, C. A., Del Bubba, M. and Brix, H. (2001). “Phosphorus removal by sands for use as media in subsurface flow constructed reed beds.” *Water research*, 35(5), 1159-1168.

Arora, K. S., Jefferys, J. L., Maul, E. A. and Quigley, H. A. (2012). “Choroidal thickness change after water drinking is greater in angle closure than in open angle eyes.” *Investigative ophthalmology and visual science*, 53(10), 6393-6402.

Augustin, A., Huilgol, P., Udupa, K. R. and K, U. B. (2016). “Effect of current density during electrodeposition on microstructure and hardness of textured Cu coating in the application of antimicrobial Al touch surface.” *J. Mech. Behav. Biomed. Mater.*, 63, 352–360.

Azarpira, H., Sadani, M., Abtahi, M., Vaezi, N., Rezaei, S., Atafar, Z., Mohseni, S. M., Sarkhosh, M., Ghaderpoori, M., Keramati, H., Hosseini Pouya, R., Akbari, A. and fanai, V. (2019). “Photo-catalytic degradation of triclosan with UV/iodide/ZnO process: Performance, kinetic, degradation pathway, energy consumption and toxicology.” *J. Photochem. Photobiol. A Chem.*, 371(November), 423–432.

Banisharif, A., Khodadadi, A. A., Mortazavi, Y., Anaraki Firooz, A., Beheshtian, J., Agah, S. and Menbari, S. (2015). “Highly active Fe<sub>2</sub>O<sub>3</sub>-doped TiO<sub>2</sub> photocatalyst for degradation of trichloroethylene in air under UV and visible light irradiation: Experimental and computational studies.” *Appl. Catal. B Environ.*, 165, 209–221.

Bart, S., Amossé, J., Lowe, C. N., Mougin, C., Péry, A. R. and Pelosi, C. (2018). “Aporrectodea caliginosa, a relevant earthworm species for a posteriori pesticide risk assessment: current knowledge and recommendations for culture and experimental design.” *Environmental Science and Pollution Research*, 25(34), 33867-33881.

Bartram, S. A. (2001). “Serious leisure careers among whitewater kayakers: A feminist perspective.” *World Leisure Journal*, 43(2), 4-11.

Belapurkar, A. D., Sherkhane, P. and Kale, S. P. (2006). “Disinfection of drinking water using photocatalytic technique.” *Curr. Sci.*, 91(1), 73–76.

Birben, N., Uyguner-Demirel, C. and Bekbolet, M. (2016). “Photocatalytic Removal of Microbiological Consortium and Organic Matter in Greywater.” *Catalysts*, 6(6), 91.

- Boano, F., Caruso, A., Costamagna, E., Ridolfi, L., Fiore, S., Demichelis, F. and Masi, F. (2020). "A review of nature-based solutions for greywater treatment: Applications, hydraulic design and environmental benefits." *Science of the total environment*, 711, 134731.
- Borlaf, M., Colomer, M. T., Moreno, R. and Ortiz, A. L. (2014). "Rare earth-doped TiO<sub>2</sub> nanocrystalline thin films: Preparation and thermal stability." *Journal of the European ceramic society*, 34(16), 4457-4462.
- Bromiley, G. D. and Shiryaev, A. A. (2006). "Neutron irradiation and post-irradiation annealing of rutile (TiO<sub>2-x</sub>): effect on hydrogen incorporation and optical absorption." *Physics and Chemistry of Minerals*, 33(6), 426-434.
- Bustarret, E. (2015). "Superconductivity in doped semiconductors." *Physica C: Superconductivity and its Applications*, 514, 36-45.
- Cai, W., Borlace, S., Lengaigne, M., Van Rensch, P., Collins, M., Vecchi, G. and Jin, F. F. (2014). "Increasing frequency of extreme El Niño events due to greenhouse warming." *Nature climate change*, 4(2), 111-116.
- Čater, M., Zorec, M. and Marinšek Logar, R. (2014). "Methods for Improving Anaerobic Lignocellulosic Substrates Degradation for Enhanced Biogas Production." *Springer Sci. Rev.*, 2(1-2), 51-61.
- Chan, F. L. and Tanksale, A. (2014). "Review of recent developments in Ni-based catalysts for biomass gasification." *Renewable and Sustainable Energy Reviews*, 38, 428-438.
- Chen, X., Casas, M. E., Nielsen, J. L., Wimmer, R. and Bester, K. (2015). "Identification of Triclosan-O-Sulfate and other transformation products of Triclosan formed by activated sludge." *Sci. Total Environ.*, 505, 39-46.
- Chong, J. X., Buckingham, K. J., Jhangiani, S. N., Boehm, C., Sobreira, N., Smith, J. D. and Bamshad, M. J. (2015). "The genetic basis of Mendelian phenotypes: discoveries, challenges and opportunities." *The American Journal of Human Genetics*, 97(2), 199-215.
- Christova-Boal, D., Eden, R. E. and McFarlane, S. (1996). "An investigation into greywater reuse for urban residential properties." *Desalination*, 106(1-3), 391-397.
- Ciabattia, I., Cesaro, F., Faralli, L., Fatarella, E. and Tognotti, F. (2009). "Demonstration of a treatment system for purification and reuse of laundry wastewater." *Desalination*, 245(1-3), 451-459.
- Dalahmeh, S. S., Assayed, M. and Suleiman, W. T. (2009). "Themes of stakeholder participation in greywater management in rural communities in Jordan." *Desalination*, 243(1-3), 159-169.
- Dalahmeh, S. S., Pell, M. and Vinnerås, B. (2012). "Efficiency of Bark , Activated Charcoal , Foam and Sand Filters in Reducing Pollutants from Greywater." *Water. Air. Soil Pollut.*, 223, 3657-3671.

- Dayeh, S. A., Chen, R., Goo, Y. and Sim, J. (2017). "Progress in doping semiconductor nanowires during growth." *Mater. Sci. Semicond. Process.*, 62, 135–155.
- De Angelis, G. (2007). "Third or additional language acquisition. Multilingual Matters."
- Dixon, A., Butler, D., Fewkes, A. and Robinson, M. (2000). "Measurement and modelling of quality changes in stored untreated grey water." *Urban Water*, 1(4), 293-306.
- Dixon, L., Postrado, L., Delahanty, J., Fischer, P. J. and Lehman, A. (1999). "The association of medical comorbidity in schizophrenia with poor physical and mental health." *The Journal of nervous and mental disease*, 187(8), 496-502.
- Donner, S. D. and Kucharik, C. J. (2008). "Corn-based ethanol production compromises goal of reducing nitrogen export by the Mississippi River." *Proceedings of the National Academy of Sciences*, 105(11), 4513-4518.
- Drechsel, P., Qadir, M. and Wichelns, D. (Eds.). (2015). "Wastewater: economic asset in an urbanizing world." *Springer*.
- Edwin, G. A., Gopalsamy, P. and Muthu, N. (2014). "Characterization of domestic gray water from point source to determine the potential for urban residential reuse: a short review." *Applied Water Science*, 4(1), 39-49.
- Elsheikh, M. H., Shnawah, D. A., Sabri, M. F. M., Said, S. B. M., Hassan, M. H., Bashir, M. B. A. and Mohamad, M. (2014). "A review on thermoelectric renewable energy: Principle parameters that affect their performance." *Renewable and sustainable energy reviews*, 30, 337-355.
- Eriksson, E., Auffarth, K., Henze, M., and Ledin, A. (2002). "Characteristics of grey wastewater." *Urban water*, 4(1), 85-104.
- Eslami, H., Ehrampoush, M. H., Ghaneian, M. T., Mokhtari, M. and Ebrahimi, A. (2017). "Effect of Organic Loading Rates on biodegradation of linear alkyl benzene sulfonate, oil and grease in greywater by Integrated Fixed-film Activated Sludge (IFAS)." *J. Environ. Manage.*, 193, 312–317.
- Etchepare, R. and van der Hoek, J. P. (2015). "Health risk assessment of organic micropollutants in greywater for potable reuse." *Water research*, 72, 186-198.
- Eyre, B. D. and Ferguson, A. J. (2009). "Denitrification efficiency for defining critical loads of carbon in shallow coastal ecosystems." In *Eutrophication in Coastal Ecosystems* (pp. 137-146). Springer, Dordrecht.
- Fatta-Kassinos, D., Bester, K. and Kümmerer, K. (Eds.). (2010). "Xenobiotics in the urban water cycle: mass flows, environmental processes, mitigation and treatment strategies" vol (6), Springer Science and Business Media.
- Fernández-ibáñez, P., Polo-lópez, M. I., Malato, S., Wadhwa, S., Hamilton, J. W.



- J., Dunlop, P. S. M., Sa, R. D., Magee, E., Shea, K. O., Dionysiou, D. D. and Byrne, J. A. (2015). "Solar photocatalytic disinfection of water using titanium dioxide graphene composites." *Chem. Eng. J.*, 261, 36–44.
- Finley, S., Barrington, S. and Lyew, D. (2009). "Reuse of domestic greywater for the irrigation of food crops." *Water, air, and soil pollution*, 199(1), 235-245.
- Friedler, E., Kovalio, R. and Galil, N. I. (2005). "On-site greywater treatment and reuse in multi-storey buildings." *Water Sci. Technol.*, 51(10), 187–194.
- Fujishima, A., Rao, T. N., and Tryk, D. A. (2000). "Titanium dioxide photocatalysis." *Journal of photochemistry and photobiology C: Photochemistry reviews*, 1(1), 1-21.
- Garland, G. M., Suddick, E., Burger, M., Horwath, W. R. and Six, J. (2011). "Direct N<sub>2</sub>O emissions following transition from conventional till to no-till in a cover cropped Mediterranean vineyard (*Vitis vinifera*)." *Agriculture, ecosystems and environment*, 141(1-2), 234-239.
- Ghaitidak, D. M. and Yadav, K. D. (2013). "Characteristics and treatment of greywater—a review." *Environmental Science and Pollution Research*, 20(5), 2795-2809.
- Ghunmi, L. A., Zeeman, G., Fayyad, M. and Lier, J. B. Van. (2011). "Grey water treatment systems: A review." *Crit. Rev. Environ. Sci. Technol.*, 41(7), 657–698.
- Gorgich, M., Mata, T. M., Martins, A., Caetano, N. S. and Formigo, N. (2020). "Application of domestic greywater for irrigating agricultural products: A brief study." *Energy Reports*, 6, 811–817.
- Grčić, I., Vrsaljko, D., Katančić, Z. and Papić, S. (2015). "Purification of household greywater loaded with hair colorants by solar photocatalysis using TiO<sub>2</sub>-coated textile fibers coupled flocculation with chitosan." *Journal of Water Process Engineering*, 5, 15-27.
- Gross, A., Azulai, N., Oron, G., Ronen, Z., Arnold, M. and Nejidat, A. (2005). "Environmental impact and health risks associated with greywater irrigation: a case study." *Water science and technology*, 52(8), 161-169.
- Gross, A., Kaplan, D. and Baker, K. (2007). "Removal of chemical and microbiological contaminants from domestic greywater using a recycled vertical flow bioreactor (RVFB)." *Ecological engineering*, 31(2), 107-114.
- Gross, A., Shmueli, O., Ronen, Z., and Raveh, E. (2007). "Recycled vertical flow constructed wetland (RVFCW)-a novel method of recycling greywater for irrigation in small communities and households." *Chemosphere*, 66(5), 916–923.
- Gross, N., Suding, K. N., Lavorel, S. and Roumet, C. (2007). "Complementarity as a mechanism of coexistence between functional groups of grasses." *Journal of Ecology*, 95(6), 1296-1305.

- Gulyas, H., Choromanski, P., Furmanska, M., Muelling, N. and Otterpohl, R. (2007, November). "Photocatalytic oxidation of biologically treated greywater in the presence of powdered activated carbon." In *International Conference on Sustainable Sanitation, Food and Water Security for Latin America, Fortaleza, Brazil*.
- Gupta, S. M. and Tripathi, M. (2012). "A review on the synthesis of TiO<sub>2</sub> nanoparticles by solution route." 10(2).
- Hajduk, T. (2018). "Research of Deposit Accumulated on Heat Exchange Surfaces in the Light of Thermal Degradation of Heat Exchange Aparatus of Steam Power Plants Part I: Study of Real Sediments." *Polish Marit. Res.*, 25(1), 99–107.
- Han, H. and Bai, R. (2011). "Effect of thickness of photocatalyst film immobilized on a buoyant substrate on the degradation of methyl orange dye in aqueous solutions under different light irradiations." *Ind. Eng. Chem. Res.*, 50(21), 11922–11929.
- Han, Y., Qiu, S., Zeng, H., Ma, F., Wang, J., Qiu, Y. and An, X. (2018). "Short-term effects of tourmaline on nitrogen removals and microbial communities in a sequencing batch reactor at low temperatures." *Int. J. Environ. Res. Public Health*, 15(6).
- Hanjra, M. A. and Qureshi, M. E. (2010). "Global water crisis and future food security in an era of climate change." *Food policy*, 35(5), 365-377.
- Harrow, D. I., Felker, J. M. and Baker, K. H. (2011). "Impacts of triclosan in greywater on soil microorganisms." *Applied and Environmental Soil Science*, 2011.
- Hassanshahi, N. and Karimi-Jashni, A. (2018). "Comparison of photo-Fenton, O<sub>3</sub>/H<sub>2</sub>O<sub>2</sub>/UV and photocatalytic processes for the treatment of gray water." *Ecotoxicol. Environ. Saf.*, 161(March), 683–690.
- Healy, M. G. and Rodgers, M. (2007). "Treatment of Dairy Wastewater Using Constructed Wetlands and Intermittent Sand Filters and intermittent sand filters." (June 2014).
- Hernández Leal, L., Zeeman, G., Temmink, H., and Buisman, C. (2007). "Characterisation and biological treatment of greywater." *Water Sci. Technol.*, 56(5), 193–200.
- Herrmann, J. (1999). "Heterogeneous photocatalysis: fundamentals and applications to the removal of various types of aqueous pollutants." 53, 115–129.
- Huo, K., Gao, B., Fu, J., Zhao, L. and Chu, P. K. (2014). "Fabrication, modification, and biomedical applications of anodized TiO<sub>2</sub> nanotube arrays." *Rsc Advances*, 4(33), 17300-17324
- Ibhadon, A. O. and Fitzpatrick, P. (2013). "Heterogeneous photocatalysis: recent advances and applications." *Catalysts*, 3(1), 189-218.

- Jacobs, H. E. and Van Staden, S. (2008, May). "Direct on-site greywater reuse—an illicit or illustrious option." In *WISA 2008 Biennial Conference and Exhibition* (pp. 18-22).
- Jamrah, A., Al-Futaisi, A., Prathapar, S. and Al Harrasi, A. (2008). "Evaluating greywater reuse potential for sustainable water resources management in Oman." *Environmental monitoring and assessment*, 137(1), 315-327.
- Janet, C. M., Navaladian, S., Viswanathan, B., Varadarajan, T. K. and Viswanath, R. P. (2010). "Heterogeneous wet chemical synthesis of superlattice-type hierarchical ZnO architectures for concurrent H<sub>2</sub> production and N<sub>2</sub> reduction." *The Journal of Physical Chemistry C*, 114(6), 2622-2632.
- Jefferson, B., Laine, A., Parsons, S., Stephenson, T. and Judd, S. (2000). "Technologies for domestic wastewater recycling." *Urban water*, 1(4), 285-292.
- Jenkins, B., Baxter, L. L., Miles Jr, T. R. and Miles, T. R. (1998). "Combustion properties of biomass." *Fuel processing technology*, 54(1-3), 17-46.
- Jeong, H., Broesicke, O. A., Drew, B. and Crittenden, J. C. (2018). "Life cycle assessment of small-scale greywater reclamation systems combined with conventional centralized water systems for the City of Atlanta, Georgia." *Journal of Cleaner Production*, 174, 333-342.
- Jong, J., Lee, J., Kim, J., Hyun, K., Hwang, T., Park, J. and Choung, Y. (2010). "The study of pathogenic microbial communities in graywater using membrane bioreactor." *Desalination*, 250(2), 568-572.
- Justicia, I., Ordejón, P., Canto, G., Mozos, J. L., Fraxedas, J., Battiston, G. A. and Figueras, A. (2002). "Designed self-doped titanium oxide thin films for efficient visible-light photocatalysis." *Advanced materials*, 14(19), 1399-1402.
- K V, A., Veeraiah, M. K., P, H. and M, M. (2014). "Synthesis and Characterisation of Poly (Vinylpyrrolidone) – Nickel (II) Complexes." *IOSR J. Appl. Chem.*, 7(8), 61–66.1
- Kamińska, G. and Marszałek, A. (2020). "Advanced treatment of real grey water by SBR followed by ultrafiltration-performance and fouling behavior." *Water (Switzerland)*, 12(1).
- Kar, R., Gupta, O. and Das, M. K. (2012). "Studies on the Effect of Feed Gas Temperature on Ranque-Hilsch Vortex Tube." *International Journal of Scientific and Research Publications*, 2(11).
- Kariuki, F. W., Kotut, K. and Ngángá, V. G. (2011). "The Potential of a Low Cost Technology for The Greywater Treatment." 32–39.
- Katukiza, A. Y., Ronteltap, M., Niwagaba, C. B., Kansiime, F. and Lens, P. N. L. (2014). "Grey water treatment in urban slums by a filtration system: Optimisation of the filtration medium." *J. Environ. Manage.*, 146, 131–141.

Kobayashi, Y., Peters, G. M., Ashbolt, N. J., Heimersson, S., Svanström, M. and Khan, S. J. (2015). "Global and local health burden trade-off through the hybridisation of quantitative microbial risk assessment and life cycle assessment to aid water management." *Water research*, 79, 26-38.

Koby, M., Demirbas, E., Ozyonar, F., Sirtbas, G. and Gengec, E. (2017). "Treatments of alkaline non-cyanide, alkaline cyanide and acidic zinc electroplating wastewaters by electrocoagulation." *Process Saf. Environ. Prot.*, 105(December), 373–385.

Krishnana, V., Ahmad, D. and Jeru, J. B. (2011). "Influence of Organizational Culture on Knowledge Sharing." *Proc. Eur. Conf. Knowl. Manag. ECKM*, 762(October 2007), 470–480.

Lamine, M., Bousselmi, L. and Ghrabi, A. (2007). Biological treatment of grey water using sequencing batch reactor. *Desalination*, 215(1-3), 127-132.

Lazarova, V., Hills, S. and Birks, R. (2003). "Using recycled water for non-potable, urban uses: a review with particular reference to toilet flushing." *Water Science and Technology: Water Supply*, 3(4), 69-77.

Leal, L. H., Temmink, H., Zeeman, G. and Buisman, C. J. N. (2010). "Bioflocculation of grey water for improved energy recovery within decentralized sanitation concepts." *Bioresour. Technol.*, 101(23), 9065-9070.

Le-Minh, N., Khan, S. J., Drewes, J. E. and Stuetz, R. M. (2010). "Fate of antibiotics during municipal water recycling treatment processes." *Water research*, 44(15), 4295-4323.

Li, C. Y., Wu, X. Y., Tong, J. B., Yang, X. X., Zhao, J. L., Zheng, Q. F. and Ma, Z. J. (2015). "Comparative analysis of human mesenchymal stem cells from bone marrow and adipose tissue under xeno-free conditions for cell therapy." *Stem cell research & therapy*, 6(1), 1-13.

Li, D., Liu, S., Mi, L., Li, Z., Yuan, Y., Yan, Z. and Liu, X. (2015). "Effects of feedstock ratio and organic loading rate on the anaerobic mesophilic co-digestion of rice straw and cow manure." *Bioresour. Technol.*, 189, 319–326.

Li, F., Wichmann, K. and Otterpohl, R. (2009). Review of the technological approaches for grey water treatment and reuses. *Science of the total environment*, 407(11), 3439-3449.

Li, M., Xu, G., Guan, Z., Wang, Y., Yu, H. and Yu, Y. (2019). "Synthesis of Ag/BiVO<sub>4</sub>/rGO composite with enhanced photocatalytic degradation of triclosan." *Sci. Total Environ.*, 664, 230–239.

Li, X., Xing, Y., Jiang, Y., Ding, Y. and Li, W. (2009). "Antimicrobial activities of ZnO powder-coated PVC film to inactivate food pathogens." *International journal of food science and technology*, 44(11), 2161-2168.

- Liu, E. K., He, W. Q. and Yan, C. R. (2014). “White revolution’to ‘white pollution’—agricultural plastic film mulch in China.” *Environmental Research Letters*, 9(9), 091001.
- Liu, L., Oza, S., Hogan, D., Perin, J., Rudan, I., Lawn, J. E. and Black, R. E. (2015). “Global, regional, and national causes of child mortality in 2000–13, with projections to inform post-2015 priorities: an updated systematic analysis.” *The Lancet*, 385(9966), 430-440.
- Long, J. M. and Holtzman, D. M. (2019). “Alzheimer disease: an update on pathobiology and treatment strategies.” *Cell*, 179(2), 312-339.
- Long, M., Wang, P., Fang, H. and Hu, W. (2019). “Progress, challenges, and opportunities for 2D material based photodetectors.” *Advanced Functional Materials*, 29(19), 1803807.
- Lu, D., Willard, D., Patel, I. R., Kadwell, S., Overton, L., Kost, T. and Cone, R. D. (1994). “Agouti protein is an antagonist of the melanocyte-stimulating-hormone receptor.” *Nature*, 371(6500), 799-802.
- Lu, H., Ma, H. and Tao, G. (2009). “Spectrophotometric determination of triclosan in personal care products.” *Spectrochim. Acta - Part A Mol. Biomol. Spectrosc.*, 73(5), 854–857.
- Luo, Y., Guo, W., Ngo, H. H., Nghiem, L. D., Hai, F. I., Zhang, J. and Wang, X. C. (2014). “A review on the occurrence of micropollutants in the aquatic environment and their fate and removal during wastewater treatment.” *Science of the total environment*, 473, 619-641.
- Maheshwari, D. K. (Ed.). (2010). “Plant growth and health promoting bacteria.” (Vol. 18), Springer Science and Business Media.
- Maimon, A., Friedler, E. and Gross, A. (2014). “Parameters affecting greywater quality and its safety for reuse.” *Science of the Total Environment*, 487, 20-25.
- Manna, S. (2018). “Treatment of gray water for reusing in non-potable purpose to conserve water in India.” *International Journal of Applied Environmental Sciences*, 13(8), 703-716.
- Manu, D. S. and Thalla, A. K. (2017). “Influence of various operating conditions on wastewater treatment in an AS-biofilm reactor and post-treatment using TiO<sub>2</sub> based Solar / UV Photocatalysis.” 3330(December).
- Marschall, J., Mermel, L. A., Fakhri, M., Hadaway, L., Kallen, A., O’Grady, N. P. and Yokoe, D. S. (2014). “Strategies to prevent central line–associated bloodstream infections in acute care hospitals: 2014 update.” *Infection Control & Hospital Epidemiology*, 35(7), 753-771.
- Matos, C., Pereira, S., Amorim, E. V., Bentes, I. and Briga-Sá, A. (2014). “Wastewater and greywater reuse on irrigation in centralized and decentralized systems—An integrated approach on water quality, energy consumption and CO<sub>2</sub> emissions.” *Science of the total environment*, 493, 463-471.

- Merz, C., Scheumann, R., El Hamouri, B, and Kraume, M. (2007). “Membrane bioreactor technology for the treatment of greywater from a sports and leisure club.” *Desalination*, 215(1-3), 37-43.
- Mishra, V. and Cherkauer, K. A. (2010). “Retrospective droughts in the crop growing season: Implications to corn and soybean yield in the Midwestern United States.” *Agricultural and Forest Meteorology*, 150(7-8), 1030-1045.
- Misra, R. K. and Sivongxay, A. (2009). “Reuse of laundry greywater as affected by its interaction with saturated soil.” *Journal of hydrology*, 366(1-4), 55-61.
- Nolde, E. (2000). “Greywater reuse systems for toilet flushing in multi-storey buildings—over ten years experience in Berlin.” *Urban water*, 1(4), 275-284.
- Nolde, E. (2005). “Greywater recycling systems in Germany—results, experiences and guidelines.” *Water Science and Technology*, 51(10), 203-210.
- O’Toole, J., Sinclair, M., Malawaraarachchi, M., Hamilton, A., Barker, S. F. and Leder, K. (2012). “Microbial quality assessment of household greywater.” *Water research*, 46(13), 4301-4313.
- Oteng-Peprah, M., Acheampong, M. A. and DeVries, N. K. (2018). “Greywater characteristics, treatment systems, reuse strategies and user perception—a review.” *Water, Air and Soil Pollution*, 229(8), 1-16.
- Oteng-Peprah, M., Vries, N. de and Acheampong, M. A. (2020). “Households’ willingness to adopt greywater treatment technologies in a developing country – Exploring a modified theory of planned behaviour (TPB) model including personal norm.” *J. Environ. Manage.*, 254, 109807.
- Ottoson, J. and Stenström, T. A. (2003). “Faecal contamination of greywater and associated microbial risks.” *Water research*, 37(3), 645-655.
- Parjane, S. B. and Sane, M. G. (2011). “Performance of grey water treatment plant by economical way for Indian rural development.” 3(4), 1808–1815.
- Parjane, S. B. and Sane, M. G. (2011). “Performance of grey water treatment plant by economical way for Indian rural development.” *International Journal of ChemTech Research*, 3(4), 1808-1815.
- Pathan, A. A., Mahar, R. B. U. X. and Ansari, K. (2011). “Preliminary Study of Greywater Treatment through Rotating Biological Contactor.” *Mehran Univ. Res. J. Eng. Technol.*, 30(3), 531–538.
- Pidou, M. (2006). Hybrid membrane processes for water reuse.
- Pidou, M., Avery, L., Stephenson, T., Jeffrey, P., Parsons, S. A., Liu, S., ... and Jefferson, B. (2008). Chemical solutions for greywater recycling. *Chemosphere*, 71(1), 147-155.

- Pidou, M., Memon, F. A., Stephenson, T., Jefferson, B. and Jeffrey, P. (2007, September). "Greywater recycling: treatment options and applications." In *Proceedings of the Institution of Civil Engineers-Engineering Sustainability* 160 (3), 119-13, Thomas Telford Ltd.
- Pinto, U., Maheshwari, B. L. and Grewal, H. S. (2010). "Effects of greywater irrigation on plant growth, water use and soil properties." *Resources, Conservation and Recycling*, 54(7), 429-435.
- Prathapar, S. A., Jamrah, A., Ahmed, M., Al Adawi, S., Al Sidairi, S. and Al Harassi, A. (2005). "Overcoming constraints in treated greywater reuse in Oman." *Desalination*, 186(1-3), 177-186.
- Priyanka, K., Behera, M. and Neelancherry, R. (2020). "Graywater Treatment in Sequencing Batch Reactor Using Simultaneous Nitrification, Denitrification and Phosphorus Removal, with Kinetic Studies of Phosphate Adsorption onto Corncob." *J. Hazardous, Toxic, Radioact. Waste*, 24(3), 1–8.
- Priyanka, K., Remya, N. and Behera, M. (2019). "Comparison of titanium dioxide based catalysts preparation methods in the mineralization and nutrients removal from greywater by solar photocatalysis." *J. Clean. Prod.*, 235, 1–10.
- Quan, B., Li, X., Zhang, H., Zhang, C., Ming, Y., Huang, Y., Xi, Y., Weihua, X., Yunguo, L. and Tang, Y. (2019). "Technology and principle of removing triclosan from aqueous media: A review." *Chem. Eng. J.*, 378(April), 122185.
- Raspolli Galletti, A. M., D'Alessio, A., Licursi, D., Antonetti, C., Valentini, G., Galia, A. and Nassi O Di Nasso, N. (2015). "Midinfrared FT-IR as a tool for monitoring herbaceous biomass composition and its conversion to furfural." *J. Spectrosc.*, 2015(December), 0–13.
- Revitt, D. M., Erklsson, E. and Donner, E. (2012). "The implications of household greywater treatment and reuse for municipal wastewater flows and micropollutant loads." *Water Res.*, 45(4), 1549–1560.
- Reynaert, E., Greenwood, E. E., Ndwandwe, B., Riechmann, M. E., Sindall, R. C., Udert, K. M. and Morgenroth, E. (2020). "Practical implementation of true on-site water recycling systems for hand washing and toilet flushing." *Water research* X, 7, 100051.
- Reynaert, E., Morgenroth, E., Ziemba, C. and Lariv, O. (2018). "Chemical composition, nutrient-balancing and biological treatment of hand washing greywater." 144, 752–762.
- Reza, K. M., Kurny, A. and Gulshan, F. (2017). "Parameters affecting the photocatalytic degradation of dyes using TiO<sub>2</sub>: a review." *Appl. Water Sci.*, 7(4), 1569–1578.
- Rice, E. W., Baird, R. B. and A.D. Eaton. (2017). "Standard Methods for the Examination of Water and Wastewater 23rd Edition." *Am. Public Heal. Assoc. Am. Water Work. Assoc.*

- Sahariah, B. P. and Chakraborty, S. (2015). “Comparative study on response of thiocyanate shock load on continuous and fed batch anaerobic-anoxic-aerobic sequential moving bed reactors.” *Environ. Eng. Res.*, 20(1), 65–72.
- Saidi, A., Masmoudi, K., Nolde, E., Amrani, B. El and Amraoui, F. (2017). “Organic matter degradation in a greywater recycling system using a multistage moving bed biofilm reactor (MBBR).” *Water Sci. Technol.*, 76(12), 3328–3339.
- Salager, J. L. (2002). “Surfactants types and uses.” *FIRP booklet*, 300.
- Samayamanthula, D. R., Sabarathinam, C. and Bhandary, H. (2019). “Treatment and effective utilization of greywater.” *Appl. Water Sci.*, 9(4), 1–12.
- Schouten, M. (2009). “Strategy and performance of water supply and sanitation providers: UNESCO-IHE PhD Thesis.” *CRC press*.
- Seetha, N., Bhargava, R. and Kumar, P. (2010). “Effect of organic shock loads on a two-stage activated sludge-biofilm reactor.” *Bioresour. Technol.*, 101(9), 3060–3066.
- Shafran, A. W., Gross, A., Ronen, Z., Weisbrod, N. and Adar, E. (2005). “Effects of surfactants originating from reuse of greywater on capillary rise in the soil.” *Water science and technology*, 52(10-11), 157-166.
- Sharma, A., Burn, S., Gardner, T. and Gregory, A. (2010). “Role of decentralised systems in the transition of urban water systems.” *Water Science and Technology: Water Supply*, 10(4), 577-583.
- Sharma, R., Engemann, S., Sahota, P. and Thakkar, M. M. (2010). “Role of adenosine and wake-promoting basal forebrain in insomnia and associated sleep disruptions caused by ethanol dependence.” *Journal of neurochemistry*, 115(3), 782-794.
- Song, S. J., Ito, K., Ala, U., Kats, L., Webster, K., Sun, S. M. and Pandolfi, P. P. (2013). “The oncogenic microRNA miR-22 targets the TET2 tumor suppressor to promote hematopoietic stem cell self-renewal and transformation.” *Cell stem cell*, 13(1), 87-101.
- Spuhler, D., Rengifo-Herrera, J. A. and Pulgarin, C. (2010). “The effect of Fe<sup>2+</sup>, Fe<sup>3+</sup>, H<sub>2</sub>O<sub>2</sub> and the photo-Fenton reagent at near neutral pH on the solar disinfection (SODIS) at low temperatures of water containing Escherichia coli K12.” *Applied Catalysis B: Environmental*, 96(1-2), 126-141.
- Spuhler, D., Rengifo-herrera, J. A., Spuhler, D. and Andre, J. (2010). “The effect of Fe<sup>2+</sup>, Fe<sup>3+</sup>, H<sub>2</sub>O<sub>2</sub> and the photo-Fenton reagent at near neutral pH on the solar disinfection ( SODIS ) at low temperatures of water containing Escherichia coli K12 Applied Catalysis B : Environmental.” (January 2016).
- Stylidi, M., Kondarides, D. I. and Verykios, X. E. (2003). “Mechanistic and kinetic study of solar-light induced photocatalytic degradation of Acid Orange 7 in aqueous TiO<sub>2</sub> suspensions.” 05.



- Stylidi, M., Kondarides, D. I. and Verykios, X. E. (2003). "Pathways of solar light-induced photocatalytic degradation of azo dyes in aqueous TiO<sub>2</sub> suspensions." *Applied Catalysis B: Environmental*, 40(4), 271-286.
- Susilawati, R., Papendick, S. L., Gilcrease, P. C., Esterle, J. S., Golding, S. D. and Mares, T. E. (2013). "Preliminary investigation of biogenic gas production in Indonesian low rank coals and implications for a renewable energy source." *Journal of Asian Earth Sciences*, 77, 234-242.
- Susilawati, U. I. (2013). "Faktor-Faktor Yang Berhubungan Dengan Keluhan Musculoskeletal Disorders Pada Pegawai Pengguna Komputer Di PT. Nusantara V Pekanbaru Tahun 2013." 242, 27–30.
- Svardal, K. and Kroiss, H. (2011). "Energy requirements for waste water treatment." *Water Science and Technology*, 64(6), 1355-1361.
- Tchobanoglous, G., Burton, F. L. and Stensel, H. D. (2003). Wastewater engineering treatment and reuse (No. 628.3 T252s). Boston, US: McGraw-Hill Higher Education.
- Teh, X. Y., Poh, P. E., Gouwanda, D. and Chong, M. N. (2015). "Decentralized light greywater treatment using aerobic digestion and hydrogen peroxide disinfection for non-potable reuse." *Journal of cleaner production*, 99, 305-311.
- Temmink, H. and Klapwijk, B. (2004). "Fate of linear alkylbenzene sulfonate (LAS) in activated sludge plants." *Water research*, 38(4), 903-912.
- Temmink, H., Zeeman, G. and Buisman, C. J. N. (2010). "Comparison of Three Systems for Biological Greywater Treatment." 155–169.
- Teoh, W. Y., Scott, J. A. and Amal, R. (2012). "Progress in heterogeneous photocatalysis: from classical radical chemistry to engineering nanomaterials and solar reactors." *The Journal of Physical Chemistry Letters*, 3(5), 629-639.
- Tian, H., Ji, X., Yang, X., Zhang, Z., Lu, Z., Yang, K. and Rao, Z. (2016). "Structural basis of Zika virus helicase in recognizing its substrates." *Protein & cell*, 7(8), 562-570.
- Tombola, R., Buttiglieri, G., Auset, M. and Gonzalez-Olmos, R. (2019). "Recycled corrugated wire hose cover as biological carriers for greywater treatment in a sequential batch biofilm reactor." *J. Environ. Manage.*, 240(February), 475–484.
- Travis, M. J., Weisbrod, N. and Gross, A. (2008). "Accumulation of oil and grease in soils irrigated with greywater and their potential role in soil water repellency." *Science of the Total Environment*, 394(1), 68-74.
- Travis, M. J., Wiel-Shafran, A., Weisbrod, N., Adar, E. and Gross, A. (2010). "Greywater reuse for irrigation: effect on soil properties." *Science of the Total Environment*, 408(12), 2501-2508.
- Tseng, D. H., Juang, L. C. and Huang, H. H. (2012). "Effect of oxygen and

hydrogen peroxide on the photocatalytic degradation of monochlorobenzene in TiO<sub>2</sub> aqueous suspension.” *Int. J. Photoenergy*, 2012(2).

Umezawa, N. and Ye, J. (2012). “Role of complex defects in photocatalytic activities of nitrogen-doped anatase TiO<sub>2</sub>.” *Physical Chemistry Chemical Physics*, 14(17), 5924-5934.

Wang, J., Shih, Y., Wang, P. Y., Yu, Y. H., Su, J. F. and Huang, C. pao. (2019). “Hazardous waste treatment technologies.” *Water Environ. Res.*, 91(10), 1177–1198.

Wang, S. and Wang, J. (2019). “Activation of peroxymonosulfate by sludge-derived biochar for the degradation of triclosan in water and wastewater.” *Chem. Eng. J.*, 356(May 2019), 350–358.

Wiel-Shafran, A., Ronen, Z., Weisbrod, N., Adar, E. and Gross, A. (2006).” Potential changes in soil properties following irrigation with surfactant-rich greywater.” *Ecological Engineering*, 26(4), 348-354.

World Health Organization. (2017). “Global diffusion of eHealth: making universal health coverage achievable: report of the third global survey on eHealth.”

Xie, X., Chen, C., Wang, X., Li, J. and Naraginti, S. (2019). “Efficient detoxification of triclosan by a S-Ag/TiO<sub>2</sub>@g-C<sub>3</sub>N<sub>4</sub> hybrid photocatalyst: Process optimization and bio-toxicity assessment.” *RSC Adv.*, 9(35), 20439–20449.

Ye, L., Jong, M. P. De, Kudernac, T., Wiel, W. G. Van Der and Huskens, J. (2017). “Doping of semiconductors by molecular monolayers: monolayer formation, dopant diffusion and applications.” 62(June 2016), 128–134.

Ye, M., He, C., Iocozzia, J., Liu, X., Cui, X., Meng, X. and Lin, Z. (2017). “Recent advances in interfacial engineering of perovskite solar cells.” *Journal of Physics D: Applied Physics*, 50(37), 373002.

Ying, G. G. (2006). “Fate, behavior and effects of surfactants and their degradation products in the environment.” *Environment international*, 32(3), 417-431.

Yu, H., Ding, W., Luo, J., Geng, R. and Cai, Z. (2012). “Long-term application of organic manure and mineral fertilizers on aggregation and aggregate-associated carbon in a sandy loam soil.” *Soil and Tillage Research*, 124, 170-177.

Yu, Z. L., Rahardianto, A., DeShazo, J. R., Stenstrom, M. K. and Cohen, Y. (2013). “Critical review: regulatory incentives and impediments for onsite graywater reuse in the United States.” *Water Environment Research*, 85(7), 650-662.

Zhang, B., Song, X., Zhang, Y., Han, D., Tang, C., Yu, Y. and Ma, Y. (2012). “Hydrochemical characteristics and water quality assessment of surface water and groundwater in Songnen plain, Northeast China.” *Water research*, 46(8), 2737-2748.

Zhang, K., Achari, G., Sadiq, R., Langford, C. H. and Dore, M. H. I. (2012). “An integrated performance assessment framework for water treatment plants.” *Water*

*Res.*, 46(6), 1673–1683.

Zheng, H., Wang, Z., Zhao, J., Herbert, S. and Xing, B. (2013). “Sorption of antibiotic sulfamethoxazole varies with biochars produced at different temperatures.” *Environmental Pollution*, 181, 60-67.

Ziemba, C., Larivé, O., Reynaert, E. and Morgenroth, E. (2018). “Chemical composition, nutrient-balancing and biological treatment of hand washing greywater.” *Water Res.*, 144, 752–762.

Zing-Yi, O., Othman, N., Mohamad, M. and Rashid, R. (2014). “Removal performance of lignin compound from simulated pulping wastewater using emulsion liquid membrane process.” *International Journal of Global Warming*, 6(2-3), 270-283.

Zuo, F., Wang, L., Wu, T., Zhang, Z., Borchardt, D. and Feng, P. (2010). “Self-doped  $Ti^{3+}$  enhanced photocatalyst for hydrogen production under visible light.” *Journal of the American Chemical Society*, 132(34), 11856-11857.

NATIONAL INSTITUTE OF TECHNOLOGY KARNATAKA, SURATHKAL

**List of Publications based on PhD Research Work**

S. No.	Title of the paper	Authors (in the same order as in the paper. Underline the Research Scholar's name)	Name of the Journal/ Conference/ Symposium, Vol., No., Pages	Year of Publication	Category *
1	Polymer-based Immobilized Fe <sub>2</sub> O <sub>3</sub> -TiO <sub>2</sub> /PVP catalyst preparation method and the degradation of triclosan in treated GW effluent by solar photocatalysis	<u>Sarath Chandra Pragada</u> , Arun Kumar Thalla	Journal of Environmental Management, 296, 113305. ( <b>Elsevier</b> )	2021	1
2	Integrated anaerobic-aerobic sequencing batch reactors for unrestricted reuse using GW treatment	<u>Sarath Chandra Pragada</u> , Arun Kumar Thalla	International journal of environmental science and development, 12(12), 346-354.	2021	1
3	Stability of Integrated anaerobic-aerobic-sand filter system at surfactant shock load application in GW treatment	<u>Sarath Chandra Pragada</u> , Arun Kumar Thalla	<b>Pipeline</b>	-	1
4	Internal Circulation Sequencing Batch Reactor with Multistage Inflow to Reclaim GW Quality	<u>Sarath Chandra Pragada</u> , Arun Kumar Thalla	NCCE-NITK, NITK Surathkal.	30-31 Jan 2020	3

\* Category: 1: Journal paper, full paper reviewed 2: Journal paper, Abstract reviewed 3: Conference/Symposium paper, full paper reviewed 4: Conference/Symposium paper, abstract reviewed 5: others (including papers in Workshops, NITK Research Bulletins, Short notes etc.)

*Sarath* 3/3/22

**Pragada Sarath Chandra**  
Research Scholar  
Name & Signature, with Date

**Dr. Arun Kumar Thalla**  
Research Guide  
Name & Signature, with Date

## **BIO- DATA**



**Name : PRAGADA SARATH CHANDRA**

**D.O.B : 01/07/1993**

**Address : S/O PRAGADA VENKATARAO**  
**Main street,**  
**Nandigam (Mandal, Post, Village)**  
**Srikakulam (District)**  
**Andhrapradesh- 532203.**

**Email : sarathpragada@gmail.com**

**Qualification : B.Tech (Civil Engineering)**

**M.Tech (Environmental Engineering)**

**Journals : 02**

**Int. Conference: 01**

**National Conference: 01**

